Modelling of dam breach flows; past and future mine tailings dam cases

Mònica Novell Morell

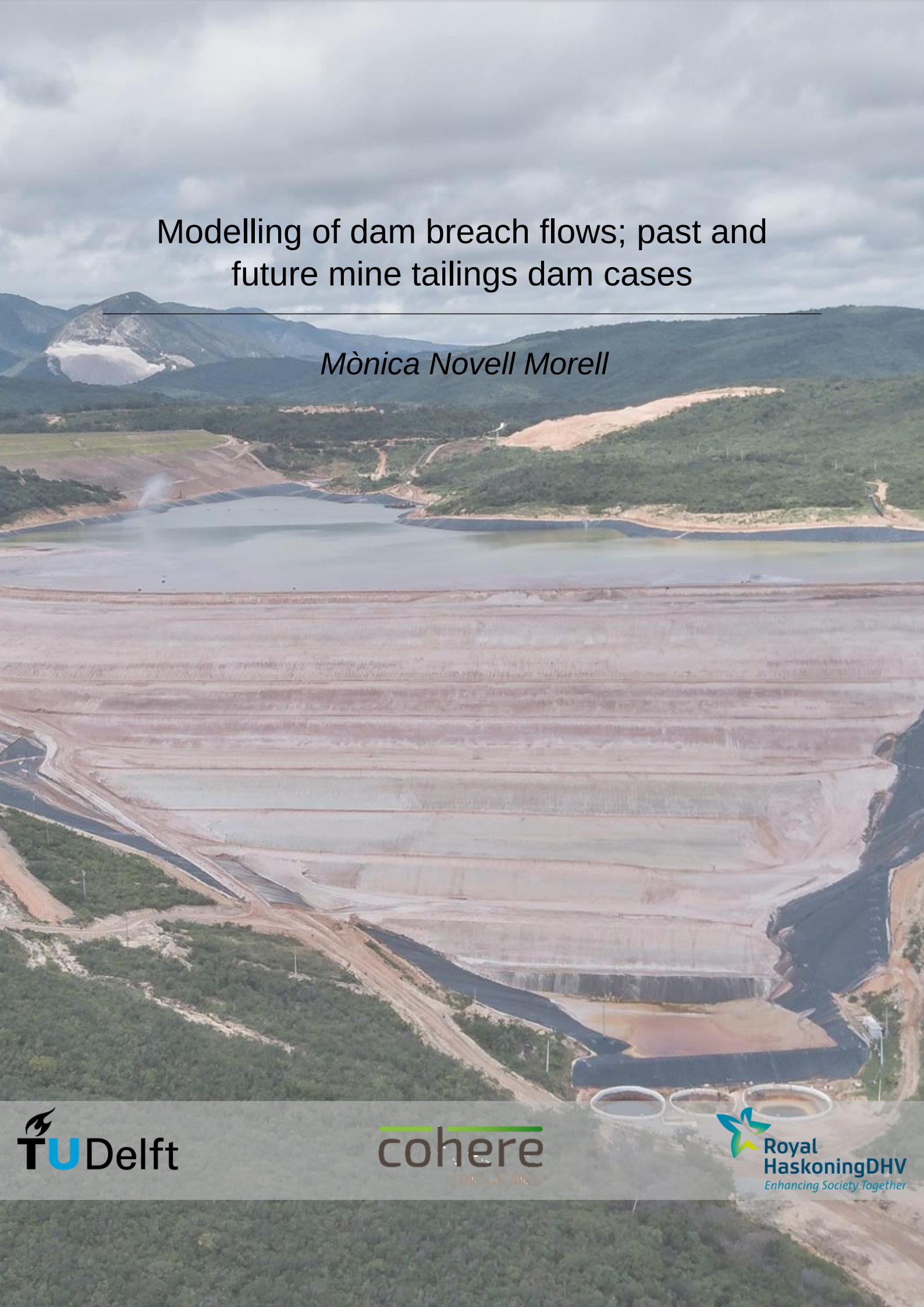

TU Delft

cohere

Royal HaskoningDHV
Enhancing Society Together

Modelling of dam breach flows; past and future mine tailings dam cases

by

Mònica Novell Morell

to obtain the degree of Master of Science in
at the Delft University of Technology,
to be defended publicly on Tuesday January 25, 2022 at 03:00 PM.

Student number:	5133238	
Project duration:	March 1, 2021 – January 25, 2022	
Thesis committee:	Dr. ir. P. J. Vardon,	TU Delft, chair
	Dr. ir. S. Slob,	Cohere Consultants
	Dr. ir. J. E. A. Storms,	TU Delft
	Prof. dr. ir. W. S. J. Uijttewaal,	TU Delft
	Dr. M. Busnelli	Royal HaskoningDHV

Cover Image: Picture from Paulo Oliveira
[https://www.meussertoes.com.br/2021/02/06/jacobina-tremores-de-terra-ou-explosoes/]

TU Delft

Preface

This Msc thesis marks the culmination of my studies at Delft University of Technology. It is written to acquire the title Master of Science in Geo-Engineering at the Civil Engineering and Geosciences faculty. This research project has been conducted in cooperation with Cohere Consultants.

First, I would especially like to thank Siefko Slob for giving me the opportunity to join Cohere Consultants and being my daily supervisor. Whenever I was lost, you helped me out and made sure I got back on track to keep going. I would also like to express my gratitude to Eliam Vlijm, for the short but insightful meetings we had. In a few sentences and comments, you were able to make me see problems from a different perspective. I would like to thank both of them for giving me the opportunity to do the Msc thesis at their company. In a few years, when I look back at my time at Cohere Consultants I will recall all the funny moments and activities we did together. Thank you for making my last study year memorable and rewarding.

Moreover, this project would not have been possible without the guidance and supervision of my graduation committee. I would like to thank Phil Vardon for agreeing on being the chair of my committee, I appreciate your feedback and all the help that you gave me throughout this project. I would also like to express my appreciation to my other supervisors Joep Storms and Marcela Busnelli, I appreciate their guidance and suggestions on the research. Specially, I would like to thank Marcela Busnelli for introducing me the numerical models used and for all the meetings we had. Last but not least, I would like to thank Wim Uijttewaal for joining the committee, your help was substantial for me in order to carry on with the project, especially due to the interdisciplinary nature of this research. I experienced our meetings as intense and challenging, but also fruitful and educational. Thank you all for your feedback, insights, availability and patience during this thesis process. In many ways, a thesis is actually more a team effort than it is individual work and I personally appreciate everybody's help.

Special thanks to my roommates Koen and Stephan for joining me on this Msc thesis journey. Thank you for all the moments when you listened to my problems and helped me out with new suggestions. I deeply appreciate your support and necessary distraction during the last months of my thesis work. Lastly, I would like to thank my family and friends for their unconditional support and making my student life in Delft unforgettable.

Mònica Novell Morell
Delft, January 2022

Abstract

Tailings storage facilities (TSF) are engineered structures that retain mixed waste material (known as mine tailings material) from mining processes in liquid or slurry form. One of the issues regarding TSF management is the lack of site investigation and sample analyses, which cause the uncertainty of geotechnical properties of mine tailings materials. For a proper operation of tailings storage facilities, the owner should study the material involved and understand the physical and chemical properties associated with it. In case of mine tailings dam failure, the resulting flood wave supposes an environmental, social and economical disaster for society. The failure rate of TSFs is an average of one to two failures a year worldwide. Well-known examples of mine tailings dams failure happened that in the state of Minas Gerais in Brazil, are the Feijão dam failure in 2015 and dam B-I near Brumadinho in 2019.

Mine tailings dam break studies use numerical models to predict the flooding area and assess the possible damaged area. Historically, these studies were carried out according to Newtonian modelling principles, but the presence of solids within the fluid suggests that the resulting flood wave of a TSF failure should be treated as a non-Newtonian fluid. Absence of laboratory data regarding the geotechnical properties of mine tailings materials make difficult the prediction of such flood wave, since the composition of the mixture is unknown. Therefore, the aim of this research is to study the flow behaviour of mine tailings materials in case of failure of tailings storage facilities. Understanding the flow behaviour of the non-Newtonian fluid is essential to analyse the possible failure event for an existing structure, in order to plan and organise emergency procedures that anticipate and mitigate downstream damages.

In the first phase of this project the fluid mechanics theory was studied. It was essential to understand the basic concepts of flow behaviour and the governing equations. Once the fundamental theory was clear, it was more feasible to understand the science of rheology and distinguish between Newtonian and non-Newtonian fluids. The starting point of the research part was to assess all the terms that compose the O'Brien quadratic rheological model. A sensitivity analysis of the all the parameters of the rheological model was carried out and it was concluded that the volumetric concentration is the property that influences the flow behaviour the most.

The second part of the project was to introduce and validate the numerical models used. The models chosen for this Msc thesis were FLO-2D and HEC-RAS, since both were able to account non-Newtonian fluids for the simulations. One of the input boundaries needed for both models was the breach hydrograph. The prediction of the breach hydrograph was carried out with the FLO-2D model, which was able to estimate the outflow rate according to the volume released and the duration of failure. Then, the same hydrograph was introduced in HEC-RAS together with the same input parameters used in FLO-2D, in order to compare the results of each model. Prior to simulations, the governing equations of each model had been studied to understand the inputs needed and the results obtained. Both models used the Shallow Water Equations as principle, but each model integrated the O'Brien rheological model in a different manner.

The third part of the research was a sensitivity analysis with FLO-2D, where the variables were the volumetric concentration, the Manning's roughness value and the breach hydrograph. The results analysed were the initial flooding area (short moment after failure) and the final inundated area (after a certain time of failure). It was found that the volumetric concentration was the property that influences the initial inundated area the most. An increase of volumetric concentration means more solids within the mixture and less fluid, causing more difficulties for the mixture to flow. The second parameter was the breach hydrograph and lastly the Manning's roughness value. Regarding the final inundated area, the duration of failure was the most sensitive parameter, specially when it was reduced. Then, the volumetric concentration and finally the Manning's roughness value.

The main difference between FLO-2D and HEC-RAS was the implementation of the O'Brien rheological model in the governing equations; it was concluded from the sensitivity analysis carried out in the rheological model that the volumetric concentration was the parameter that influenced the most the flow behaviour. Therefore, for the sensitivity analysis carried out with HEC-RAS only the volumetric concentration property was changed. It was important to note that the non-Newtonian feature in the HEC-RAS model was still a trial version and it had not been tested yet. That was the reason why the results obtained with HEC-RAS were inconsistent with the FLO-2D results and the flow theory.

Finally, an application of FLO-2D to predict the flooding area in case of dam breach was carried out in two TSF of Minas Gerais. The predictions were given with a range of possible solutions, varying the volumetric concentration and the duration of failure. The realism of the range of values used was obtained from the sensitivity analyses performed with FLO-2D. The results were compared with an energy-line approach that was based in two empirical formulas that linked the volume of the reservoir with the angle of reach, which is the ratio between the elevation of the TSF's crest and the distance travelled by the mixture. From the results obtained, the energy-line approach represented an overestimation of the inundated area in comparison with the results obtained with FLO-2D.

To conclude, from the results obtained the volumetric concentration was the parameter that influence the flow behaviour the most. Analysing the O'Brien quadratic rheological model, the volumetric concentration appeared in each term, thus it was expected. Regarding the numerical models, the inputs that affected the result the most were the volumetric concentration and the duration of failure. A decrease of the volumetric concentration meant that the fluid had less solids within the mixture and it would be easier for it to flow, leading to a more extensive flooding area. Reducing the duration of failure, thus increasing the peak discharge, implied higher velocity values and a larger inundated area near the failure location. The results obtained with the energy-line approach resulted in an overestimation of the inundated area in comparison with the results from the numerical models. However, it supposed a good first approximation to delimit the inundated area in case of failure if complex models could not be used. Overall, what this project does offer is a good understanding of the geotechnical properties and input values that should be considered when modelling the flood wave of a tailings storage facility failure.

List of Figures

List of Tables

List of Symbols

Latin symbols	Dimensions and Units	Definition
a	$[L/T^2]$	Acceleration field in the Cartesian coordinate system
a_i	$-$	Empirical coefficient in the dispersive shear stress
A	$[L^2]$	Area
b	$[M/L^{-1} \cdot T^2]$	Coriolis forces
C_v	-	Volumetric concentration
$C*$	-	Maximum volumetric concentration
D_i	$[mm]$	Particle size ($i = 10, 30, 50, 60$)
d_s	$[m]$, $[mm]$	Sediment size
E	*[m]*	Energy head
e	-	Void ratio
Fr	-	Froude number
f	$[M/L^{-1} \cdot T^2]$	Friction forces
$\overline{F_{ext}}$	$[M/L \cdot T^2]$	External forces field in Cartesian Coordinate system
$\overline{F_p}$	$[M/L \cdot T^2]$	Pressure forces field in Cartesian Coordinate system
$\overline{F_s}$	$[M/L \cdot T^2]$	Shear forces field in Cartesian Coordinate system
G	$[L/T^2]$	Gravitational acceleration field
H	$[m]$	Total flow depth
H'	$[m]$	Elevation of the crest's tailing storage facility
h	$[L]$	Longitude between the plane of reference and the topography
K	$[T/L^{1/3}]$ = $[s/m^{1/3}]$	Resistance parameter
k	$[N \cdot s^n/m^2]$	Consistency index
k'	-	von Kármán constant
L	$[L]$	Longitudinal length scale
L'	$[m]$	Longitude of the flooding area
l_m	$[L]$	Prandtl mixing length
m	$[M]$	Mass
n	$[T/L^{1/3}]$ = $[s/m^{1/3}]$	Manning's roughness value
n_{td}	$[T/L^{1/3}]$ = $[s/m^{1/3}]$	Manning's resistance value for turbulent flow
n'	-	Porosity
N	-	Flow index
P	$[M/L^{-1} \cdot T^2]$	Pressure force
Q	$[L^3/T]$ = $[m^3/s]$	Discharge
q	$[L^3/T]$	Influx term
R	$[L]$	Hydraulic radius
Re	-	Reynolds number
S	-	Dimensionless slope
S_0	-	Channel slope
S_f	-	Friction slope
S_{MD}	-	Mud-debris friction slope
S_{td}	-	Turbulent-dispersive friction slope
S_y	-	Yield friction slope
S_v	-	Viscous friction slope
t	$[T]$	Time
(u', v')	$[L/T]$	Instantaneous fluctuating velocities
$\overline{V} = (u, v, w)$	$[L/T]$	Velocity field in Cartesian Coordinate system
V^*	$[L^3]$	Volume
V_R	$[Mm^3]$	Total volume released
V_S	$[Mm^3]$	Total volume of solids
V_T	$[Mm^3]$	Total volume of mixture
V_W	$[Mm^3]$	Total volume of water
$\overline{W}$	$[M/L \cdot T^2]$	Weight forces field in Cartesian Coordinate system
$\overline{X} = (x, y, z)$	$[L]$	Cartesian Coordinate system

Greek symbols	Dimensions and Units	Definition
α	*[°]*	Angle of reach
α_1	-	Empirical parameter for the yield strength
α_2	-	Empirical parameter for the viscosity
β_1	-	Empirical parameter for the yield strength
β_2	-	Empirical parameter for the viscosity
ρ	$[M/L^3]$	Density
ρ_m	$[kg/m^3]$	Density of the mixture
ρ_s	$[kg/m^3]$	Density of particles
ρ_w	$[kg/m^3]$	Density of water
μ	$[M/L \cdot T]$ = $[N \cdot s/m^2]$	Viscosity
μ_t	$[M/L \cdot T]$ = $[N \cdot s/m^2]$	Turbulent eddy viscosity
λ	-	Linear volumetric concentration
γ	$[1/T]$ = $[s^{-1}]$	Shear rate
τ	$[M/L \cdot T^2]$ = $[N/m^2]$	Total shear stress
τ_b	$[M/L \cdot T^2]$ = $[N/m^2]$	Bottom shear stress
τ_{MD}	$[M/L \cdot T^2]$ = $[N/m^2]$	Mud-debris shear stress
τ_d	$[M/L \cdot T^2]$ = $[N/m^2]$	Dispersive shear stress
τ_t	$[M/L \cdot T^2]$ = $[N/m^2]$	Turbulent shear stress
τ_v	$[M/L \cdot T^2]$ = $[N/m^2]$	Viscous shear stress
τ_y	$[M/L \cdot T^2]$ = $[N/m^2]$	Yield strength
ζ	$[m]$	Water surface elevation
φ	-	Water surface slope
ψ	*[°]*	Inclination angle of the current velocity direction

Contents

1 Introduction

1.1. Problem definition

In Brumadinho (Minas Gerais, Brazil), on January 25th 2019, a mine tailing storage facility, dam B-I owned by Vale S.A., failed catastrophically. It caused 250 casualties and more than 100 people were missing. Cameras were placed around dam B-I for monitoring purposes, so there are videos of the failure in real time. Those videos (Guardian, 2019) clearly show a slope failure starting from the crest, which dropped and the area around the toe region bulged outwards before the surface of the dam broke apart. The total collapse involved a volume released of $9.7\ Mm^3$ of mudflow that flowed through the downstream area at a high velocity. Studies performed to investigate the causes of failure of dam B-I concluded that the combination of a steep slope constructed dam, high water level within the reservoir and weak fine mine tailings material within the dam created the conditions for failure (Robertson et al., 2019).

Nevertheless, it was not the first time that an incident like this one took place; in 2015 near the town of Mariana (Brazil), the Fundão tailings storage facility also failed. After 16 days the mud flood reached the sea, where its impact affected thousands of marine fauna and flora species. It was the most serious environmental disaster in recent Brazilian history (Miranda and Marques, 2016).

There are over 769 tailings storage facilities in Brazil. Most of these dams are constructed in a step-by-step construction method, which leads to a continuously changing state of vertical loads during construction. After the accidents in Brumadinho and Mariana, the National Mining Agency in Brazil banned the construction of mine tailings dams with the same design method as those two structures: the upstream method. Additionally, it was announced a mandatory decommissioning of same type of dams up to 2021 (Palu and Julien, 2019). When a dam fails, loss of life, environmental, human and economic damage are direct consequences of such event, which depend on the magnitude of the mudflow and its velocity.

Mine tailings storage facilities are dams with large volumes of largely saturated mine tailings materials behind it. These structures contain the leftover part of the ore of many years of mining activities. The hazard of dam failure in combination with the impacts of the resulting flood wave makes these structures high-risk objects. Two major dam failure in Brazil, Mariana dam failure and the Brumadinho (dam B-I) failure in 2015 and 2019 are evidence of such risk.

Mine tailings dam failure can happen due to several causes, for instance insufficient spillway capacity, structural defects, unstable slopes, seepage, piping, overtopping or earthquakes. In case of mine tailings dam failure, the extents of inundated area are driven by the size of the impoundment, the extension of the breach, the peak discharge, the flow velocity, roughness between soil-material, rheology of the mixture, the properties and mineralogy of the sediments involved and the downstream topography. When failure happens, the resulting flood wave is a mix of water and mine tailings particles within the reservoir. The amount of volume and water are a characteristic of each facility, thus the resulting flood

wave in case of failure is different for each structure. For safety assessment and evacuation planning a predictive model is of key importance. Models are used to identify areas prone to flooding, to evaluate the risk involved, as well as suggesting measures to minimise flood damage and develop emergency plans. In this thesis and to avoid confusion, the mixture of water and mine tailings material is referred as hyper-concentrated sediment fluid.

1.2. Research objective

The objective of the research is to determine the degree of influence of mine tailing material's properties and the flow behaviour of a flood wave caused by tailings dam breach, which is predicted with numerical models. This research aims to delimit the impacted zones resulting from the dam failure and identify which material properties influences the most on the damaged area.

From the objective stated the following main research question is:

How does the flow behaviour affect the area impacted by a hyper-concentrated sediment fluid resulting from a dam break?

To find an answer to this question, the following sub-questions are defined:

1. What properties affect flow behaviour of a hyper-concentrated sediment fluid?
2. Which parameters are the most critical for modelling the dam break flow model?
3. In what way does a non-Newtonian fluid model perform better than water based model for breach modelling?
4. From the properties of mine tailing dams, is it possible to accurately determine beforehand the flow behaviour?
5. What are the limitations of the existing modelling softwares used?
6. Are the simpler methods an accurate approach to delimit the inundated area?

1.3. Structure

This Msc thesis is divided into different chapters that are aimed to answer the research questions:

- Chapter 2 contains the fluids mechanics theory together with a description of the equations involved. Next, an explanation of the type of fluids that theory distinguishes. Lastly, the science of rheology and rheological models are explained. The aim of this part is to get familiar with the theory and equations that are the basis for the subsequent research.
- Chapter 3 describes all the terms and components involved in the rheological model. A sensitivity analysis is carried out to see which parameters influence the most on the result. Different cases are considered to test the robustness of the model. Additionally, the description of the event near Brumadinho of the dam B-I in Minas Gerais, Brazil.
- Chapter 4 introduces the numerical models used. The governing equations are explained for each model and also a comparison between them. Two benchmark tests are performed in order to calibrate the models according to fluid's mechanics laws.
- Chapter 5 starts with the parameters that are needed for the analysis, ranges for values that these parameters may take and predictions of what is expected. Thereafter, the comparison of numerical simulations with different input values.

- Chapter 6 shows how the model can be applied in order to predict the resulting inundated area in case of mine tailings dam failure and the results obtained are compared with an energy-line approach. This method is based on two empirical equations that link the volume of the reservoir with the distance travelled by the fluid. The comparison is carried out for two tailings storage facilities.
- Chapter 7 discusses on the results from the numerical models used and simulations performed.
- Chapter 8 concludes on the observed results, answers the research questions and suggests some recommendations.

2

Background

This chapter includes an overview of the main findings of theoretical background information on fluid mechanics. A fluid is a substance whose molecules move freely past each other and mechanics is the field of science focused on the motion of material bodies. This thesis is centered in the mechanics when a certain material is in a fluid phase, which is the science of energy, motion, deformation and properties of fluids (Elger et al., 2020). The first section 2.1 of this chapter is focused on the governing equations of fluid behaviour. Section 2.2 treats the physical properties of fluids and sediments. Finally, section 2.3 explains the basis of rheology, types of fluids and the models involved.

2.1. Fluid mechanics

In this section, differential equations of fluid dynamics are presented that describe the motion of fluids. Density, velocity and temperature are the considered variables that provide a spatiotemporal description of the distribution of the fluid in statistical terms (because of the averaging over elementary volumes). External forces give information regarding the actions applied on fluids and the main objective of the equations is to predict and describe the evolution of the aforementioned variables in time and space under the action of such forces (Coussot, 2005). Assuming incompressible flow (constant density) and constant viscosity, the following equations are based on three fundamental physical principles (Anderson and Wendt, 1995): conservation of mass, momentum and energy.

2.1.1. Continuity equation

The continuity equation is a partial differential equation that describes the law of conservation of mass when applied to a fixed volume. The mass conservation principle means that in absence of any source of matter, the amount of matter considered must remain constant during any displacement (Coussot, 2005). The continuity equation analyses a specific volumetric region in space called control volume (CV). A CV observes motion in specific locations (Eulerian method), the matter inside a CV can only change over time due to mass flowing across the boundaries (Elger et al., 2020). For a CV, the physical interpretation of the continuity equation is:

$$\frac{d\, m_{cv}}{dt} = 0 \tag{2.1}$$

If mass passes through the boundaries, then equation 2.1 can be rewritten as:

$$\frac{d\, m_{cv}}{dt} = \sum m_i - \sum m_o \tag{2.2}$$

In equation 2.2, the first term describes the accumulation rate of mass inside the CV. Σm_i and Σm_o represent the inflow and outflow rates at which the mass enters and leaves the system, respectively. Therefore, the accumulation concept is the variation in the mass quantity inside the CV respect time. If accumulation is positive, mass inside the CV increases ($\Sigma m_i > \Sigma m_o$). On the contrary, accumulation is negative when mass decreases in the CV ($\Sigma m_i < \Sigma m_o$); or is zero when it stays the same ($\Sigma m_i = \Sigma m_o$).

The physics of the mass conservation are summarised as a balance equation applied at an instant time with units (kg/s):

accumulation + (net outflow of mass) = accumulation + (inflow - outflow) = 0

To derive the continuity equation for a certain infinitesimally small CV (dx, dy, dz), first a Cartesian coordinate system $\overline{X} = (x, y, z)$ is defined, where *x* and *y* are the longitudinal and horizontal coordinates and *z* represents the vertical coordinate, oriented positive upwards. The velocity field is given by $\overline{V} = (u, v, w)$, where *u*, *v* and *w* are the depth-averaged velocities in the Cartesian coordinates *x*, *y* and *z* respectively (Figure 2.1).

The accumulation term follows as:

$$\frac{d\ m_{cv}}{dt} = \left(\frac{\partial \rho}{\partial t}\right)(dxdydz) \tag{2.3}$$

where the mass in the CV equals the density of the fluid (ρ) times the control volume (dx, dy, dz), where the volume is constant with time.

The net outflow mass results in:

$$m_{net} = \left(\frac{\partial(\rho u)}{\partial x} + \frac{\partial(\rho v)}{\partial y} + \frac{\partial(\rho w)}{\partial z}\right)(dxdydz) \tag{2.4}$$

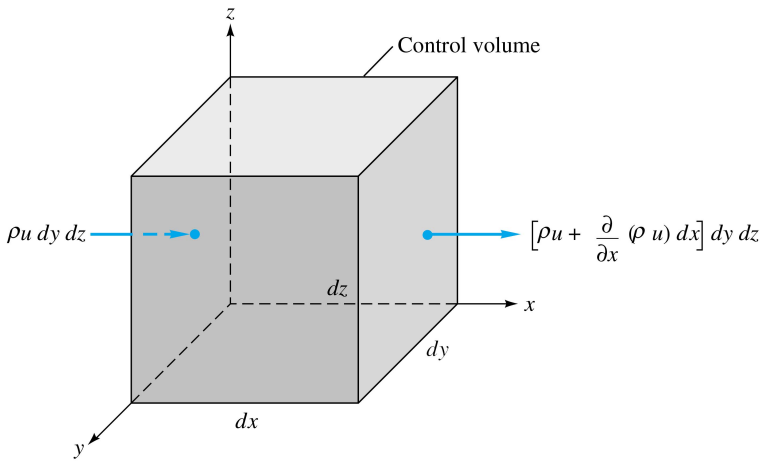

Figure 2.1: Infinitesimally small CV with inflow and outflow rates for x-direction. Source: White, 2003.

Applying equations 2.3 and 2.4 to the mass balance and dividing by the volume of CV, the conservation of mass for an infinitesimal control volume is obtained:

$$\frac{\partial \rho}{\partial t} + \frac{\partial(\rho u)}{\partial x} + \frac{\partial(\rho v)}{\partial y} + \frac{\partial(\rho w)}{\partial z} = 0 \tag{2.5}$$

Assuming incompressible flow, equation 2.5 in Cartesian coordinates is:

$$\frac{\partial u}{\partial x} + \frac{\partial v}{\partial y} + \frac{\partial w}{\partial z} = 0 \tag{2.6}$$

Dimensions and units for the continuity equation are:

$$\frac{(mass/time)}{(volume)} = \frac{kg/s}{m^3} \tag{2.7}$$

A more detailed and extensive derivation of the continuity equation can be found in Elger et al., 2020 and White, 2003.

2.1.2. Momentum equation

The Navier-Stokes equation or momentum equation has the theoretical basis in the Newton's second law. The second law of Newton states that the sum of external forces is proportional to the acceleration, with the mass of the particle serving as the constant of proportionality (Elger et al., 2020):

$$\sum \overline{F_{ext}} = m\overline{a} = m\frac{d\overline{V}}{dt} \tag{2.8}$$

$\overline{a}$ is the acceleration vector in the Cartesian coordinates, which is equivalent as the derivative of the velocity vector $\overline{V}$. Note that $m\overline{V}$ is the momentum of one particle.

Two categories are considered for the external forces $\overline{F_{ext}}$: surfaces forces such as the pressure force $\overline{F_p}$ and shear force $\overline{F_s}$; and only one body force, weight $\overline{W}$. Therefore, extending equation 2.8 with the stated forces gives:

$$\overline{F_p} + \overline{F_s} + \overline{W} = \rho V^* \frac{d\overline{V}}{dt} \tag{2.9}$$

Note that $V*$ is the volume considered and $\overline{V}$ is the velocity field. Elger et al., (2020) contains the thorough derivation methodology for the linear momentum equation. The following Navier-Stokes equation gives the result for a system of particles assuming constant density and viscosity:

$$\rho\frac{d\overline{V}}{dt} = \rho\overline{g} - \nabla P + \mu\nabla^2\overline{V} \tag{2.10}$$

The Navier-Stokes equations in Cartesian coordinates are:

$$\rho\left(\frac{\partial u}{\partial t} + u\frac{\partial u}{\partial x} + v\frac{\partial u}{\partial y} + w\frac{\partial u}{\partial z}\right) = \rho g_x - \frac{\partial P}{\partial x} + \mu\left(\frac{\partial^2 u}{\partial x^2} + \frac{\partial^2 u}{\partial y^2} + \frac{\partial^2 u}{\partial z^2}\right) \tag{2.11}$$

$$\rho\left(\frac{\partial v}{\partial t} + u\frac{\partial v}{\partial x} + v\frac{\partial v}{\partial y} + w\frac{\partial u}{\partial z}\right) = \rho g_y - \frac{\partial P}{\partial y} + \mu\left(\frac{\partial^2 v}{\partial x^2} + \frac{\partial^2 v}{\partial y^2} + \frac{\partial^2 v}{\partial z^2}\right) \tag{2.12}$$

$$\rho\left(\frac{\partial w}{\partial t} + u\frac{\partial w}{\partial x} + v\frac{\partial w}{\partial y} + w\frac{\partial w}{\partial z}\right) = \rho g_z - \frac{\partial P}{\partial z} + \mu\left(\frac{\partial^2 w}{\partial x^2} + \frac{\partial^2 w}{\partial y^2} + \frac{\partial^2 w}{\partial z^2}\right) \tag{2.13}$$

In the system of Navier-Stokes equations (2.11, 2.12 and 2.13) the parameters involved are:

- *u*, *v* and *w* are the velocities in the Cartesian coordinates *x*, *y* and *z* respectively.
- $\overline{g} = (g_x, g_y, g_z)$ is the gravitational acceleration field.
- ρ is the density of the fluid
- *P* is the pressure

The left term of the equations is the local acceleration (variation of velocity in time) and the three next the convective acceleration (increases when the particle moves through regions of spatially varying velocities); on the right side the external forces: the weight of the particle divided by the volume, then the pressure difference and last one the diffusive acceleration terms (viscous stresses).

The dimensions and units of Navier-Stokes equations are:

$$\frac{Force}{Volume} = \frac{N}{m^3} = \frac{kg}{m^2 \cdot s^2} \tag{2.14}$$

Therefore, continuity equation (2.6) and momentum equations (2.11, 2.12 and 2.13) present four unknowns *u*, *v*, *w* and *P*. White, 2003 presents the boundary conditions for these equations.

2.1.3. Energy equation

The First Law of Thermodynamics states that heat is a form of energy that cannot be created or destroyed, but can only be transferred from one location to another or converted. Because heat transport is not treated in this project, the energy equation is not explored in this thesis. See White, 2003 for more details on the derivation technique and the terms used.

2.1.4. Shallow Water Equations

Because it is complex to define fluid motion using the three-dimensional Navier-Stokes partial differential equations, the two-dimensional Shallow Water Equations (SWE) are derived using two assumptions and boundary conditions (Vreugdenhil, 1994):

- The vertical momentum exchange is minor compared to the horizontal one, since the vertical velocity (*w*) is smaller than the two horizontals components (*u* and *v*). Parameterisation of the processes in the vertical direction is relatively easy and saves on computational effort.
- Assume hydrostatic pressure distribution.
- Kinematic and dynamic boundary conditions at the free water surface and at the solid bottom.

The assumptions and boundary conditions allow to reduce the 3D Navier-Stokes equations to a 2D system, with only the continuity equation and momentum equation in the *x* and *y* directions.

An hypothetical physical domain is depicted in Figure 2.2:

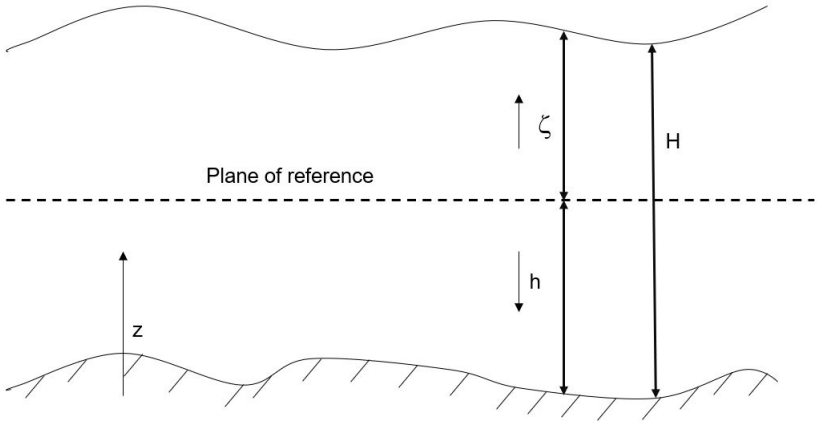

Figure 2.2: Flow with a free surface and fixed bottom. After Spee, 2010.

It is assumed a Cartesian coordinate system where *x* and *y* are the horizontal coordinates and *z* represents the vertical coordinate, oriented positive upwards. The water level is the distance between the plane of reference and the free surface, which is represented by the function ζ at specific position *(x,y)* and time *t*. The bottom part is the time-independent depth below the plane of reference, $h(x,y)$. The total water depth is defined by the function:

$$H(x,y,t) = \zeta(x,y,t) + h(x,y) \tag{2.15}$$

The depth-averaged Shallow Water Equations are defined by the continuity equation:

$$\frac{\partial \zeta}{\partial t} + \frac{\partial uH}{\partial x} + \frac{\partial vH}{\partial y} = 0 \tag{2.16}$$

and the momentum equation in *x* and *y* directions:

$$\frac{\partial u}{\partial t} + u\frac{\partial u}{\partial x} + v\frac{\partial u}{\partial y} - b_u = -g\frac{\partial \zeta}{\partial x} - S_f + \mu\left(\frac{\partial^2 u}{\partial x^2} + \frac{\partial^2 u}{\partial y^2}\right) \tag{2.17}$$

$$\frac{\partial v}{\partial t} + u\frac{\partial v}{\partial x} + v\frac{\partial v}{\partial y} + b_v = -g\frac{\partial \zeta}{\partial y} - S_f + \mu\left(\frac{\partial^2 v}{\partial x^2} + \frac{\partial^2 v}{\partial y^2}\right) \tag{2.18}$$

b represents the Coriolis forces and S_f the friction forces, based on Manning's equation:

$$S_f = \frac{n^2 V^2}{H^{4/3}} \tag{2.19}$$

where *n* is the Manning's value $[T/L^{1/3}]$ that defines the roughness of the surface.

2.1.5. 1-D Saint-Venant equation

To simplify the situation even more, it is possible to express the Shallow Water Equations (SWE) in one dimension i.e., the 1D Saint Venant Equations. The following assumptions are considered (Akan and Iyer, 2021):

- Velocity is uniformly distributed over a channel section.
- Incompressible flow.
- Diffusive terms and Coriolis forces are neglected.

For a 1D situation, it makes sense to express the equations in terms of discharge (*Q*, noting that *Q=A*u*). The continuity equation results in:

$$\frac{\partial A}{\partial t} + \frac{\partial Q}{\partial x} = q \tag{2.20}$$

where *A* is the cross-sectional flow area, *Q* is the discharge and *q* an influx term, an inflow of fluid that depends on the situation considered (precipitation, melt water, etc.).

The momentum equation is:

$$\frac{\partial Q}{\partial t} + \frac{\partial}{\partial x}\left(\frac{Q^2}{A}\right) + gA\frac{\partial H}{\partial x} - gAS_0 + gAS_f = 0 \tag{2.21}$$

S_0 is the longitudinal channel slope and S_f the friction slope, which is based on the Manning's equation.

Equations 2.20 and 2.21 can also be expressed in terms of velocity, noting that $Q = u * A$ (*u* being the velocity in x-direction):

$$\frac{\partial H}{\partial t} + \frac{\partial Hu}{\partial x} = 0 \tag{2.22}$$

$$\frac{\partial u}{\partial t} + u\frac{\partial u}{\partial x} + g\frac{\partial H}{\partial x} = g(S_0 - S_f) \tag{2.23}$$

2.2. Physical properties: fluids and sediments

The consequent literature study provides a general summary of the relevant properties in hyper-concentrated sediment flows. All flows have certain characteristics by which their physical conditions may be described. Therefore, the most useful properties for this project are introduced.

1. SEDIMENT SIZE

The properties of a single sediment particle reflect its history. For instance, sediment size (d_s) is associated to the transport medium and its velocity. Shape and roundness of a particle depend on the distance and intensity of the movement. The mineral composition indicates the possible source area and the travelled distance. From such properties, one can obtain an overview of the characteristics of the source material and source area of the processes of erosion, transport and deposition (Chien and Wan, 1999). Sediment size of the material involved influences on the amount of bed load and suspended load that the fluid transports along the area. The coarser the material is, the fluid will be less capable to carry particles over long distances and deposition of solids will take place.

2. SEDIMENT PARTICLE DENSITY

Particle density (ρ_s) is defined as the mass of a unit volume of sediment solids. Particle densities generally fall between 2.60 and 2.75 g/cm^3 for natural mineral particles (Haan et al., 1994). However, the tailings material considered in this thesis is man-made and product of the mining industry. These materials are the remaining part after the process of separating the valuable fraction from the uneconomic fraction of ore. Since it is not a natural soil, the specific gravity value mentioned before is not applicable, but from geotechnical analyses performed in samples of mine tailings and the specific gravity ranges from 3.08 to 3.2 g/cm^3 (Hu et al., 2017, Morgenstern et al., 2016). Thus, for a mixture with a specific volumetric concentration, the density of the mixture will be higher than natural soils.

3. MIXTURE DENSITY

The density of the water-sediment mixture (ρ_m in kg/m^3) is estimated with the following constitutive equation:

$$\rho_m = \rho_w + (\rho_s - \rho_w) * C_v \tag{2.24}$$

where ρ_w is the water density (1000 kg/m^3), ρ_s is the particle density (kg/m^3) and C_v is the volumetric concentration. Saturated materials are assumed for equation 2.24, so all the voids between the particles are filled with water and there is no air within the mixture (Stanford and Sánchez, 2020).

4. YIELD STRENGTH

Critical shear stress that must be exceeded before irreversible deformation and flow occurs. When the applied stress is below this threshold value, the fluid deforms elastically, with complete strain recovery after removal of the stress. When the yield stress is exceeded, the mixture behaves like a viscous liquid, with the viscosity decreasing as the shear rate increases (D. Boger et al., 2006). Yield strength is symbolised by τ_y, in N/m^2.

5. VISCOSITY

Viscosity (also known as dynamic or absolute viscosity) measures the resistance to deformation of a fluid under shear stress. Viscosity is the constant of proportionality that relates the shear stresses in a moving fluid to the strain rate (White, 2003):

$$\tau = \mu \cdot \gamma \tag{2.25}$$

where τ is the shear stress in N/m^2, μ is the viscosity in $N \cdot s/m^2$ and γ the rate of strain in s^{-1}. It is possible that the linear relationship between the shear stress and shear rate is not satisfied, therefore the viscosity can decrease or increase according to the shear rate. A further explanation can be found

in section 2.3.

As it was stated by Newton, the viscosity concept is produced when a layer of fluid moves in relation to another layer, so a higher internal friction demands a higher force to develop a greater rate of deformation. A highly viscous fluid requires more stress to achieve the same velocity gradient as a fluid with a low viscosity. As a result, viscosity is a material attribute that considers the fluid's lubricity in order for it to flow (Franco and Partal, 2010). The viscosity of a fluid can be influenced by several aspects:

- Decreasing the volumetric concentration reduces the colloidal interaction, leading to a fluid less cohesive and less viscous.
- Temperature dependency: increasing temperature results in less viscosity.
- Influence of the shape and type of material involved in the mixture.

6. VOLUMETRIC CONCENTRATION

Expressed as a percentage, it is the ratio of total volume of sediments (V_S in Mm^3) to the total volume of the mixture (water plus sediment, V_T in Mm^3).

$$C_v = \frac{V_S}{V_T} \tag{2.26}$$

The physics of flowing water and sediment is a continuum that ranges between clear water flow to mud flow. Despite multiple attempts to identify, classify and catalog different types of flow events, the distinction between fluid flow and soil mass movement is yet unclear. O'Brien et al., 1993 presented four different categories to distinguish hyper-concentrated sediment flows: water floods, mud flood, mudflows and landslides. Figure 2.3 shows a progressive transition from water floods to mud flood, mudflows and landslides as the sediment load increases and becomes coarser and Table 2.1 lists the four different categories of sediment flows and their characteristics:

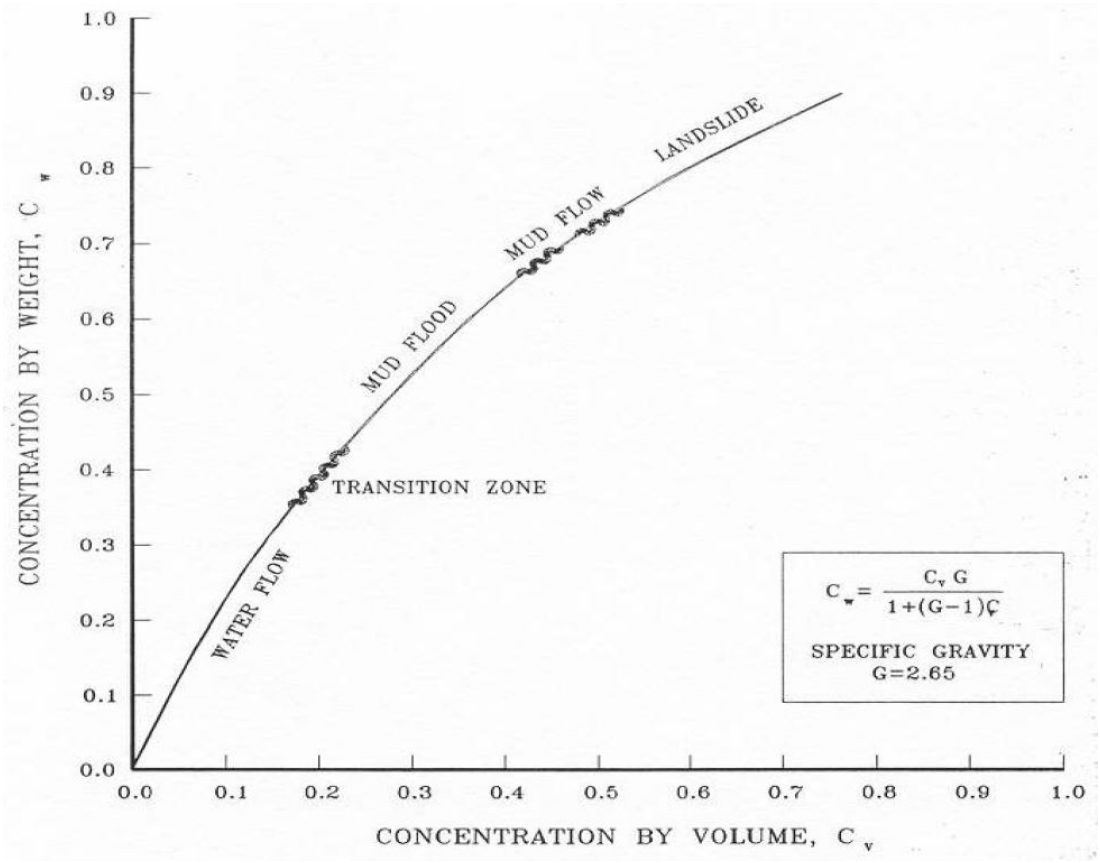

Figure 2.3: Classification of hyper-concentrated sediment flows. Source FLO-2D Software, 2019.

Table 2.1: Flow behaviour as a function of volumetric concentration (C_v). Source FLO-2D Software, 2019

TYPE OF FLOW	C_v	CHARACTERISTICS
Landslide	0.65 - 0.80	Flow will not occur; failure by rock sliding.
	0.55 - 0.65	Slow creep prior to failure; block sliding failure with internal deformation during the slide.
Mudflow	0.48 - 0.55	Flow evident; slow creep sustained mudflow; plastic deformation under its own weight; cohesive.
	0.45 - 0.48	Cohesive flow; mixing.
Mud flood	0.40 - 0.45	Flow mixes easily; shows fluid properties in deformation; spreads on horizontal surface but maintains an inclined fluid surface; waves appear but dissipate rapidly.
	0.35 - 0.40	Marked settling of gravels and cobbles; spreading nearly complete on horizontal surface; liquid surface with two fluid phases appears; waves travel on surface.
	0.30 - 0.35	Separation of water on surface; waves travel easily; most sand and gravel has settled out and moves as bedload.
	0.20 - 0.30	Distinct wave action; fluid surface; all particles resting on bed in quiescent fluid condition.
Water flood	<0.20	Water flood with conventional suspended load and bedload.

The first category are flows with a volumetric concentration less than 20% are basically water floods with high bed load (sediment that moves by saltation, rolling, or sliding in the flow layer just above the bed) and suspended load material (sediment that stays in suspension over a lengthy period of time due to turbulence). The second category are mud floods, which happen when bed load increases with high concentrations in the suspended load. Increasing the amount of sediments,leads to a range of sediment concentrations between 20 to 45% by volume for mud floods. Mud floods are difficult to distinguish from water floods because their flow behavior is similar, as seen in Table 2.1, but their fluid properties are clearly different, with substantially higher viscosity and density.

The third category describes a very viscous, hyper-concentrated sediment flow commonly known as mudflow, with sediment concentrations that range from 45 to 55% in terms of volume. Mudflows are non-homogeneous, transitory flood events in which the fluid characteristics of the water alter significantly as it flows down steep watershed channels or across alluvial fans. Mudflows are made of a fine sediment fluid matrix that can sustain boulder transport. Its behavior is a function of the parameters of the fluid matrix, channel geometry, slope, and roughness. The concentration of fine sediments in the fluid matrix influences the properties of the fluid such as viscosity, density and yield strength. The governing property of a mudflow is the high viscosity (see section 2.3.1), which causes it to move slowly, far slower than water floods on the same slope (FLO-2D Software, 2019). Lastly, a landslide is defined as the movement of a mass of rock or earth down a slope, therefore flow will not occur. Landslides occurs when forces acting down-slope (mostly gravity) exceed the strength of the earth materials that composed that same slope (Highland, Bobrowsky, et al., 2008).

2.3. Rheology

Rheology is the study of how materials deform under stress. Most materials can resist shear stress for short periods but eventually deform and exhibit fluid behaviour over time (Krishnan et al., 2010). The most important rheological properties that define the motion of non-Newtonian fluids are the yield strength and the viscosity.

2.3.1. Types of fluids

Two different types of fluids are distinguished: Newtonian and non-Newtonian.

1. NEWTONIAN FLUIDS

In simple shear and at constant temperature and pressure, the Newtonian fluid exhibits a linear relationship between the applied shear stress (τ) and the rate of shear (γ) with viscosity (μ) as the constant of proportionality. Since the shear stress is directly proportional to the rate of shear, plotting these two variables results in a straight line passing through the origin and the slope is the value of the viscosity. Examples of Newtonian fluids would be water, alcohol or gasoline (White, 2003, Krishnan et al., 2010).

$$\tau = \mu \cdot \gamma \tag{2.27}$$

where τ is the shear stress in N/m^2, μ is the viscosity in $N \cdot s/m^2$ and γ the shear rate in s^{-1}.

2. NON-NEWTONIAN FLUIDS

At very high solid concentrations, fluid behaviour begins to deviate from the linear relationship between shear stress and shear rate. It has been proved that many fluids do not follow the *Newton's law of viscosity*. These are called non-Newtonian fluids. In order to visualise the behaviour of non-Newtonian fluids, rheograms display graphical representations of the rheological characteristics, a graph of rate of shear (γ) versus shear stress (τ).

There are three ways to characterise the behaviour of non-Newtonian fluids (Krishnan et al., 2010):

- *Visco-elastic behaviour:* system that experiences a mix of viscous fluid-like behaviour and of elastic solid-like behaviour. For tension in an ideal elastic solid, stress in a sheared state is directly proportional to strain and the constant of proportionality is the Young's modulus (Hooke's law).

- *Time-dependent behaviour:* the relation between shear stress and strain shows further dependence on the duration of shearing. For instance: thixotropic behaviour (material is sheared at constant shear rate and the viscosity decreases with he duration of shearing); or rheopectic behaviour (viscosity or the shear stress values increase with time of shearing) (Figure 2.4).

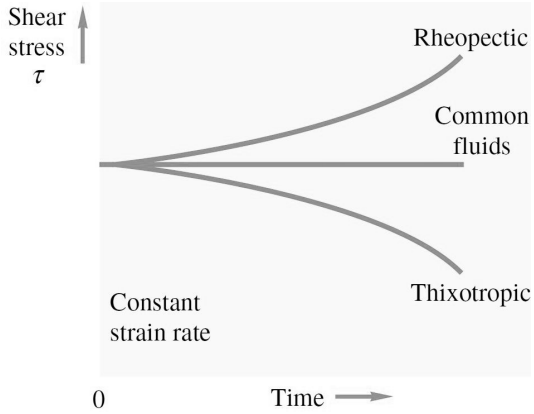

Figure 2.4: Rheological behaviour of time-dependent fluids. Source: White, 2003.

- *Time-independent behaviour:* system for which the value of strain at a specific point within the fluid is determined only by the shear stress value at that same point, or vice versa. Also known as purely viscous or inelastic fluids, there exist two types:

  1. Shear-thinning or pseudoplastic behaviour: viscosity decreases with increasing shear rate.
  2. Shear-thickening or dilatant behaviour: viscosity increases with increasing shear rate.

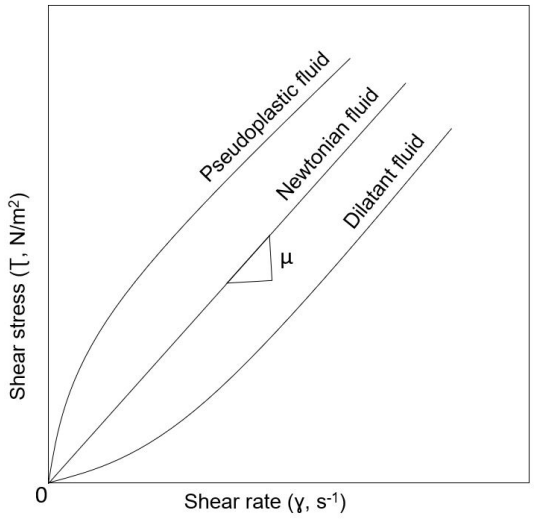

Figure 2.5: Rheological behaviour of time-independent fluids. After: Alderman, 1997.

Furthermore, non-Newtonian fluids can also be characterised by the existence of a threshold stress (yield stress, τ_y) which must be exceeded for the fluid to deform or flow. The yield stress value or yield strength of the fluid has been described in section 2.2. The following non-Newtonian fluids exhibit a time-independent behaviour and can be classified as:

- Shear-thinning or yield-pseudoplastic behaviour: viscosity decreases with increasing shear rate.
- Shear-thickening or yield-dilatant behaviour: viscosity increases with increasing shear rate.
- Visco-plastic or Bingham plastic behaviour: There is a linear relation between the shear stress and the rate of shear after achieving a non-zero stress value (yield strength) to commence significant flow.

The following rheogram illustrates the effect of yield strength and viscosity on the behaviour of a fluid.

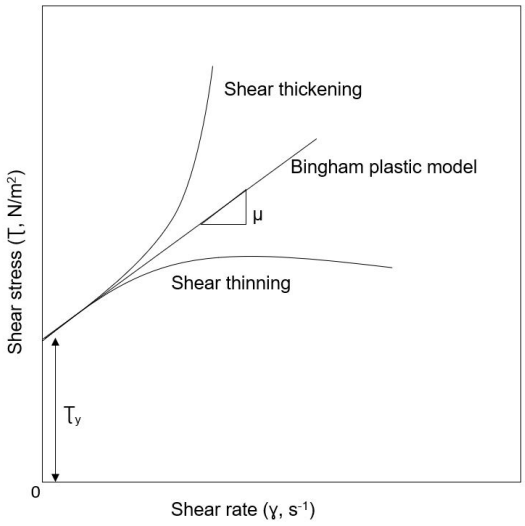

Figure 2.6: Rheological behaviour of time-independent fluids with yield strength. After: Elger et al., 2020.

2.3.2. Rheological models

A variety of rheological models are available to describe flow behaviour of the aforementioned non-Newtonian fluids (D. V. Boger, 2013, Alderman, 1997 and Krishnan et al., 2010). Only the time-independent fluids are considered in this section, since the time-dependent and visco-elastic behaviours are out of the scope of this project.

1. OSTWALD-DE WAELE POWER LAW MODEL

This is a two parameter model described by:

$$\tau = k\gamma^N \tag{2.28}$$

where τ is the shear stress, γ is the shear rate, k the consistency index ($N \cdot s^n/m^2$) and N the flow index (dimensionless). This model applies to:

- Pseudo-plastic behaviour: decreasing the viscosity makes the fluid thinner. The flow index (N) must range from 0 to 1.
- Dilatant behaviour: the increasing viscosity results in a thicker fluid. In this case, the flow index (N) must be higher than 1.

2. BINGHAM PLASTIC MODEL

This is a two parameter model to describe visco-plastic fluids:

$$\tau = \tau_y + \mu\gamma \tag{2.29}$$

where τ_y is the yield strength and μ is the viscosity ($N \cdot s/m^2$).

3. HERSCHEL-BULKLEY MODEL

The strain experienced by the fluid is related to the stress in a non-linear way (Saasen and Ytrehus, 2019). The constitutive equation is written as:

$$\tau = \tau_y + k(\gamma)^N \tag{2.30}$$

Where τ_y is the yield strength, γ is the shear rate, k is the consistency index ($N \cdot s^n/m^2$) and N is the flow index (dimensionless). The consistency factor depends on the curvature exponent, while N defines the degree of viscosity of the fluid.

- Yield-pseudoplastic behaviour: shear-thinning behaviour. The flow index (N) must be lower than 1.
- Yield-dilatant behaviour: shear-thickening behaviour. The flow index (N) must be higher than 1.

4. O'BRIEN MODEL

This is a quadratic rheological model that describes the rheology of hyper-concentrated sediment flows. The resulting quadratic formulation of the final shear stress includes cohesion between particles, viscosity of the fluid, collision between particles and turbulence (Julien and Lan, 1991). The model separates the stress-strain relationship in four different terms:

$$\tau = \tau_y + \tau_v + \tau_t + \tau_d \tag{2.31}$$

where:

- τ_y: yield strength of the fluid (N/m^2).
- τ_v: viscous shear stress of the fluid (N/m^2). It relates the friction between sediment particles and fluid.
- τ_t: turbulent shear stress of the fluid (N/m^2). Term that accounts for turbulence within the fluid.
- τ_d: dispersive shear stress of the fluid (N/m^2). Describes the interaction between sediment particles within the mixture.

It is a model proposed to analyse fluids with dilatant behaviour, considering or not yield strength. The approach is similar to the Herschel-Bulkley model when the flow index (N) is higher than 1. A further explanation of the model is introduced in section 3.4.

3

Tailings storage facilities

Tailings storage facilities are geotechnical structures made of waste material, product of many years of mining activities. Tailings dams usually increase in height with time and the storage area hold large volumes of fine-grained material. Section 3.1 introduces the existing types of tailings storage facilities, followed by section 3.2 which describes the historical failure of the mining storage facility (dam B-I) near Brumadinho. Section 3.3 explains the geotechnical properties of the materials stored in the reservoir. Then, section 3.4 and 3.5 analyse in more detail the rheological model used and a sensitivity analysis of each term is done in the consequent section 3.6.

3.1. Types of tailings dams

The construction process of a mine tailing dam begins with the construction of a starter dam, which is usually only a few meters high. Once the initial volume is filled, the starter dam is raised. There are three different ways for raising a tailings dam (Berghe et al., 2011):

1. Upstream method: by constructing a new dam on the tailings material that has already consolidated. Part of the new dam will be placed on top of the first one and the remaining part on top of the waste, moving the crest further upstream. The same procedure can be done multiple times, creating an upstream dam with 3 or more different sub-dams, which are situated on top of each other. The height and volume of the structure will increase every time, making it unstable, since part of the dam is resting on weaker materials from mining activities (Dutch Risk Reduction Team, 2019).
2. Downstream method: once the volume behind the starter dam is as its maximum, the next dam is placed on top of the previous one but the extra support needed is placed in front of the started dyke, thus raising the crest further downstream. This method requires more material and available space for the upcoming new dams.
3. Centreline method: imported material is placed on top of the existing dam to raise the structure's height. This technique is an intermediate approach between the upstream and downstream methods.

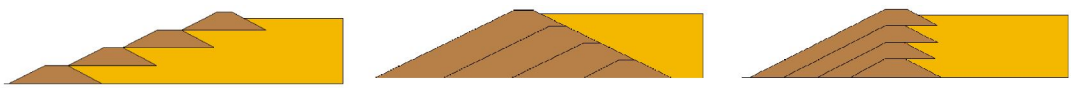

Figure 3.1: Types of methods for raising tailing dams. From left to right: upstream, downstream and centreline. Source: Berghe et al., 2011.

Of the three construction methods, tailing dams constructed by the upstream technique are potentially the most unstable structures. If the groundwater pressure increases, seepage or liquefaction might happen, resulting in collapse of the dam, allowing the material to flow out.

3.2. Example of a past event

Tailing storage facilities are one of the largest man-made and technically challenging structures in geotechnical practice (Davies, 2002). Worldwide, failure of tailing storage facilities occur at relatively high rates; Wallingford, 2019 estimated that the failure rate over the last 100 years for a world inventory of 18.401 mine sites is 1.2% - higher than the failure rate for conventional water dams, 0.01%. Failure of mine tailing dams involves irreversible damages to ecosystems and large economic impact to society, where the impact is defined by the quantity of volume released and its toxicity.

3.2.1. Feijão dam B-I

On the 25th January 2019, the tailings dam B-I suffered a catastrophic failure, at the Córrego do Feijão iron ore mine, 9 kilometres east of Brumadinho city, in the state of Minas Gerais, Brazil. The mine was owned by Vale S.A. and in 2018 it produced 8.5 million tons of iron ore. Dam B-I was constructed using the upstream method in 15 stages between 1976 and 2013. The dam had a height of 86 meters and a crest length of 720 meters, with an impoundment volume of 12,7 Mm^3, (Robertson et al., 2019).

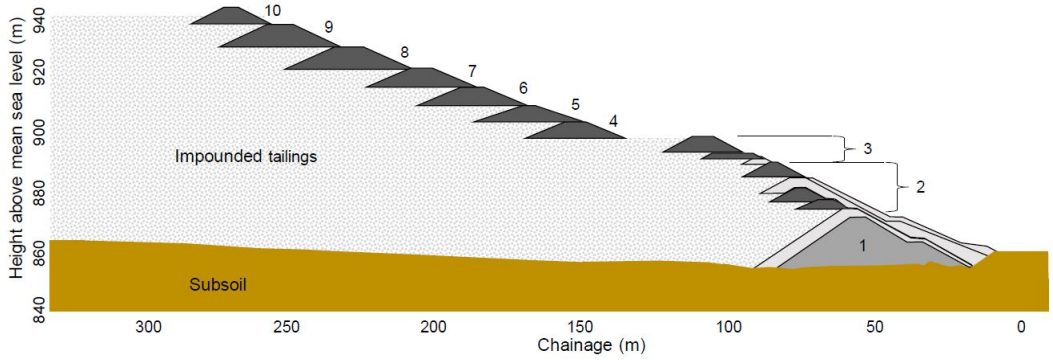

Figure 3.2: Cross-section of dam B-I. Source: Robertson et al., 2019

At 12.28 (local time) the tailings dam collapsed and released $9.7\ Mm^3$ of material (water plus tailings), approximately 75% of the total volume. The cameras recorded the rapid movements of the mudflow, which traveled through the mine's canteen and offices, also houses, farms and roads downstream and finally, after 2 hours, it reached the Paraopeba river 10 km downstream. Over 248 people died, 2.8$ billion worth of property were lost or damaged and it supposed an environmental disaster (Raman and Liu, 2019a).

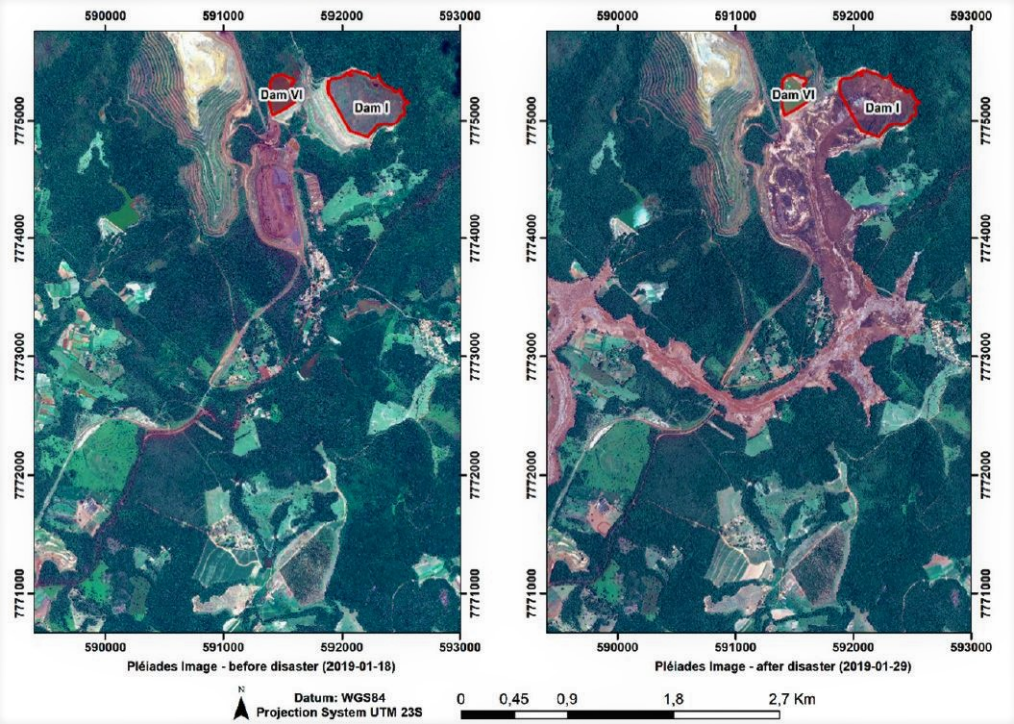

Figure 3.3: Satellite images taken before and after the collapse. Source: F Gama et al., 2020

An expert panel of geotechnical engineers was assembled to review and assess relevant data to determine the causes of failure. According to Robertson et al., 2019 and available monitoring videos on-site, the slope failure started from the dam crest and spread around the area around the last raising. A mud wave of 30 m height was released and the entire slope collapse happened in less than 10 s, where 75% of the impounded volume flowed out in less than 5 min. Flow liquefaction is the main reason of dam B-I failure and it was caused by six different reasons: a design with a steep slope, large volumes of water near the crest, lack of internal drainage within the reservoir, high iron content in the material, intense season rainfall and the upper portions of the slope over weaker fine tailings.

3.3. Mine tailings properties

Mine tailings are the by-product from the mining industry, a mixture of crushed rock and processing fluids that remain after the extraction of ore materials (Kossoff et al., 2014). Mine tailings are commonly stored and pumped into a sedimentation pond. Over the last few decades, the amount of tailings produced has expanded considerably due to advancements in mining technologies and growing demand for minerals and metals. Because tailings can contain toxic substances, heavy metals, and chemicals added during mineral processing, tailings often generate serious environmental and ecological problems. Furthermore, mine tailings are used for the construction of tailings dams, therefore the physical-mechanical properties of mine tailings have a great impact on the safety of those dams (Du et al., 2018).

The mine tailings are distinguished between coarse particles at the bottom of the reservoir and fine tailings suspended in the free water in the upper part (Du et al., 2018). Coarse and fine mine tailings are used to construct upstream dams, but the tailings particles located at the starter dyke may be subjected to high values of normal and shear stresses as the embankments are gradually raised. The coarse particles experience crushing and collision between them and fine particles are generated, which results in changes in the mechanical properties of tailings. A large amount of fines lead to a reduction of permeability, which cause an excess of pore pressure and a potential risk of liquefaction (Bhanbhro et al., 2021).

To characterise the mechanical properties of mine tailings, values regarding the basic geotechnical properties for iron mine tailings are summarised in Table 3.1:

Table 3.1: Geotechnical properties of coarse and fine iron mine tailings.

	Source: Du et al., 2018		Source: Hu et al., 2017	
PROPERTIES	**COARSE TAILINGS**	**FINE TAILINGS**	**COARSE TAILINGS**	**FINE TAILINGS**
Specific gravity (-)	3.127	3.183	3.230	3.080
Natural water content (%)	-	15.66	43 - 54	43
D_{10} (mm)	0.013	0.012	0.051	0.005
D_{30} (mm)	0.040	0.020	0.093	0.012
D_{50} (mm)	0.088	0.038	0.120	0.030
D_{60} (mm)	0.107	0.049	0.160	0.045
Coefficient of uniformity	8.230	4.080	3.110	8.820
Coefficient of curvature	1.150	0.680	1.050	0.590
Initial void ratio, e	0.880	1.110	0.740	1.410

3.4. Rheological model for tailings material

In Section 2.3.2, four rheological models were presented to usually analyse the flow behaviour of non-Newtonian fluids. The material involved in a tailing dam failure is a hyper-concentrated sediment fluid (O'Brien et al., 1993), therefore, the rheological model used in this project is the one proposed by O'Brien and Julien, 1985: the O'Brien quadratic model.

From the four models, the quadratic model is the most complex. Unlike the Bingham plastic model or Herschel-Bulkley, the O'Brien model accounts for turbulent and dispersive behaviour. It decomposes the stress-strain relationship into four different components (already introduced in section 2.3.2), so the resulting equation is:

$$\tau = \tau_y + \tau_v + \tau_t + \tau_d \tag{3.1}$$

where τ_y is the yield strength, τ_v is the viscous shear stress, τ_t is the turbulent shear stress and τ_d is the dispersive shear stress. The total shear stress is defined as the force needed to start deformation (τ in N/m^2). The rate of shear (γ in s^{-1}) in the O'Brien quadratic model is defined as the vertical integration over of the velocity profile (Iverson, 1997), which leads to:

$$\gamma = \frac{3\overline{u}}{H} \tag{3.2}$$

where $\overline{u}$ is the depth-averaged velocity and H the flow depth.

The following sections will elaborate on each term of equation 3.1 and how it contributes to the shear stress.

3.4.1. Yield strength

The yield strength property is an intrinsic value of the fluid, since it depends on the number of bonds between particles. Thus, the more particles there are, a higher shear stress is needed to start the flow. Although it is a complex property to quantify, when solid particles are small enough to sample and the fluid can be reconstituted, laboratory techniques such as tilt tests or vane tests can estimate a value for the yield strength. However, it is challenging for samples of debris flows. Therefore, O'Brien and Julien, 1988 derived an empirical relation to estimate the yield strength:

$$\tau_y = \alpha_1 e^{\beta_1 C_v} \tag{3.3}$$

This approach converts two empirical parameters (α_1 and β_1) into an exponential function of the volumetric concentration. O'Brien carried out laboratory analysis of mudflow samples, from natural mudflows deposits in the Colorado Rocky Mountains (USA) (O'Brien and Julien, 1988). The values of the two empirical parameters were obtained by regression analysis for each sample (FLO-2D Software, 2019) and in the absence of tailings laboratory data, O'Brien suggests to use $\alpha_1 = 0.00172$ and $\beta_1 = 29.5$ to obtain a moderate yield stress.

The yield strength for mine tailings ranges between 30 to 100 Pa (D. Boger et al., 2006). However, it is just an approximation, since it has a high dependency on the volumetric concentration.

3.4.2. Viscous stress

The newtonian part of the equation defines the internal friction between fluid and sediment particles. From equation 2.25 it can be seen that only the viscosity value is required to obtain a relationship between stress and strain. The viscosity is calculated using an exponential relation based on the volumetric concentration and two empirical parameters (α_2 and β_2):

$$\mu = \alpha_2 e^{\beta_2 C_v} \tag{3.4}$$

According to O'Brien's experimental research on mudflows samples, the viscosity for a material which behaves like mine tailings (high viscosity with high sediment concentration), the empirical coefficients are $\alpha_2 = 0.000602$ and $\beta_2 = 33.1$.

3.4.3. Turbulent stress

As the sediment concentration increases in hyper-concentrated sediment flows, turbulence affects the physics of the flow behaviour. Before defining the turbulent stress term and formula, a brief introduction of laminar and turbulent flow is given.

Laminar flow is characterised by adjacent fluid layers moving smoothly with respect to each other with little or no mixing (Elger et al., 2020). Laminar flow occurs at relatively low and constant velocities (depth-averaged velocities, u and v) and a parabolic distribution function represents the velocity field, with high velocity values near the free surface. With the classical experiment of Reynolds, the transition between laminar to turbulent flow is explained. The experiment states that when velocity exceeds a certain limit value, part of the flow loses its stability and eddies are created (swirls and the corresponding current) which make the trajectory of each fluid and sediment particle chaotic, thus the motion varies randomly in time and space (Chien and Wan, 1999). Turbulent flow is associated with non-uniform and high velocity profiles.

The Reynolds number (Re, dimensionless) is the ratio between inertial and viscous forces and it is used to define the flow regime:

$$Re = \frac{\rho V L}{\mu} \tag{3.5}$$

where V and L are the velocity and length scales of the flow, ρ the fluid density and μ the viscosity.

Viscosity acts as a dissipative mechanism that mitigates perturbations, but its effects minimise as the Reynolds number increases. Thus, the tendency to instability increases together with the Reynolds number. For low values of the Reynolds number the flow is considered laminar, but once the Reynolds number exceeds a critical value (~ 2000) the flow becomes turbulent (Mathieu and Scott, 2000).

An important effect of turbulence is the transport of properties like heat, momentum or suspended matter across planes parallel to the mean flow direction by the random motions of fluid movement. As it was mentioned before, for laminar flows the depth-averaged velocities components (u and v) do not

vary at any point in space and time. Turbulence creates eddies which generate fluctuations in velocity, thus for turbulent flows the velocity field is expressed as:

$$\overline{u} = u + u' \tag{3.6}$$

$$\overline{v} = v + v' \tag{3.7}$$

where u and v are the same as for laminar flows and u' and v' are the instantaneous fluctuating velocities (turbulent component). Those turbulent velocities are represented in Figure 3.4: the particle will not follow a linear path parallel to the flow direction, since it will deviate from its original path. The velocity of the new trajectory is defined by equations 3.6 and 3.7:

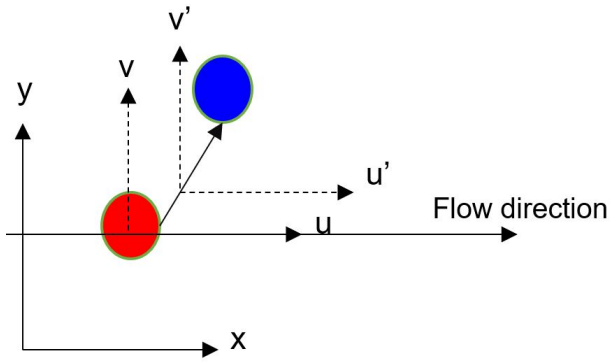

Figure 3.4: Sketch of the development of the instantaneous fluctuating velocities.

For turbulent flows, apart from the viscosity shear stress, there is the turbulent shear stress acting as an additional diffusion mechanism for transport of fluid momentum. This means that both stresses act to minimise the turbulence within the flow. The turbulent shear stress (τ_t, also known as Reynolds stress) is an exchange (vertical movements) of macroscopic eddies within the fluid that tends to even out the velocity distribution by diffusion of momentum (Southard, 2000). Reynolds defined the turbulent shear stress as:

$$\tau_t = \rho\overline{u'v'} \tag{3.8}$$

The parameters u' and v' are complex to quantify (thus the average value $\overline{u'}$, $\overline{v'}$), therefore L. Prandtl simulated momentum exchange on a macro-scale to explain the mixing phenomenon induced by turbulence. An eddy with certain initial properties (heat, concentration or momentum) is considered; that same eddy travels a distance l_m perpendicular to the flow direction and it reaches the terminal point (Figure 3.5). As the eddy was moving, its properties changed, losing the initial ones and gaining those of the new location. The Prandtl mixing length (l_m) for turbulent flow is a length that describes turbulence interchanges at any plane (Chien and Wan, 1999). u' and v' are related to each other and also are the same order of magnitude, thus:

$$u' \sim v' = l_m \frac{du}{dy} \tag{3.9}$$

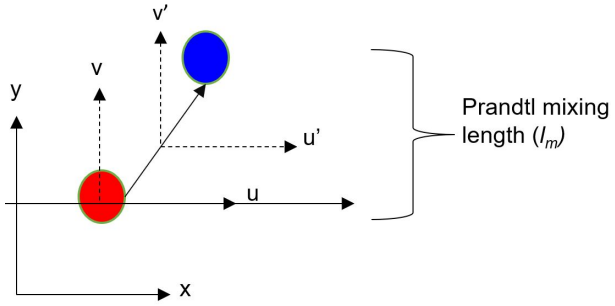

Figure 3.5: Sketch of the Prandtl mixing length concept.

The mean (depth averaged) value of the Prandtl mixing length is usually calculated as a function of the total flow depth and the von Kármán constant ($k' \sim 0.4$):

$$l_m = k' * H = 0.4 * H \tag{3.10}$$

Using equation 3.9 in equation 3.8 the turbulent shear stress results in:

$$\tau_t = \rho_m l_m^2 \gamma^2 \tag{3.11}$$

3.4.4. Dispersive stress

The dispersive stress accounts for the collision between sediment particles within the fluid. Relative movement occurs between particles and fluid, thus a resulting force exists perpendicular to the flow which depends on the volumetric concentration and the regime of the fluid. Bed load particles start to move at a certain speed, collisions between particles are generated which depend on the sediment concentration; the resulting momentum exchange occurs during collision which results in a force (Shook and Roco, 2015, Chien and Wan, 1999). Its component in the flow direction is the dispersive shear stress (τ_d) and in the vertical direction, the dispersive force (P_d).

Bagnold, 1954 formulated the dispersive shear stress and dispersive force as a function of the volumetric concentration, average sediment size and density:

$$\tau_d = a_i \rho_s (\lambda d_s \gamma)^2 \tag{3.12}$$

where a_i is an empirical coefficient (~ 0.01), ρ_s the density of sediments, λ is the linear volumetric concentration and d_s the average sediment size.

The linear volumetric concentration (λ, dimensionless) is:

$$\lambda = \left[\left(\frac{C*}{C_v} \right)^{1/3} - 1 \right]^{-1} \tag{3.13}$$

where $C*$ is the maximum possible volumetric concentration for spheres (~ 0.615) and C_v is the current volumetric concentration.

Hence, the dispersive shear stress is:

$$\tau_d = 0.01 \rho_s \left(\left(\frac{0.615}{C_v} \right)^{1/3} - 1 \right)^{-2} d_s^2 \gamma^2 \tag{3.14}$$

Further explanation regarding Bagnold's studies are available in Bagnold, 1954, Bagnold, 1956 and Hanes and Bowen, 1985.

3.5. Analysis of rheological model

In this section, each term of the O'Brien model is examined in terms to its contribution to the shear stress.

1. YIELD STRENGTH

Recalling equation 3.3, the yield strength depends on two empirical parameters (α_1 and β_1) and the volumetric concentration (C_v). Because α_1 and β_1 are fixed values, the only variable in the equation is C_v, thus it is obvious that a higher sediment concentration will lead to larger yield strength values. Looking back at section 3.4, the yield strength is a threshold value that needs to be achieved to start deformation or flow: therefore large shear stress is required to start movement. Figure 3.6 displays the relationship between yield strength values according to C_v, which ranges from concentrations below 20% (mud flood characteristics) to 70% (landslide characteristics). The yield strength increases exponentially according to C_v, with $\tau_y = 0.0628\ N/m^2$ for $C_v = 20\%$ to $\tau_y = 8366\ N/m^2$ for $C_v = 60\%$

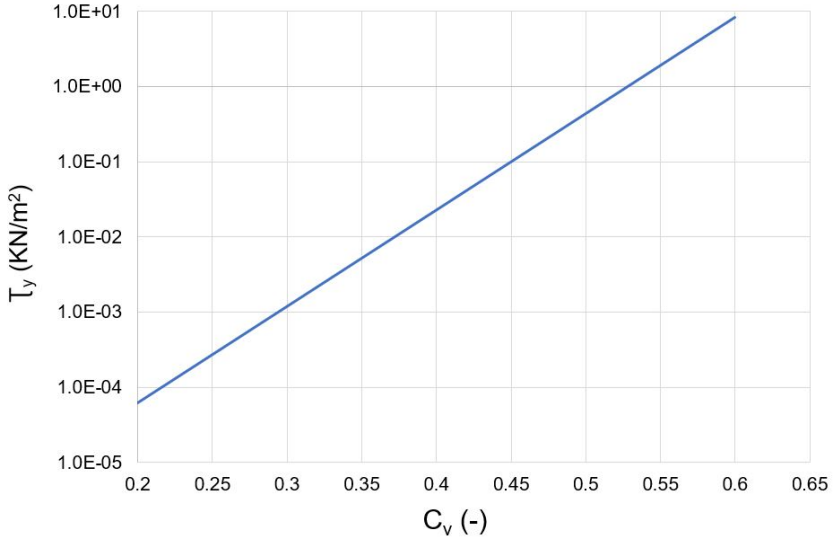

Figure 3.6: C_v versus τ_y.

2. VISCOUS SHEAR STRESS

The viscosity shear stress term provides the Newtonian behaviour to the fluid. Equation 3.4 presented the formula suggested by O'Brien et al., 1993, where the two empirical parameters derived by (α_2 and β_2) are constant, leaving only one variable: volumetric concentration (equation 3.4). Increasing C_v will make the viscosity rise exponentially (Figure 3.7):

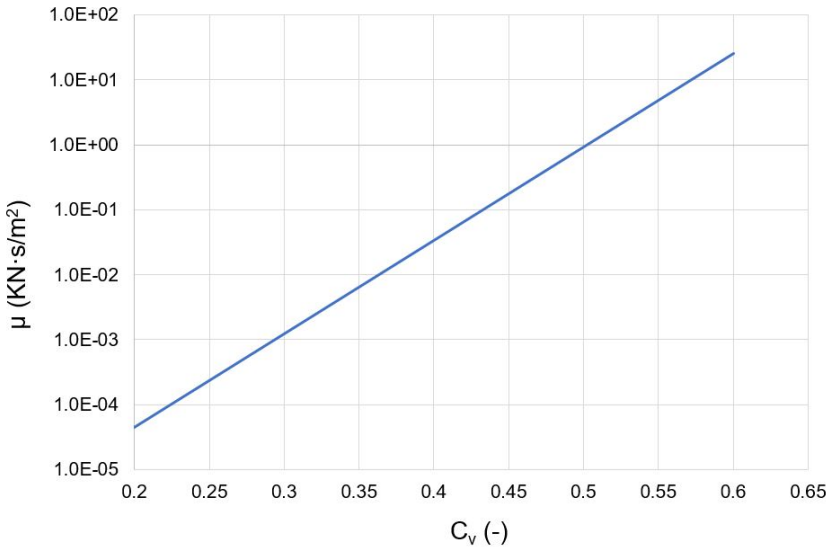

Figure 3.7: C_v versus μ.

Since high C_v values lead to more viscous fluids, larger shear stresses are needed to start flow movement. High viscosity values will also attenuate turbulence within the fluid, because viscosity is a mitigation mechanism of perturbations. In section 3.4.3, the Reynolds number was defined as a prediction of flow behaviour (laminar or turbulent) and from Reynolds equation 3.5, high C_v values of viscosity results in small Reynolds numbers, thus less turbulence.

3. TURBULENT SHEAR STRESS

The turbulent shear stress is:

$$\tau_t = \rho_m l_m^2 \gamma^2 \tag{3.15}$$

where C_v is considered in the density of the mixture formula:

$$\rho_m = \rho_w + (\rho_s - \rho_w) * C_v \tag{3.16}$$

with $\rho_w = 1000\ kg/m^3$ and $\rho_s = 3155\ kg/m^3$ (average of values from Table 3.1). More sediment particles in the fluid, increase the C_v, which leads to a linear increment of the density of the mixture (ρ_m) (Figure 3.8):

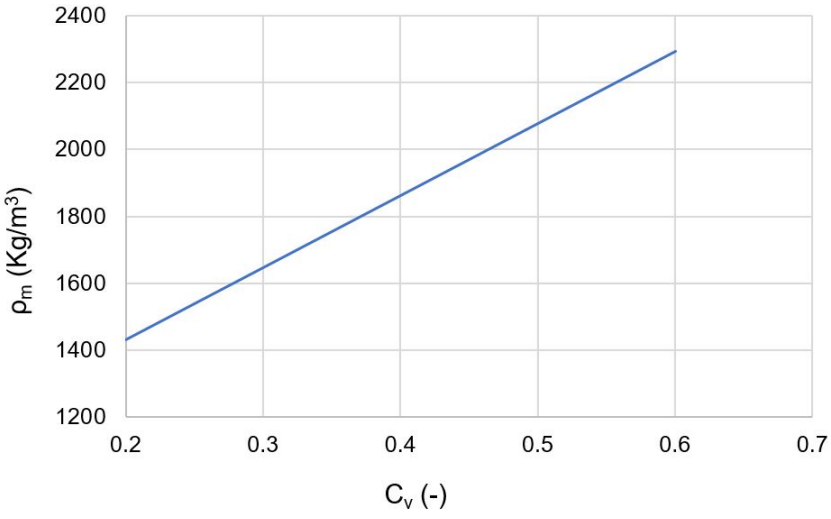

Figure 3.8: C_v versus ρ_m.

The turbulent shear stress also depends on the Prandtl mixing length (l_m), which has been described in section 3.4.3. Recalling its formula (equation 3.10), it depends on the von Kármán constant ($k' \sim 0.4$) and the total flow depth (H). The physics behind the Prandtl mixing length formula can be reflected in the turbulent shear stress. Transport of momentum over large distances by turbulent structures lead to an increase in stresses (see Figure 3.9):

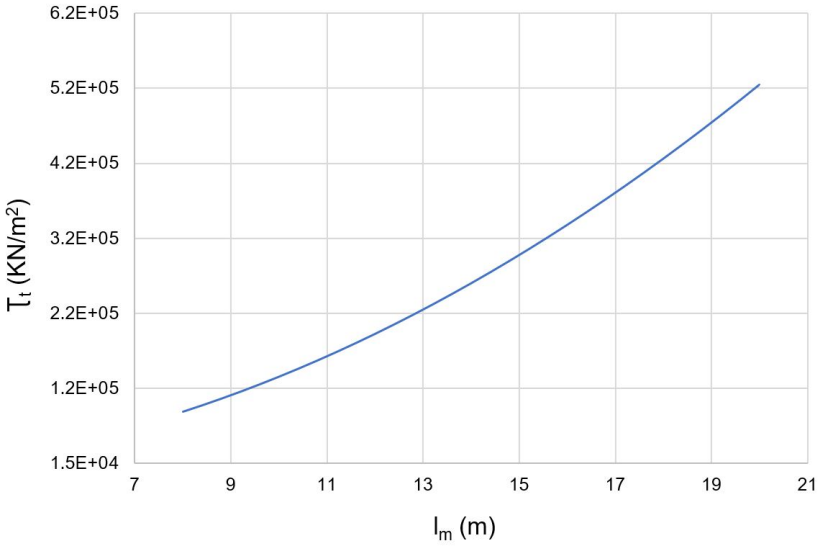

Figure 3.9: l_m versus τ_t

Figure 3.9 illustrates the influence on the Prandtl mixing length to the resulting turbulent shear stress; the other parameters in equation 3.15 have been fixed. O'Brien and Julien, 1988 states that typical shear rates for hyper-concentrated sediment flows range between 5 to 50 s^{-1}. Thus, the constants for equation 3.15 are: shear rate $\gamma = 25s^{-1}$ and $\rho_m = 2077.5kg/m^3$ (with $C_v = 50\%$ in equation 3.16).

4. DISPERSIVE SHEAR STRESS

Dispersive shear stress is present when there is significant interaction between sediment particles. Thus, it is logical to expect that the governing value in the dispersive term is the volumetric concentration (C_v). The dispersive shear stress is defined as:

$$\tau_d = a_i \rho_s (\lambda d_s \gamma)^2 = 0.01 \rho_s \left(\left(\frac{0.615}{C_v} \right)^{1/3} - 1 \right)^{-2} d_s^2 \gamma^2 \tag{3.17}$$

where a_i is an empirical coefficient (~ 0.01), ρ_s the density of sediments, λ is the linear volumetric concentration, d_s the average sediment size and γ is the shear rate (s^{-1}).

Figure 3.10 displays volumetric concentration (C_v) versus linear concentration (λ^{-2}) as it is stated in formula 3.13. It can be appreciated that for low-medium values of C_v ($20\% \sim 50\%$), λ^{-2} slightly varies, but as soon as C_v exceeds 50%, λ^{-2} raises exponentially, larger than three orders of magnitude when going from $C_v = 50\%$ to 60%. All the other input values of equation 3.17 are constant, to avoid any influence on the result, hence: $\gamma = 25\ s^{-1}$, $\rho_s = 3155\ kg/m^3$ (average value from all samples of Table 3.1) and $d_s = 0.000069\ m$ (average D_i from all samples of Table 3.1).

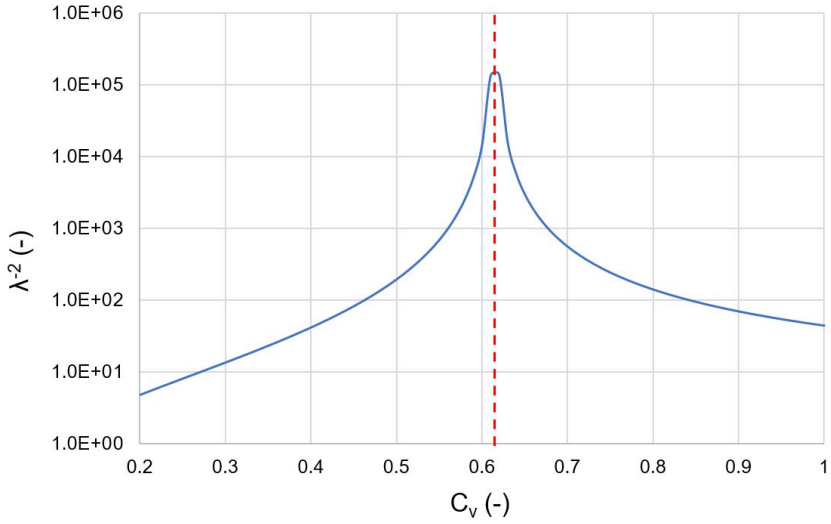

Figure 3.10: C_v versus λ^{-2}

It can be concluded from the graph that more sediment particles within the fluid will increase the value of λ^{-2}, thus the turbulent shear stress - due to more interaction and collision between particles.

Furthermore, if the volumetric concentration increases and surpasses the maximum possible volumetric concentration (C^*), λ^{-2} will decrease together with the turbulent shear stress(τ_d). One could expect that λ^{-2} and τ_d would increase with C_v, but once the ratio C^*/C_v is less than unity, λ^{-2} reduces (red line in Figure 3.10). The fluid will start behaving like a solid, therefore less interaction between particles due to the low amount of water within the mixture. It can be confirmed with Table 2.1, where for $C_v \sim 60\%$ the flow behaviour is no longer related with mudflows and it is associated with landslides, where there is no flow.

In conclusion, the effect of the volumetric concentration in the dispersive shear stress is remarkable when C_v is higher than 50% (see Figure 3.11).

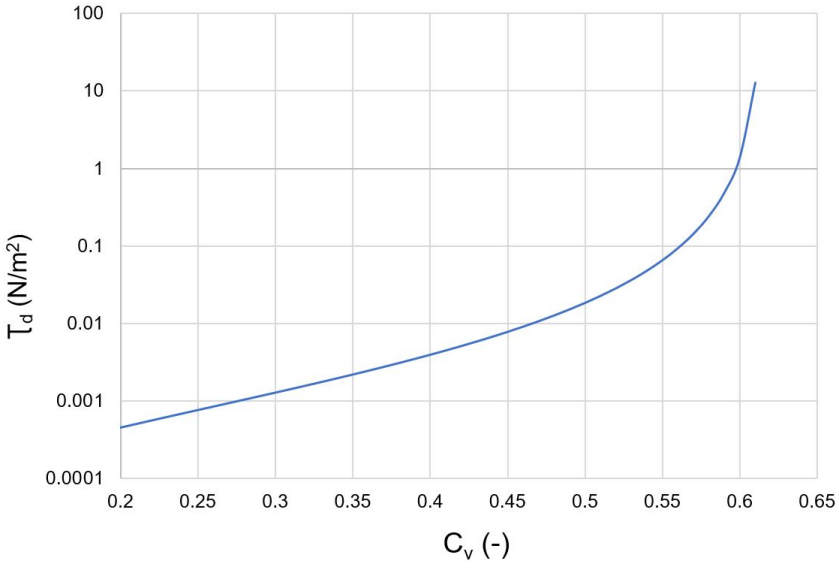

Figure 3.11: C_v versus τ_d

Another parameter in the dispersive term is the density of sediments (ρ_s). From laboratory tests from literature, it ranges between $3080 \sim 3230 kg/m^3$. Keeping constant $\gamma = 25 s^{-1}$, $C_v = 50\%$ and $d_s = 0.000069\ m$, the impact of the density of sediments in the turbulent shear stress is:

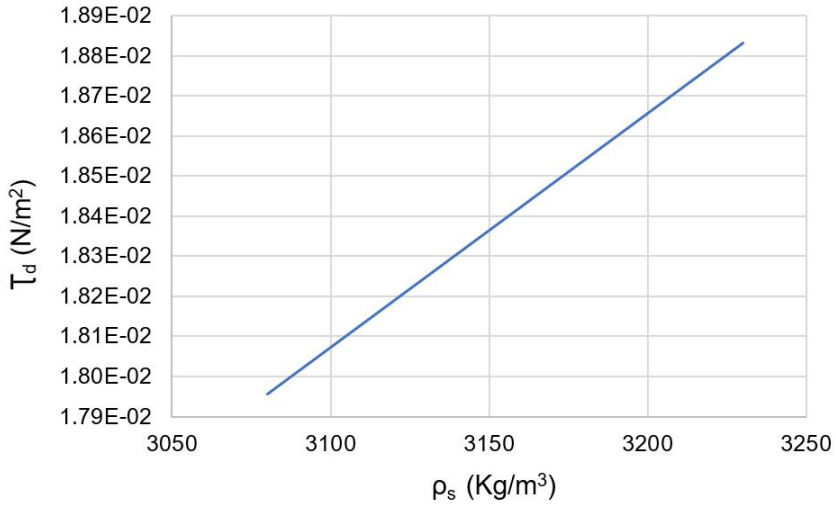

Figure 3.12: ρ_s versus τ_d

The last input parameter in the dispersive shear term is the average sediment size. From the results of the laboratory tests presented in Table 3.1, the values considered range between the average of all D_{10} to the average value of all D_{60}. The impact of the sediment size is represented in Figure 3.13, where $\gamma = 25\ s^{-1}$, $C_v = 50\%$ and $\rho_s = 3155\ kg/m^3$ are constant:

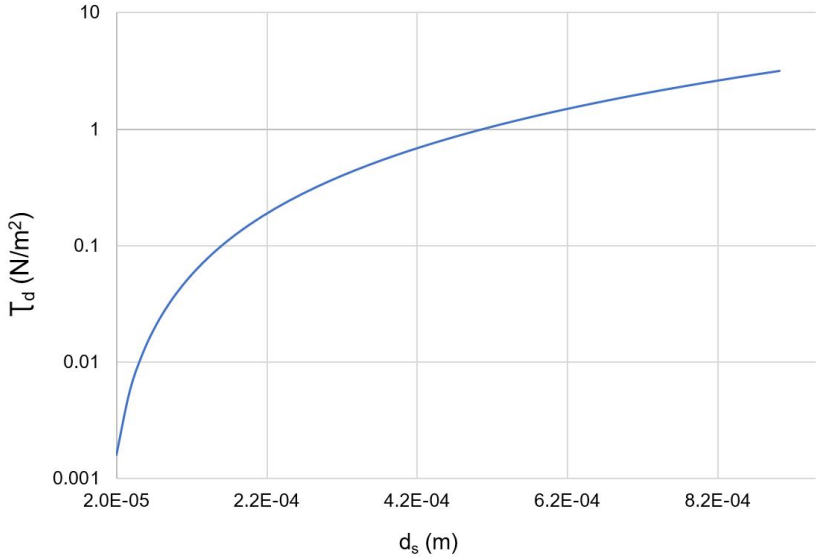

Figure 3.13: d_s versus τ_d

3.6. Sensitivity analysis

In this section, a sensitivity analysis is carried out to see which input parameter has the largest impact on the final computed shear stress. The simplified formula of O'Brien quadratic model is:

$$\tau = \tau_y + \tau_v + \tau_t + \tau_d \tag{3.18}$$

and the extended version of it is as follows (see equation 3.19):

$$\tau = (\alpha_1 e^{\beta_1 C_v}) + (\alpha_2 e^{\beta_2 C_v})\gamma + \left((\rho_w + (\rho_s - \rho_w) \cdot C_v) l_m^2\right)\gamma^2 + \left(0.01\rho_s \left(\left(\frac{0.615}{C_v}\right)^{1/3} - 1\right)^{-2} d_s^2\right)\gamma^2 \tag{3.19}$$

Firstly, one of the easiest ways to analyse the sensitivity of each parameter in the outcome is to plot all the variables in a tornado chart. For $\gamma = 25\ s^{-1}$, Figure 3.14 shows the impact on the total shear stress by the inputs that can be modified by the user and are not C_v-dependant; the range of each parameter is based on information found in literature and described in section 3.5 (see Table 2.1 and Table 3.1):

- Volumetric concentration (C_v): 20% to 55% (2.1)
- Density of the sediments (ρ_s): 3080 to $3230\ kg/m^3$ (Table 3.1).
- Sediment size (d_s): average value of $D_{10} = 0.020\ mm$ to an average value of $D_{60} = 0.090\ mm$ from the four samples in 3.1.

The center axis is set at $C_v = 45\%$, $\rho_s = 3155\ kg/m^3$ and $d_s = 0.055\ mm$. The water depth is constant for all the calculations (50 m), which leads to a Prandtl mixing length of 20 m.

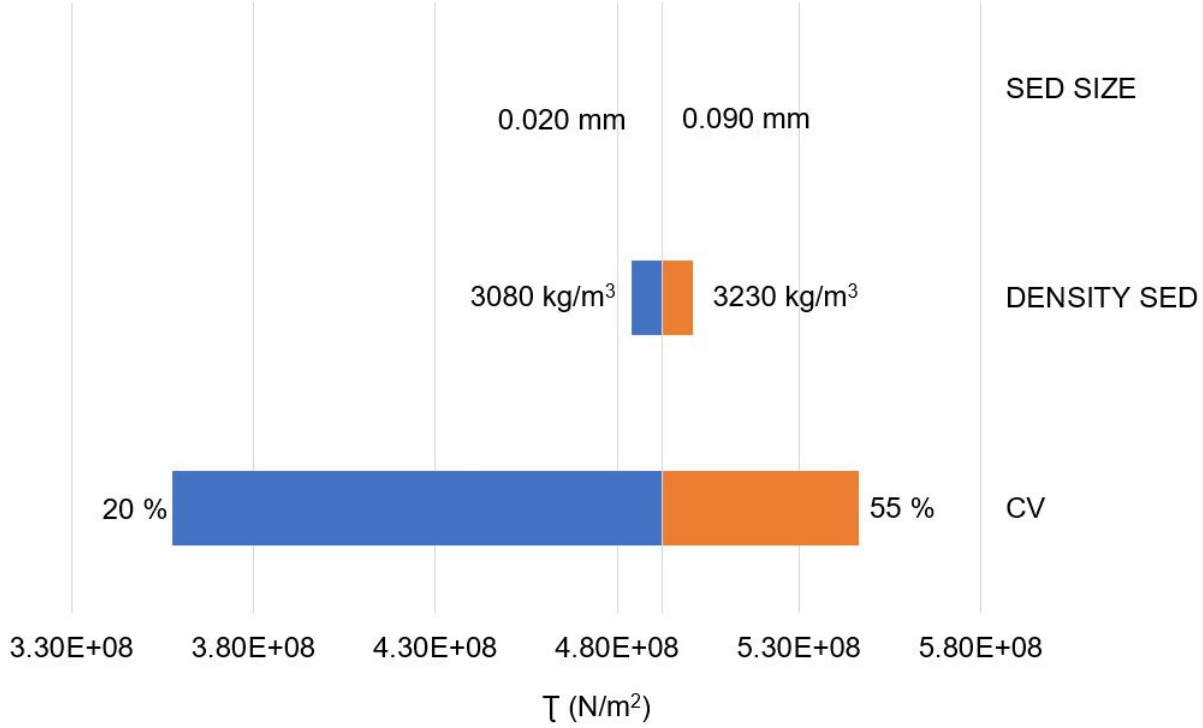

Figure 3.14: Sensitivity of each variable for the total shear stress. Constant water depth ($H = 50\ m$ that leads to $l_m = 20\ m$).

It is concluded that the most sensitive input value is the volumetric concentration. Therefore, the succeeding sensitivity analysis considers C_v as the variable parameter.

Secondly, each shear stress component is plotted to analyse its contribution to the total shear stress. According to Table 2.1, three boundaries are defined for the C_v:

1. Lower boundary: $C_v = 20\%$, mud flood characteristics.
2. Average boundary: $C_v = 45\%$, transition between mud flood and mudflow behaviour.
3. Upper boundary: $C_v = 55\%$, mudflow characteristics.

For the analysis, parameters such as density of sediments (ρ_s), sediment size (d_s) or the Prandtl mixing length are kept constant, since those are not affected by C_v. Table 3.2 displays the input values that are considered constant:

Table 3.2: Constant parameters.

DENSITY OF SEDIMENTS (ρ_s, kg/m^3)	**SEDIMENT SIZE (d_s, m)**	**PRANDTL LENGTH (m)**
3155	0.000055	20 (H = 50 m)

The C_v dependant parameters are provided in Table 3.3:

Table 3.3: Variables according to C_v

	YIELD STRENGTH (τ_y, N/m^2)	**VISCOSITY (μ, $N \cdot s/m^2$)**	**DENSITY OF THE MIXTURE (ρ_m, kg/m^3)**
Cv = 20%	0.062	0.045	1431
Cv = 45%	100.182	177.179	1969.8
Cv = 55%	1914.064	4852.075	2185.3

Introducing all the values from Table 3.2 and 3.3, and also a varying shear rate from 0 to 4 s^{-1} the resulting shear stress values for each part of equation 3.18 are in plotted in Figure 3.15, which shows the value of each component for the base situation ($C_v = 45\%$):

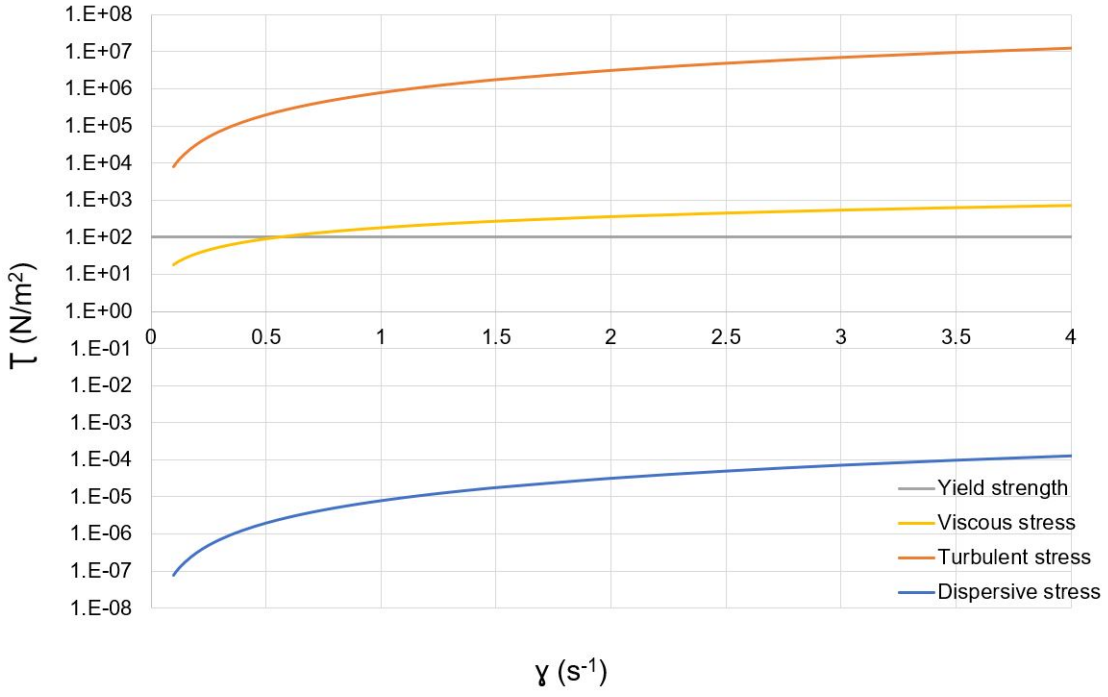

Figure 3.15: Rheogram of each shear stress.

It is evident that the normative stress is the turbulent, since it is already $1969\ N/m^2$ for a small shear rate of 0.05 s^{-1}. The second term that impacts the final shear stress is the yield strength, however it is a constant value independent of the rate of shear. Further, the viscous shear stress gradually increases

but with less intensity than the turbulent stress. Finally, the dispersive shear stress shows the least.

The turbulent shear stress depends on the density of the mixture and the Prandtl mixing length, but from these two parameters, the Prandtl length is the governing one (see equation 3.10). The Prandtl mixing length depends on the total flow depth (H). Thus a higher H leads to large values of l_m. When the height of a fluid is significant (large H), there is more available domain for eddies to be created and travel, hence creating perturbations that mix momentum over the vertical leading to increased bed shear stresses. If the instantaneous fluctuating velocities (u' and v') increase, the resulting velocities from equation 3.6 and 3.7 will also increase, leading to high values of the Reynolds number (equation 3.5), this means turbulent flow. However in this situation, the low values of viscosity are insufficient to reduce particle velocities or turbulence.

For the three situations considered before ($C_v = 20\%$, $C_v = 45\%$ and $C_v = 55\%$), the resulting flow curves are plotted in the rheogram shown in Figure 3.16:

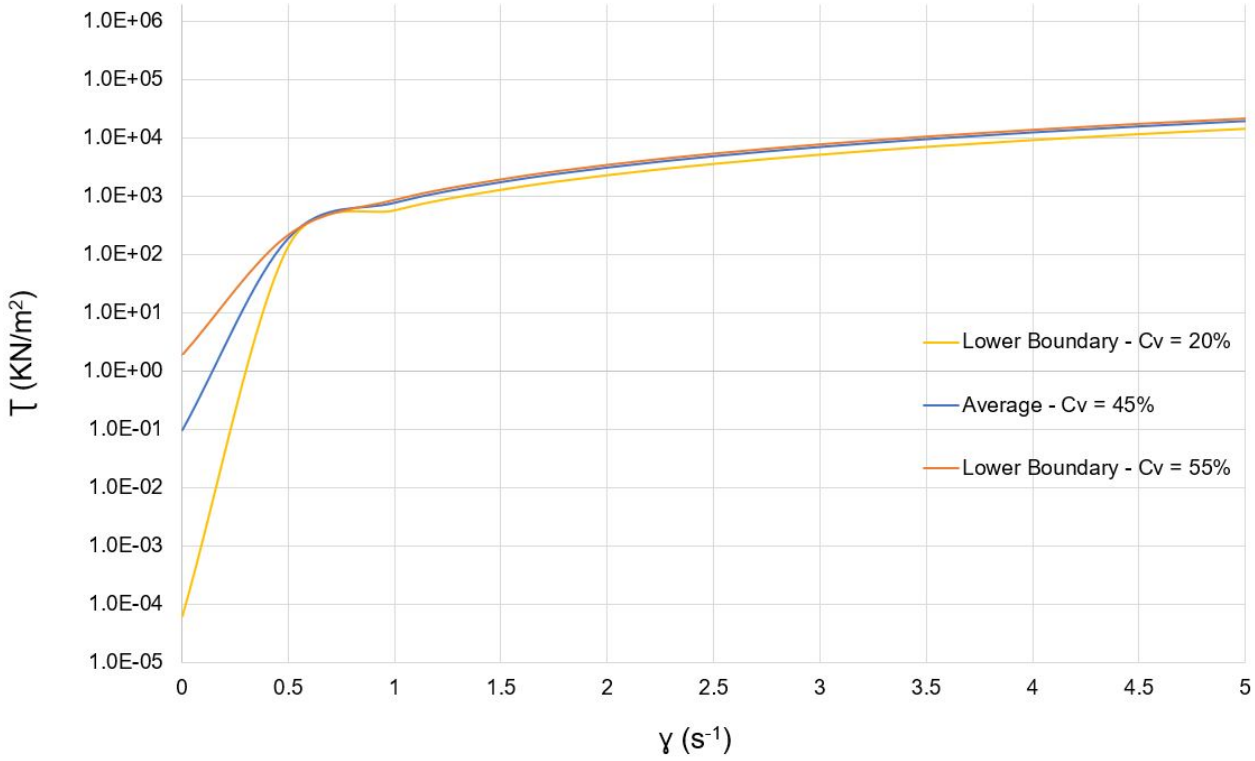

Figure 3.16: Rheogram for three different volumetric concentrations.

For the first case when $C_v = 20\%$, the yield strength value is relatively low (first point of the curve), but then the total shear stress increases mainly due to the turbulent component since the viscosity and the yield strength values are smaller. For the second case, $C_v = 45\%$ the yield strength is 100 times larger than the previous one, but the shape of the function is similar. The last case, $C_v = 55\%$, results in a high yield strength value and from that point, the final shear stress increases slightly. All curves have the same shape, but low values of C_v make the curve less steep and a lower value of the yield strength.

Shear rate values for hyper-concentrated sediment flows range between 5 to 50 s^{-1} (O'Brien and Julien, 1988). The following rheogram visualises the C_v effects, just like Figure 3.16, but the y-axis is not in a logarithmic scale:

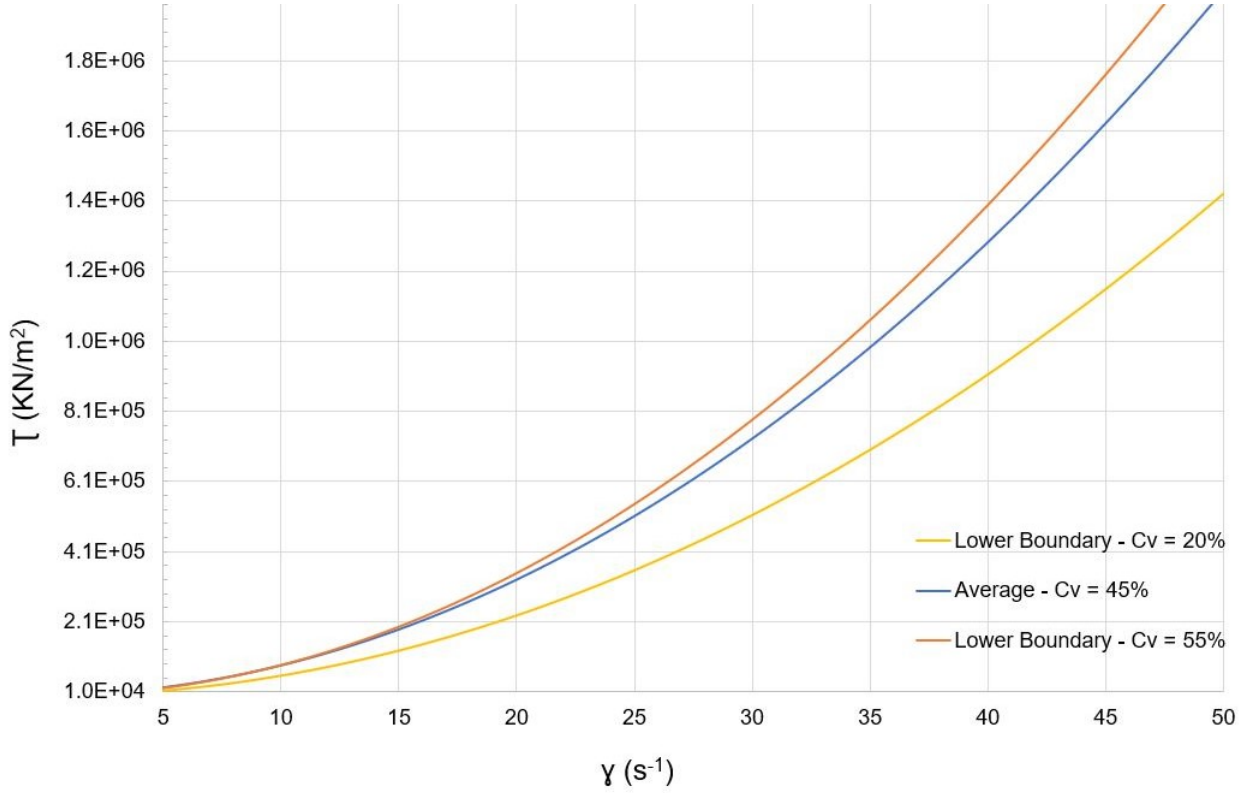

Figure 3.17: Rheogram for each scenario.

From Figure 3.17, the shape of the flow curves show the characteristics of mine tailings fluids. Recalling Figure 2.6 from section 2.3.1, from this curve the viscosity value increases with increasing shear rate. Therefore, it is shown that mine tailings exhibit a shear-thickening or yield-dilatant behaviour.

Two other extra cases are also considered: a fluid with similar characteristics as water ($C_v = 0.1\%$) (very low viscosity and yield strength, both negligible); and a fluid with $C_v = 90\%$, where no flow and landslide behaviour is expected. The resulting rheogram is shown in Figure 3.18:

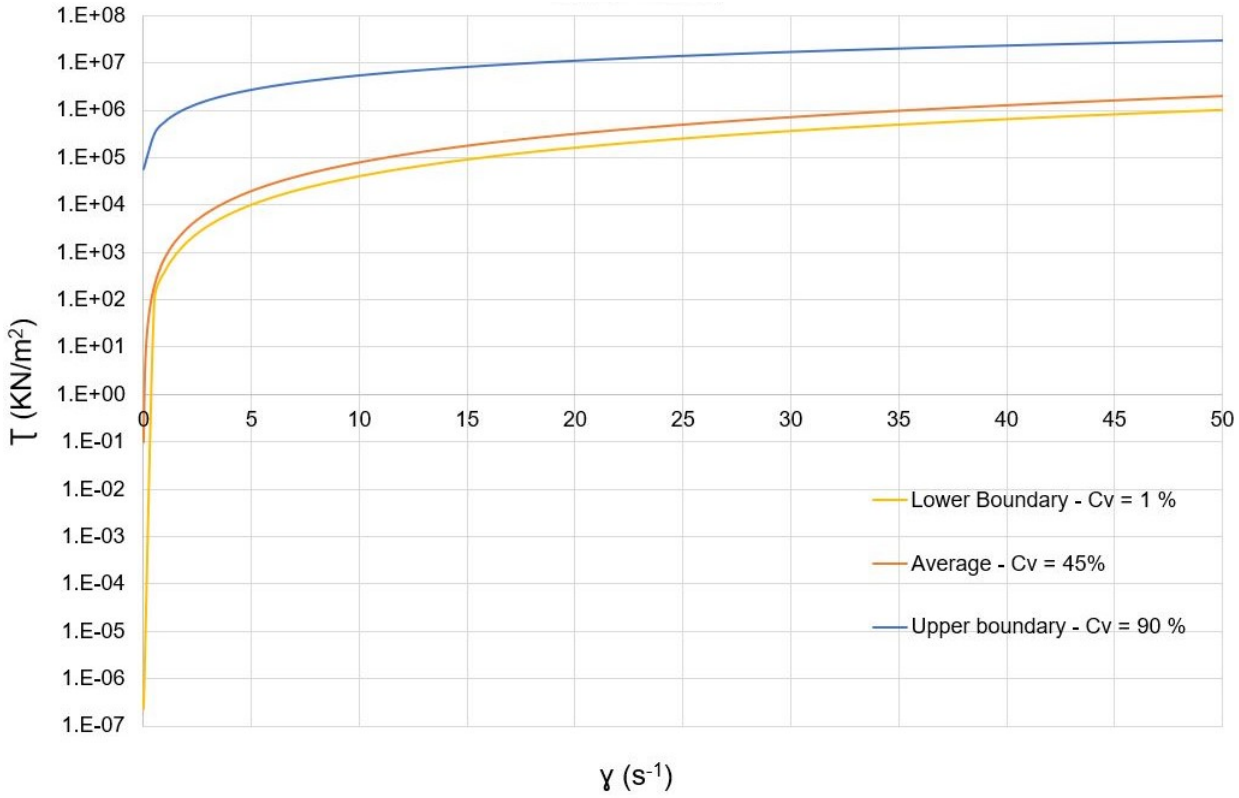

Figure 3.18: Rheogram for extreme scenarios

The range in the shear stress results for $C_v = 0.1\%$ and $C_v = 45\%$ differ less than for $C_v = 45\%$ and $C_v = 90\%$. $C_v = 45\%$ has similar shear stress values as water compared with $C_v = 90\%$. Concluding that for a landslide ($C_v = 90\%$), the required force to start movement is much higher than for fluid mixtures.

4

Modelling strategy

This chapter describes the basis for the selected models. Section 4.1 provides a general overview of models available to perform dam break studies. Section 4.2 describes the governing equations of the first model used, HEC-RAS. Section 4.3 presents the main physical processes of the second model, FLO-2D. In section 4.4 both models are compared to see the main differences between them. Finally, section 4.5 describes two benchmark tests done to calibrate both models.

4.1. Types of models

The numerical models utilise the fundamental principles of physics to simulate the breaching of earth embankments and the subsequent release of material in the downstream area. Advances during the past few years have allowed to redefine and understand the rheological behaviour of non-Newtonian fluids and implement them in the field of modelling the dynamic of fluids. The use of water based models to predict the impact of dam failure with non-Newtonian fluids governing the flow behaviour is not accurate enough. This is because water equations lead to a simple approximation of reality, since terms such as viscous dissipation, yield strength and turbulence become normative components within non-Newtonian fluid behaviour and these are ignored in water based models (Minussi and Maciel, 2012).

Different numerical methods are available for predicting the breach hydrograph, the subsequent release volume and the area of inundation. A general description of accessible models is provided, but expert judgement remains important to select the most appropriate model for a given scenario.

1. EMBREA-MUD

Model that considers the complex geotechnical, structural and hydraulic behaviour of an earth dam and its impounded reservoir (Morris et al., 2018). It is developed by Hydraulic Research Wallingford and predicts the growth of breach and the resulting volume released in the form of an hydrograph. Both breaching and outflowing processes are modelled simultaneously using the properties of the dam material, simulating the evolution of the breach opening without the need to make assumptions about the breach dimensions. It is a 2-phase model, since it considers two different fluids (Figure 4.1):

- Fluid 1: water layer with suspended solids (eroded tailings), Newtonian behaviour characterised by its depth and velocity.
- Fluid 2: mud layer with yield-dependency and non-Newtonian behaviour, which represents liquefied tailings.
- Solid layer: dam material.

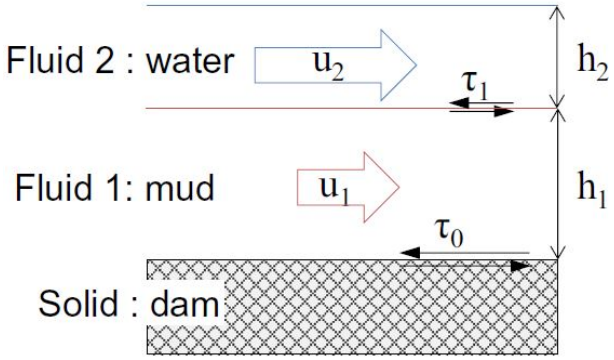

Figure 4.1: Schematic representation of 2-phase flow with EMBREA-MUD. Source Petkovšek et al., 2021.

The interaction between both fluid layers occurs as a result of shearing because of different velocities. The shear stress force is based on the Manning equation for flow resistance. Furthermore, the shear stress between mud and dam layer is computed using the Herschel-Bulkley fluid model. The model requires user-specified parameters for the dam, tailings and water inflow. The initial conditions for the dam part are the water and tailings level and a trapezoidal section, where the dam height, crest width, length and slope must be specified. Additionally, the user should select the failure method for the dam, the dam erodibility coefficient and the critical shear stress. For tailings flow, the erodibility coefficient, the yield strength, the consistency index and the flow index (Herschel-Bulkley parameters). For the water flow, the Manning roughness coefficient must be selected (Petkovšek et al., 2021).

2. RAMMS:DEBRIS FLOW

RAMMS (Rapid Mass Movements Simulation) is a software developed by a professional team at the *WSL Institute for Snow and Avalanche Research SLF* and the *Swiss Federal Institute for Forest, Snow and Landscape Research*. It is a numerical tool able to simulate runout distance, flow heights, flow velocities and impact pressure of dense flow snow avalanches, hillslope landslides and debris flows.

RAMMS uses the second-order numerical solution of the shallow water equations to model debris flows. The numerical model uses the two-parameter Voellmy model to describe the frictional behaviour of the material. Voellmy model divides the frictional resistance into two parts: a dry-Coulomb type friction and a velocity squared drag. To set up a simulation, an input hydrograph is required, an elevation file of the area and professional criteria to determine the frictional parameters for the Voellmy model (Mikoš and Bezak, 2021).

3. RIVERFLOW-2D

RiverFlow-2D allows to simulate a wide range of hyper-concentrated flows, from non-Newtonian fluids to granular material; and also specific cases such as the sudden release of tailings from dam failures. It is created by an engineering consulting firm specialized in advanced numerical model applications, Hydronia LLC (USA). It is a two-phase model (water and/or sediment) and the governing equations are the momentum and continuity equations presented in section 2.1. RiverFlow-2D presents 8 different rheological laws to model the flow resistance in the hyper-concentrated part. The input parameters needed to start a simulation are: an inflow hydrograph, the topography of the area and, depending on the rheological law, parameters such as yield strength, viscosity or volumetric concentration (Hydronia, 2017).

4.2. HEC-RAS

The Hydrologic Engineering Center (HEC) of the US Army Corps Engineers developed the River Analysis System (RAS). HEC-RAS allows to perform one/two-dimensional steady or unsteady flow water simulations,sediment transport calculations and water quality analysis (Brunner, 2016).

In this section, only the unsteady flow approach is considered, since the velocity resulting from a dam break is not constant. Assuming incompressible flow and hydrostatic pressure within the domain, HEC-RAS solves the Shallow Water Equations introduced in 2.1.4: the depth-averaged continuity equation follows as:

$$\frac{\partial \zeta}{\partial t} + \frac{\partial Hu}{\partial x} + \frac{\partial Hv}{\partial y} + q = 0 \tag{4.1}$$

where ζ is the free water surface, *H* is the total water depth, *u* and *v* are the depth-averaged velocities components in the Cartesian coordinates and *q* is an influx term from the hydrograph.

The depth-averaged momentum equation is different from the one presented in section 2.1.4, since HEC-RAS uses a modified version of the momentum equation especially formulated for debris flows (Hergarten and Robl, 2015). These equations present appropriate corrections for large topographic gradients (see equations 4.15 and 4.16):

$$\frac{\partial u}{\partial t} + u\frac{\partial u}{\partial x} + v\frac{\partial u}{\partial y} = -gcos^2\varphi\frac{\partial \zeta}{\partial x} + \mu_t\left(\frac{\partial^2 v}{\partial x^2} + \frac{\partial^2 v}{\partial y^2}\right) - \frac{\tau_x}{\rho_m R}\frac{cos\psi}{cos\varphi}\frac{u}{|\overline{V}|} \tag{4.2}$$

$$\frac{\partial v}{\partial t} + u\frac{\partial v}{\partial x} + v\frac{\partial v}{\partial y} = -gcos^2\varphi\frac{\partial \zeta}{\partial y} + \mu_t\left(\frac{\partial^2 v}{\partial x^2} + \frac{\partial^2 v}{\partial y^2}\right) - \frac{\tau_y}{\rho_m R}\frac{cos\psi}{cos\varphi}\frac{v}{|\overline{V}|} \tag{4.3}$$

where:

- τ is the total shear stress (from rheological model)
- ρ_m is the density of the mixture
- μ_t the turbulent eddy viscosity
- *R* is the hydraulic radius
- φ the water surface slope
- ψ is the inclination angle of the current velocity direction

In this set of equations, on the right hand side, the first term is the slope gradient, which is corrected by $cos^2\varphi$. The second term represents the horizontal mixing due to turbulence (μ_t), which is linked to the vertical gradient of velocities. Considering turbulence as an isotropic phenomena, it is assumed that what is produced in the vertical direction is the same as in the horizontal direction. Therefore, the turbulent eddy viscosity is equals as the viscosity defined in the original equation 2.17 and 2.18 and in the rheological model. The last term describes the friction forces within the fluid and HEC-RAS divides the total shear stress in two components:

$$\tau = \tau_b + \tau_{MD} \tag{4.4}$$

where τ_b is the bottom shear stress, based on the Manning's roughness equation (equation 2.19) and τ_{MD} is the mud-debris shear stress describes the shear stress from the rheological model.

The steps to set up a simulation with HEC-RAS are:

1. Obtain the Digital Elevation model
2. Define the computational domain
3. Set the grid size and roughness *n*-value
4. Define upstream and downstream boundary conditions
5. Plan the time step and simulation times

4.3. FLO-2D

FLO-2D is a finite volume conservation flood routing model designed by FLO-2D Software Inc. It can simulate multi-directional flow with either water or mud on different surfaces, giving the resulting temporal variation of flow velocity, flow depth and the affected area (FLO-2D Software, 2019).

Flow progression is controlled by the topography and resistance to flow. This is accomplished by numerical integration of the two dimensional equations of continuity and momentum (see section 2.1.4). For the momentum equation (equation 2.17 and 2.18) the friction slope S_f is calculated using the five shear stresses of the O'Brien rheological model. FLO-2D depth-integrates the shear stress strain relationship from the rheological model and it is given in dimensionless slope form (O'Brien et al., 1993):

$$S_f = S_y + S_v + S_{td} \tag{4.5}$$

where S_f is the dimensionless friction slope and it includes the yield slope S_y, the viscous slope S_v and the turbulent-dispersive slope S_{td}.

The first term of equation is the yield slope:

$$S_y = \frac{\tau_y}{\rho_m g H} \tag{4.6}$$

The viscous slope slope is written as:

$$S_v = \frac{K\mu u}{8\rho_m H^2} \tag{4.7}$$

K is a resistance parameter computed from Manning's roughness value (*n*):

$$K = 1460865.81(n)^{2.381} \tag{4.8}$$

The turbulent and dispersive shear stress terms are combined in one slope equation, which is equivalent to the Manning's friction slope equation (see equation 2.19):

$$S_{td} = \frac{n_{td}^2 u^2}{H^{4/3}} \tag{4.9}$$

where n_{td} is the Manning's resistance value for turbulent flow, which is obtained from:

$$n_{td} = n \cdot 0.0538 \cdot e^{6.0896 \cdot C_v} \tag{4.10}$$

FLO-2D solves the differential forms of the Saint-Venant continuity and momentum equations in 2 dimensions. The model determines the velocity and the flow depth for each time step, according to the boundary conditions given.

The procedure to set up a simulation with FLO-2D is:

1. Obtain the Digital Elevation Model
2. Define the computational area
3. Determine the cell size and time step
4. Determine Manning's roughness value.
5. Compute the breach hydrograph with the Tailings dam tool. FLO-2D incorporates this feature that is capable to determine the hydrograph through an iterative process, according to the failure duration and the volume released, both introduced by the user.

4.4. Differences between models

Flo-2D was chosen for this master thesis since it is capable to determine the breach hydrograph resulting from a dam break, according to the volume released and the duration of failure. Additionally, it can also model non-Newtonian fluids instead of water. On the contrary, HEC-RAS is unable to obtain the outflow hydrograph, but it can also model non-Newtonian fluids. Thus, the hydrograph from FLO-2D will be used as an upstream boundary for the simulations in HEC-RAS. Since the hydrographs and the input parameters will be the same, the differences between the results are expected to be similar.

The governing equations of each model are based on the Shallow Water Equations but they are implemented in the model following different approaches. The differences lie in the use of the momentum equation and are explained hereafter with the Shallow Water Equations and the 1-D Saint-Venant equation:

1. FLO-2D

The momentum equation used in FLO-2D is the 1-D Saint-Venant equation but in *(x.y)* directions in the horizontal plane (this is the 2-D Saint-Venant equation) (see equation 4.11 and 4.12):

$$\frac{\partial u}{\partial t} + u\frac{\partial u}{\partial x} + g\frac{\partial H}{\partial x} = g(S_{x,0} - S_{x,f}) \tag{4.11}$$

$$\frac{\partial v}{\partial t} + v\frac{\partial v}{\partial y} + g\frac{\partial H}{\partial y} = g(S_{y,0} - S_{y,f}) \tag{4.12}$$

For mudflows, the S_f is based on the O'Brien quadratic rheological model (equation 3.18) and converted from a shear-strain relationship into a friction slope (see equation 4.13):

$$S_f = S_y + S_v + S_{td} = \frac{\tau_y}{\rho_m H} + \frac{K\mu u}{8\rho_m H^2} + \frac{n_{td}^2 u^2}{H^{4/3}} \tag{4.13}$$

The friction slope includes the yield strength and viscosity (first and second term) and the Manning friction slope (third term) that accounts for the turbulent and dispersive shear stress. When clear water is considered as the main fluid, the yield and viscous slope disappear and only the Manning's slope is considered (as in equation 2.21).

To conclude, the momentum equation in FLO-2D is (in x-direction) expressed in equation 4.14:

$$\frac{\partial u}{\partial t} + u\frac{\partial u}{\partial x} + g\frac{\partial H}{\partial x} = g(S_0 - S_y - S_v - S_{td}) \tag{4.14}$$

2. HEC-RAS

The momentum equation defined in HEC-RAS is adapted for steep terrains, since the original Shallow Water Equations are considered for an almost horizontal free water surface, pre-requisite that is not satisfied with debris flows (Hergarten and Robl, 2015). Therefore the momentum equation can be expressed as shown in equation 4.15 and 4.16:

$$\frac{\partial u}{\partial t} + u\frac{\partial u}{\partial x} + v\frac{\partial u}{\partial y} = -gcos^2\varphi\frac{\partial \zeta}{\partial x} + \mu_t\left(\frac{\partial^2 v}{\partial x^2} + \frac{\partial^2 v}{\partial y^2}\right) - \frac{\tau_x}{\rho_m R}\frac{cos\psi}{cos\varphi}\frac{u}{|\overline{V}|} \tag{4.15}$$

$$\frac{\partial v}{\partial t} + u\frac{\partial v}{\partial x} + v\frac{\partial v}{\partial y} = -gcos^2\varphi\frac{\partial \zeta}{\partial y} + \mu_t\left(\frac{\partial^2 v}{\partial x^2} + \frac{\partial^2 v}{\partial y^2}\right) - \frac{\tau_y}{\rho_m R}\frac{cos\psi}{cos\varphi}\frac{v}{|\overline{V}|} \tag{4.16}$$

The rheological shear stress (τ) is introduced in the momentum equation with the sum of the bottom shear stress and the rheological shear stress (equation 4.4).

To compare the physics of the momentum equation between HEC-RAS and FLO-2D, the 1-D Saint-Venant equation is used. HEC-RAS transforms both shear stresses into friction dimensionless slopes by:

$$S = \frac{\tau_b}{\rho_m g H} + \frac{\tau_{MD}}{\rho_m g H} \tag{4.17}$$

Following equation 4.17, the bottom shear stress (τ_b) becomes the Manning's slope friction (S_f, equation 2.19) and the rheological shear stress (τ_{MD}) becomes the mud-debris slope (S_{MD}):

$$S = S_f + S_{MD} = S_f + [S_y + S_v + S_t + S_d] \tag{4.18}$$

The momentum equation in the 1-D Saint-Venant equation is (in x-direction):

$$\frac{\partial u}{\partial t} + u\frac{\partial u}{\partial x} + g\frac{\partial H}{\partial x} = g(S_0 - S_f - [S_y + S_v + S_t + S_d]) \tag{4.19}$$

To conclude, HEC-RAS considers all the terms in the rheological O'Brien model including the Manning's roughness, therefore there are 5 dimensionless friction slopes to take into account. On the other hand, FLO-2D depth-integrates the rheological model and accounts for the yield, viscous and Manning's slope (which considers turbulent and dispersive stress).

Table 4.1 displays the main differences between both models:

Table 4.1: Comparison between FLO-2D and HEC-RAS

\

ATTRIBUTE		FLO-2D	HEC-RAS
CATEGORY	CONCEPT		
THEORY	Governing equations	Continuity equation	Continuity equation
		Momentum equation	Momentum equation
INPUT DATA	Digital Elevation Model	Required	Required
	Manning's value	Required. Constant or variable	Required. Constant or variable
	Grid	Flooding area. Uniform mesh	Flooding area. Flexible mesh
	Dam breach schematisation	Generated by Tailings dam tool	Required as an upstream boundary condition
	Boundary conditions	Required: upstream and downstream	Required: upstream and downstream
	Other input parameters	Volume concentration, yield strength, viscosity, density of the mixture, Manning's roughness	Volume concentration, yield strength, viscosity, average sediment size, Manning's roughness
COMPUTATIONAL ALGORITHM	Numerical method	Finite volume method	Finite volume method
	Iterative method	Newton-Raphson method	Newton-Raphson method
OUTPUT	Results	Variation of flow depth, discharge, velocity and flooded area	Variation of flow depth, discharge, velocity and flooded area
	Time resolution	Seconds, minutes, hours, days	Seconds, minutes, hours, days

4.5. Benchmark tests

Before using both models to simulate failure of tailings dams. In order to check whether the proposed models satisfy equations for fluid motion it is necessary to test them.

4.5.1. HEC-RAS

The benchmark test for HEC-RAS is performed with a simple pipe, with a free surface and water as the main fluid. The pipe is 10 *m* long, 0.146 *m* wide, a 10.7% slope and a maximum elevation in the upstream boundary is 1.86 *m*. It is a 1D steady simulation and the flow direction is marked by the dashed red line (4.2).

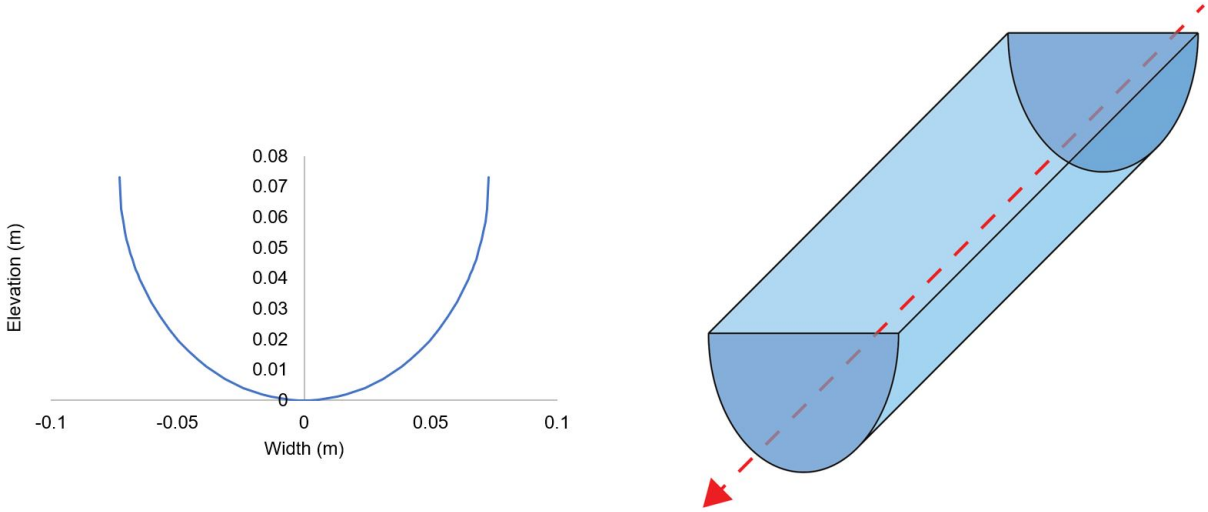

Figure 4.2: Sketch of the pipe. After Gibson et al., 2021.

Three different formulas are used to calibrate numerical with experimental results:

1. FRONT VELOCITY

In the front part of the fluid, a measure for the expected front velocity is:

$$v = \sqrt{gH} \tag{4.20}$$

where *g* is the gravity and *H* the flow depth.

2. FROUDE NUMBER

Froude number is a dimensionless ratio between inertia and gravitational forces:

$$Fr = \frac{v}{\sqrt{gH}} \tag{4.21}$$

3. ENERGY HEAD

It is also considered in the front part:

$$E = \frac{v^2}{2g} + \zeta \tag{4.22}$$

where *v* is the velocity and ζ the water surface elevation.

RESULTS

The values checks to verify the formulas have been obtained in the front part of the wave at $x = 3.17m$ at $t = 3s$. Since it is a steady simulation, it is pointless to measure all the parameters at different locations because the discharge is constant, thus the velocity too. Instead, to test the model for accuracy, the grid has been coarsened and refined and the results are calculated and compared at the same location.

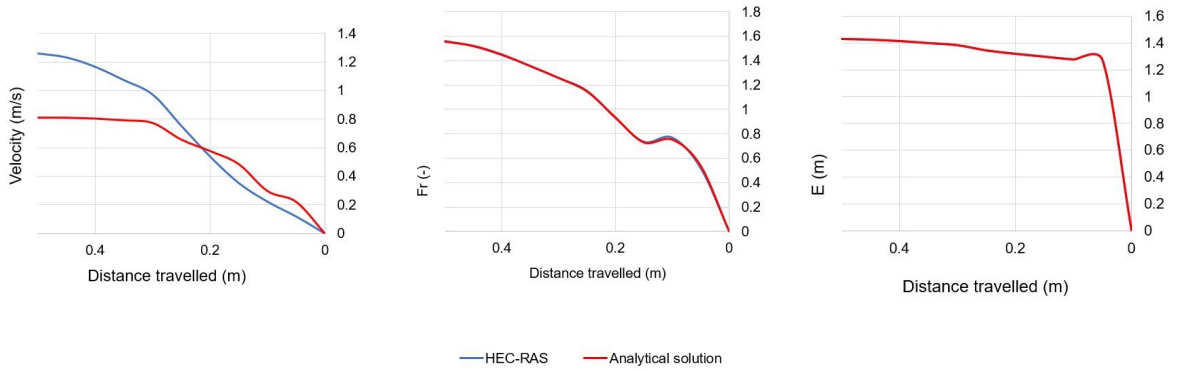

(a) Front velocity (b) Froude number (c) Energy head

Figure 4.3: Comparison between numerical and analytical solutions from the aforementioned formulas.

Figure 4.3 shows a comparison between the numerical and analytical solution for a grid with 3966 cells. HEC-RAS (numerical solution) determines the front velocity, Froude number and energy head over distance and time. The analytical solution of the same aforementioned parameters is calculated with equations 4.20, 4.21 and 4.22. The required inputs of the equations are flow depth (H), front velocity (v) and water surface elevation (ζ); which are obtained with HEC-RAS. Thus, the results with HEC-RAS are expected to be similar as the equations results. It can be seen that the front velocity is in the same order of magnitude, therefore the principle stated by equation 4.20 is conserved. More exact are the results for the Froude number (Figure 4.3 b)) and Energy Head elevation (Figure 4.3 c)), where both functions are overlapped.

The same results are retrieved for a coarser mesh of 444 cells and for a finer mesh of 35964 cells. For the coarse grid, the results are less accurate and less similar, but the computational time is reduced. On the contrary, for a finer mesh the results are still in the same order of accuracy as in the average grid (3996 cells) but the computational time increases considerably. The values obtained for a coarser and finer grid are available in Appendix A.

4.5.2. FLO-2D

FLO-2D is a flood routing model for delineating flood hazards, regulating floodplain zoning or designing flood mitigation; therefore it is designed for large scale situations. A simple pipe case like the one in HEC-RAS is not possible and it leads to numerical instability, since FLO-2D uses hours as the main computational time and cell sizes int the grid are in the order of 30 meters. Thus, to calibrate FLO-2D, the failure of the Feijão dam B-I explained in section 3.2.1 is modelled and the results are compared with the the actual event. First, the study of the causes of failure and consequences is presented (Robertson et al., 2019). Then, the required parameters for FLO-2D are determined based on the characteristics of the failure of dam B-I, in order to obtain a result that is similar to reality. Once the input parameters are established, the model is run with water to verify the front velocity equation 4.20. Again, the numerical solution obtained with FLO-2D is compared with the analytical solution from equation 4.20 (using the results obtained with FLO-2D of velocity and flow depth at certain time steps and locations). Lastly, the same simulation is carried out with hyper-concentrated sediment fluid, with the C_v that was obtained in section 3.6.

FLO-2D models mud and debris flow according to the quadratic rheological model presented in 2.3.2. A debris flow is a mass of loose mud, sand, soil, rock, water, and air that moves down a slope under gravity's effect. The moving material must be loose and capable of flowing through the downstream area. It was concluded from section 3.6 that the volumetric concentration (C_v) is the most sensitive parameter, followed by the density of sediments (ρ_m) and the sediment size (d_s). Thus, the first step is to determine the volumetric concentration of the mixture.

BENCHMARK TEST: FAILURE OF DAM B-I

Robertson et al., 2019 present an assessment of the technical cause(s) for the failure of dam B-I, together with technical and laboratory data from samples pre-failure, detailed image analysis, utilizing satellite, radar, video, drone, and LiDAR data.

Before failure, Robertson et al., 2019 estimated that the total volume (water plus tailings) within the reservoir was 12.7 Mm^3 (V_T), by comparing the pre-dam topography and pre-failure LiDAR point clouds. An averaged in situ void ratio of 1.0 was calculated from historical samples available, which is in line with the values presented in Table 3.1. A void ratio of 1.0 implies a porosity value of 0.5 and a volumetric concentration of 50%, meaning that 50% of the total volume of tailings were voids. Mine tailings of dam B-I are described as very loose and saturated, but the material in the impoundment is not homogeneous and part of tailings above the water level were unsaturated. The periodic review of dam mine safety Bureau, 2017 monitored the groundwater level on a monthly basis by 93 piezometers, 37 water level indicators and other instruments. The results show that the ground water level fluctuates between 20 *m* to 5 *m* below the surface (Figure 4.4), verifying that not all the tailings were saturated. Since the void ratio is not constant over the entire reservoir, some areas within the reservoir will have low values of porosity and void ratio, or vice versa. From all the geotechnical monitoring carried out in dam B-I, Bureau, 2017 measured a volume of mine tailings of 7.7 Mm^3 (V_S). From the information available, Robertson et al., 2019 estimated a water volume (V_W) within the reservoir of approximately 5 Mm^3.

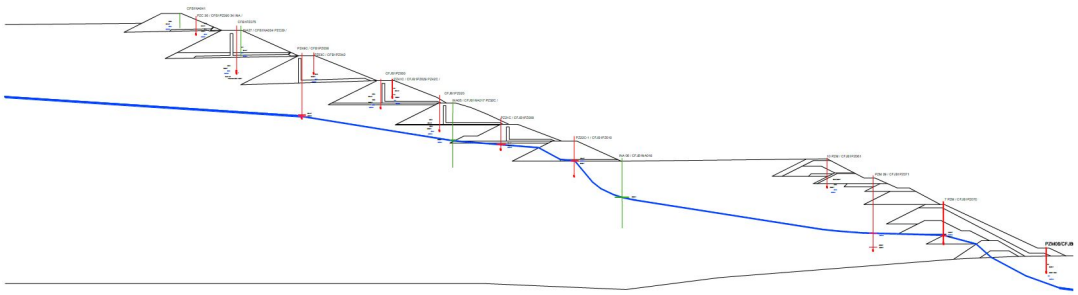

Figure 4.4: Estimated groundwater level of dam B-I. Source: Bureau, 2017

Robertson et al., 2019 evaluated the volume released (V_R in Table 4.2) after failure by comparing the pre and post-failure topographies of dam B-I. For this Msc thesis, it is assumed that the entire volume of water in the reservoir flowed out, therefore there is conservation of water volume before and after failure. Thus, if the total and water volumes are known, the volume of tailings released out can be calculated. Table 4.2 summarises the volumes before and after failure.

Table 4.2: Volumes before and after failure for dam B-I.

	VOLUMES PRE-FAILURE (Mm^3)	**VOLUMES POST-FAILURE (Mm^3)**
Total (V_T and V_R)	12.7	9.7
Water (V_W)	5.0	5.0
Tailings (V_S)	7.7	4.7

The post-failure volumes allow to derive the volumetric concentration of the mixture that flowed over the downstream area:

$$C_v = \frac{V_S}{V_R} = 0.48 \tag{4.23}$$

A C_v of 0.48 means a porosity value of $n = 0.52$ and a void ratio of $e = 1.08$, which corresponds to a very loose and saturated material.

With the C_v calculated, the other input values for the rheological model are obtained (see Table 4.3). The sediment size and density of sediments are not dependant on the volumetric concentration, thus they are the average value from laboratory data of mine tailings samples before failure (Robertson et al., 2019).

Table 4.3: Geotechnical properties of mine tailings of dam B-I.

PROPERTY	VALUE	EQUATION
Volumetric concentration, C_v (-)	0.48	Equation 4.23
Yield strength, τ_y (N/m^2)	242.74	Equation 3.3
\ Viscosity, μ $(N \cdot s/m^2)$	478.26	Equation 3.4
Density of sediments, ρ_s (kg/m^3)	4500	-
Density of the mixture, ρ_m (kg/m^3)	2680	Equation 2.24
Sediment size, d_S (m)	0.00010845	-

Once the values that govern flow behaviour are defined, the input parameters mentioned in Table 4.1 to set up a simulation with FLO-2D are:

1. DIGITAL ELEVATION MODEL AND COMPUTATIONAL DOMAIN

Obtained from *Shuttle Radar Topography Mission (SRTM)-Downloader*, plugin available for QGIS. Computational domain is delimited according to the extension of the observed flooding area.

2. COMPUTATIONAL TIME AND CELL SIZE

Cell size of 30 m and a time step of 30 seconds guarantees numerical stability, according to the Courant-Friedrich-Lewy condition.

3. BREACH HYDROGRAPH

The reservoir was emptied in approximately 5 to 7 minutes (Robertson et al., 2019, Ghahramani et al., 2020 and Lumbroso et al., 2021). The Tailings dam tool from FLO-2D predicts the breach hydrograph of 6 minutes as the failure duration, with a $Q_{peak} = 1.8 * 10^5\ m^3/s$.

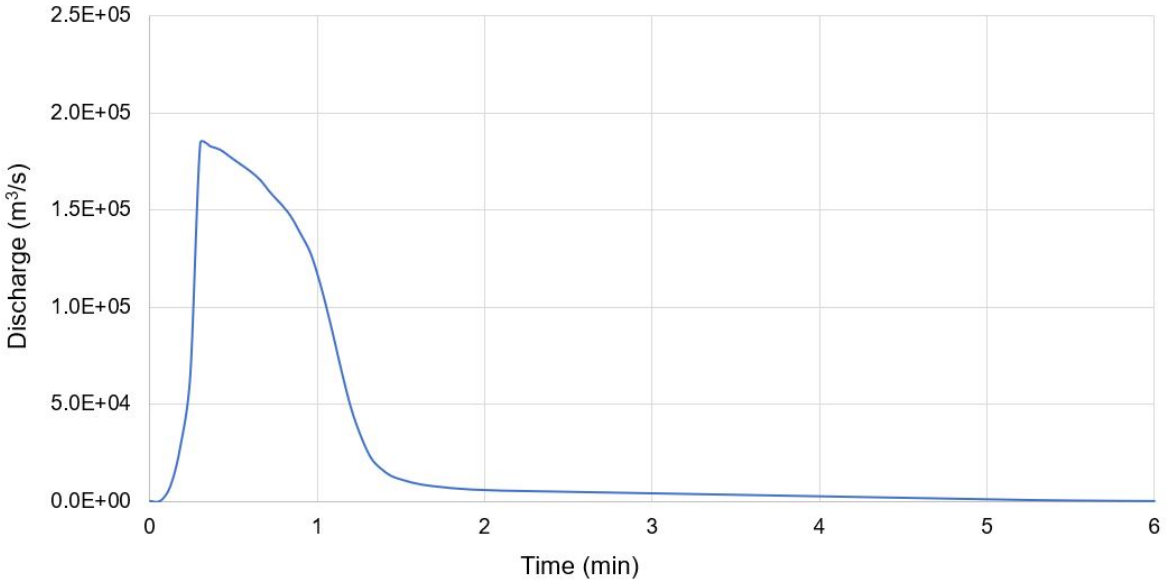

Figure 4.5: Breach hydrograph for the failure of dam B-I (6 minutes).

4. MANNING'S ROUGHNESS

The Manning's roughness is the only value which cannot be retrieved from theory, because expert judgement is required to estimate which roughness coefficient is the most suitable for the occasion. Therefore, it is the only unknown.

From Arcement and Schneider, 1989 the ranges for roughness coefficients for flood plains with vegetation are:

Table 4.4: Manning's values for flood plains with vegetation. Source: Arcement and Schneider, 1989.

AMOUNT OF VEGETATION	**n** $[s/m^{1/3}]$
Small	0.001 - 0.010
Medium	0.011 - 0.025
Large	0.025 - 0.050
Very large	0.050 - 0.100
Extreme	0.100 - 0.200

Several analyses with different *n* values and a from all the simulations carried out with FLO-2D, $n = 0.03$ is the best option to obtain an output that matches the reality of the environment and the events. *n* is not a dimensionless parameter, its units are $[s/m^{1/3}]$; however they are often omitted. In this project, the units of Manning's roughness value will not be added when the *n* is mentioned.

RESULTS

In this section, the failure of the mine tailing dam B-I has been modelled, first with water as the main fluid and then with hyper-concentrated sediment fluid with a $C_v = 48\%$.

1. WATER

Prior to run the model with a non-Newtonian fluid, the Brumadinho failure has been analysed with water. The input parameters are the aforementioned ones, except for the C_v, which is 0. The idea for using water as the main fluid is to verify the evolution of the front wave velocity and asses the increase of the velocity front with equation 4.20. The comparison of the front velocity between the numerical and analytical solution is analysed in 4 different long-sections. Figure 4.6 shows the maximum velocity value per cell registered for the whole simulation time, which gives an approximation of the flooding area. The initial inundated area (Figure 4.6) is measured with the maximum velocity values registered per cell, since these represent the locations reached by the fluid for the entire simulation time. If a specific timestep within the duration time was considered, the fluid would not have had sufficient time to reach further locations, which would result in an underestimation of the flooded area. It can be seen that the maximum velocity values are registered near the failure location and then they minimise over distance. In addition, over the entire domain, higher velocity values are registered in the centreline of the flooded area in comparison with its edges, where the fluid is deposited and barely flowing.

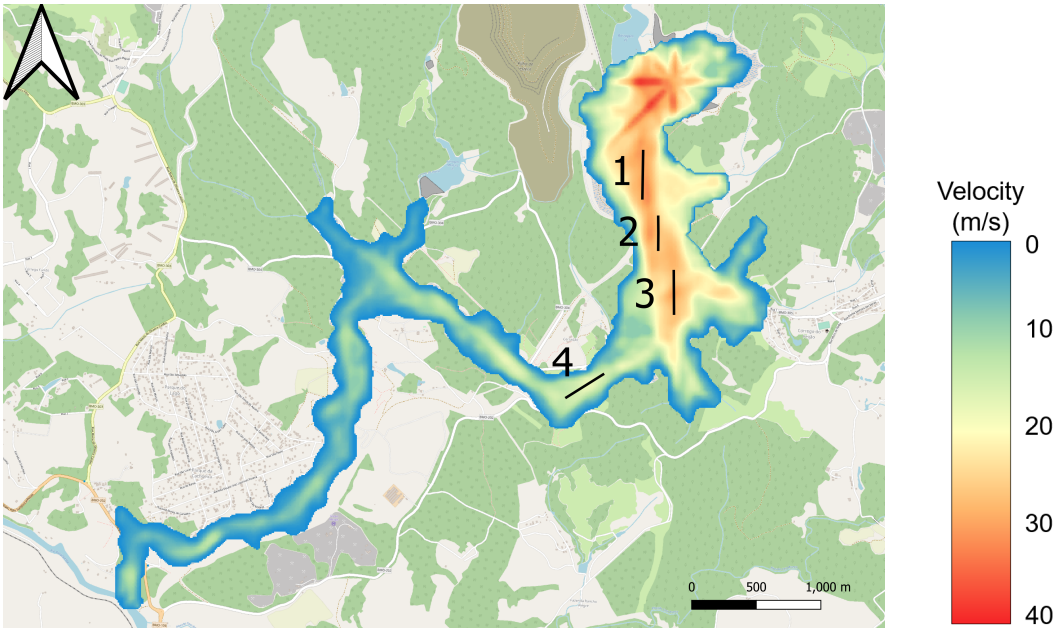

Figure 4.6: Primary impact zone with water and the long sections considered.

To compare the evolution of front velocity with equation 4.20 with the numerical analysis, the result is illustrated for long-section 3 in Figure 4.7.

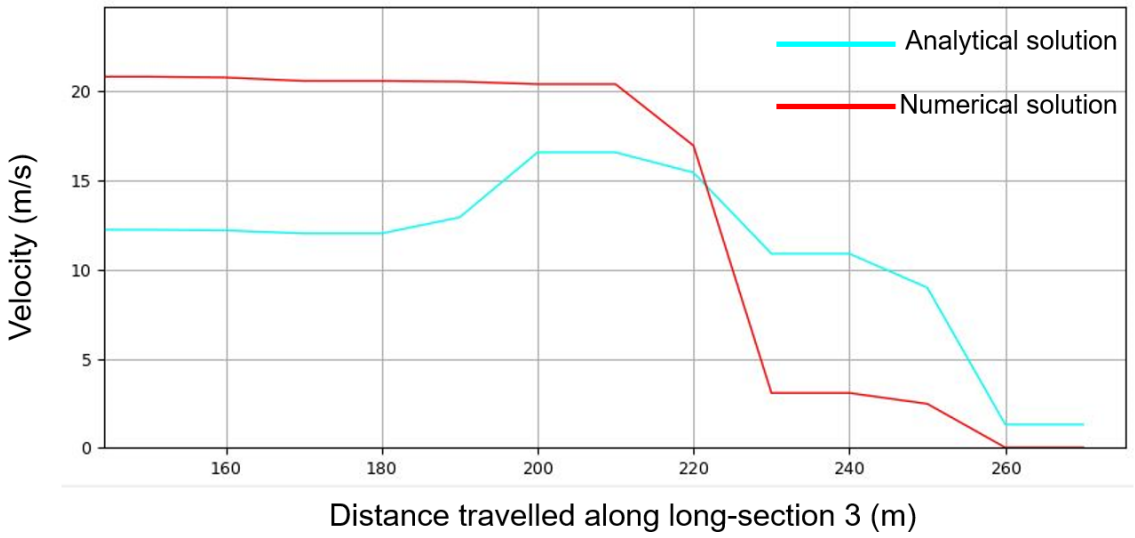

Figure 4.7: Comparison of theoretical and numerical front velocities in long-section 3.

The increase in the front velocity is in the same order of magnitude, therefore it results in a plausible approximation. The analyses for the other long-sections are in Appendix A.

2. HYPER-CONCENTRATED SEDIMENT FLUID

Once the front velocity has been verified with water, the simulation with a hyper-concentrated sediment fluid is carried out. Table 4.5 summarises the input parameters, its values used for the simulation and the results obtained.

Table 4.5: Input values and results from the simulation of failure of dam B-I.

FLO-2D INPUT PARAMETERS	RESULTS FROM FLO-2D
$C_v = 48\%$	Area of inundation = 3.1 Mm^2
Manning's roughness = 0.03	Peak velocity = 36.7 m/s
Failure duration = 6 *min*	Arrival time at the river = 2.5 *h*

The results from FLO-2D are compared with the data retrieved from literature, where other simulations and studies were performed.

- Area of inundation of 2.7 - 3.0 Mm^2 (Ghahramani et al., 2020, Lumbroso et al., 2021).
- Arrival time at the River Paraopeba was between 2 - 3 hours (Lumbroso et al., 2021, Raman and Liu, 2019b).
- Peak velocity of 33 m/s (Robertson et al., 2019, Lumbroso et al., 2021).

The primary impact zone of the flood wave is measured with the maximum velocity value map for each grid element registered during the entire simulation interval (Figure 4.8), because that area accounts for the regions where the mudflow is moving (moments after failure). These maximum velocity values consider the locations inundated by the mixture for the entire simulation time, thus it is possible to calculate the area of the primary impact zone. If the initial inundated area was measured for a specific timestep within the simulation interval, low velocity values would not have had enough time to reach further inundated locations, leading to an underestimation of the flooded area. The initial inundated area for hyper-concentrated sediment fluid for the dam B-I failure is $3.1\ Mm^2$.

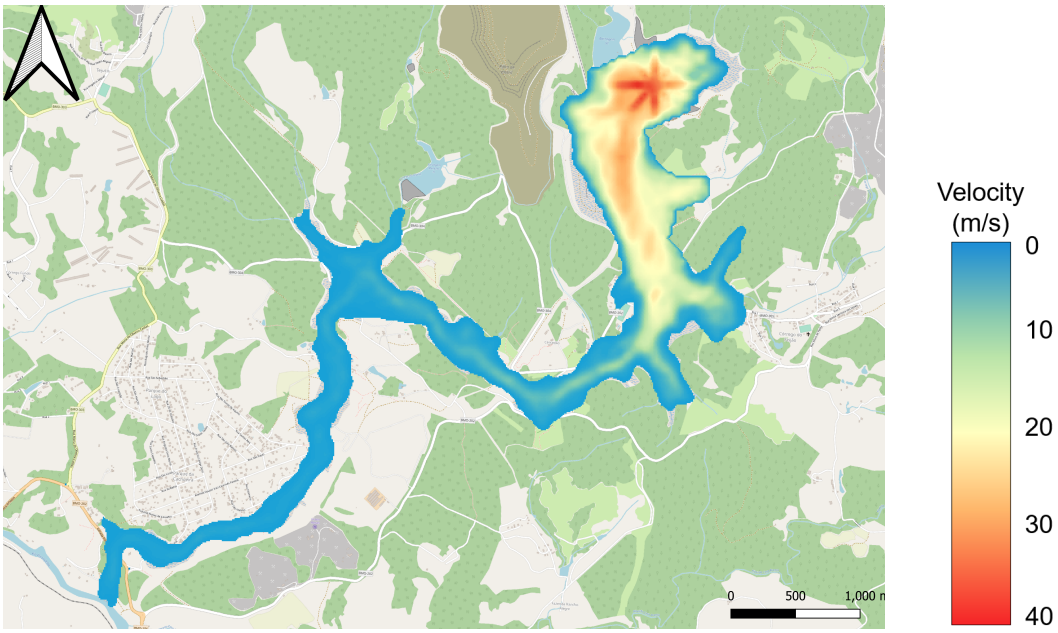

Figure 4.8: Primary impact zone after failure of dam B-I. The inundated area is measured with the maximum velocity value per cell during the entire simulation time.

Because of the sudden release of tailings, maximum velocities are registered near the dam area and thereafter decrease over distance, due to the friction forces within the fluid and between the fluid and the terrain. Higher velocity values are measured at the centreline of the flooded area, where also higher flow depths are registered. Lower velocity values are registered at the edges of the inundated area.

The total area of inundation (minutes, hours after failure) is delimited with the total flow depth map for each grid element obtained for the entire simulation time. Accounting for the maximum flow depths values allow to determine the total area where the mixture is accumulated over entire simulation time, since the fluid can still be in a deposition and accumulating process after a long time of failure. Therefore, it is more suitable to consider the flow depth values registered for the entire failure rather than a specific time step within the interval simulation. It is larger than the primary impact zone, since the mudflow is accumulated after certain time but not flowing. This area is $3.3\ Mm^2$.

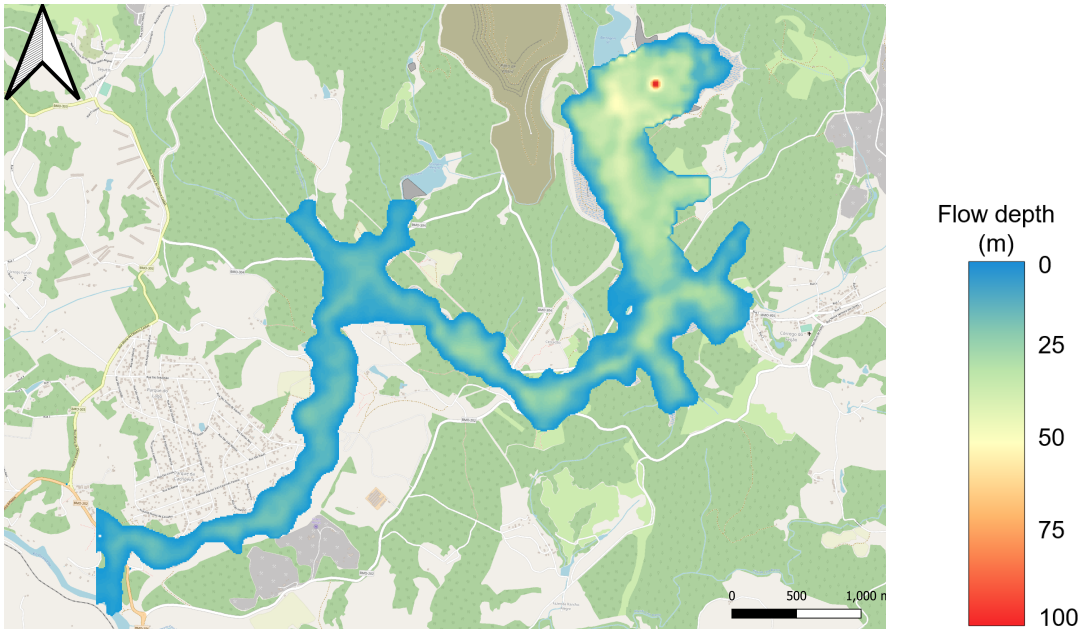

Figure 4.9: Final inundation area after failure of dam B-I. Area delimited with the map of maximum flow depth value per cell.

In conclusion, comparing the results obtained with FLO-2D (Table 4.5) and the literature available, FLO-2D is capable to perform the effects of failure of mine tailings dams.

5

Numerical results

The modelling strategy began in section 3.5 when assessing the rheological model and determining which parameter influences the most the total shear stress. It was concluded that the volumetric concentration was the one with greatest influence, followed by the density of sediments and sediment size. Thereafter, section 4 provided an explanation of the governing equations for each model: FLO-2D and HEC-RAS. Then, the input parameters for each model were described. Additionally, the failure event of 2019 in Brumadinho was modelled with FLO-2D, according to public data from the characteristics of the dam and the reservoir. In order to test the robustness of the models, this chapter provides a sensitivity analysis according to the parameter that influences the most the rheological model, the volumetric concentration. Furthermore, input parameters of the model are also added in the sensitivity analysis of the model. These parameters are the Manning's roughness value (*n*) and the duration of failure (*t*). Section 5.1.1 presents the variables for the sensitivity analysis and the ranges considered for them. A prediction of the outcome is explained according to the parameter and value considered. Section 5.1.2 provides the results of the sensitivity analysis carried out with FLO-2D. The results considered are: initial inundated area or primary impact zone (moment right after failure), which is determined with the map of maximum velocity value registered for each element over the entire simulation time; the final inundated area (hours after failure), which is the area delimited with the map of maximum flow depth values obtained for each element for the entire simulation duration. Section 5.1.3 explains the results obtained and the realism behind every value chosen, thus, a further classification of the parameters is obtained. Section 5.1.4 comments on the results regarding the final flooded area. Then, in section 5.2 the sensitivity analysis is carried out with HEC-RAS, but only with volumetric concentration as variable.

5.1. FLO-2D: Dam B-I failure

5.1.1. Parameters considered

The results obtained in section 4.5.2 are used as basis for the sensitivity analysis. The parameters altered are explained hereafter together with predictions of each variation.

1. VOLUMETRIC CONCENTRATION

The starting value $C_v = 0.48$ is derived in section 4.5.2 from the released volumes. To test the model against the sensitivity to the volumetric concentration, the total failure volume is maintained constant ($V_R = 9.7 Mm^3$). Whereas, volumes (V_W and V_S) are modified to obtain several C_v, which will influence porosities, void ratio and the resulting the flow behaviour. Table 5.1 shows the volumes.

Table 5.1: Different volumes and their implications.

	V_R **(**Mm^3**)**	V_W **(**Mm^3**)**	V_S **(**Mm^3**)**	C_v **(%)**	*n'* (-)	*e* (-)
SCENARIO 1	9.7	7.0	2.7	28	0.72	2.59
SCENARIO 2	9.7	5.3	4.4	45	0.55	1.20
REALITY	9.7	5.0	4.7	48	0.52	1.06
SCENARIO 3	9.7	4.85	4.85	50	0.50	1.00
SCENARIO 4	9.7	4.4	5.3	55	0.45	0.83
SCENARIO 5	9.7	2.7	7.0	72	0.28	0.39

- Scenario 1 (V_W » V_S): the volume of water is more than twice the quantity of sediments, meaning that the entire mixture is governed by water. The porosity and void ratios are large, which implies that the mixture is in a very loose state and saturated. High velocity values are expected near the failure location, since the small amount of particles are not sufficient to take into account the viscosity, yield strength and dispersive effects within the fluid. According to Table 2.1, this situation implies a mud flood behaviour, similar to water according to the test evaluation on the rheological model in section 3.5. The yield, viscous and dispersive shear stresses are not predominant and the flow behaviour is governed by the turbulent shear stress. Furthermore a more extensive primary impact zone is expected, since it will be easier for the fluid to flow and inundate the downstream area. Thus, the primary flooding area will be similar to the final inundation area. Less amount of solids will be accumulated along the drainage path, due to the low amount of sediments and its ease to move into the downstream area. The high velocities in the fluid will give an arrival time at the River Paraopeda shorter than reality of 2.5 hours.
- Scenario 2 (V_W > V_S): the amount of water is less than scenario 1 but still higher than the considered sediments volume. The material is found in a very loose state, with a void ratio higher than unity and a porosity value of 0.55 (*n'*). Thus, the material is saturated. Different from case 1, the increment in the volumetric concentration will result in a higher the yield strength, viscosity, turbulent and dispersive shear stresses. This will minimise the velocity and turbulence within the fluid. From the sensitivity analysis done in section 3.5, for a $C_v = 45\%$, the governing shear stress is the turbulent component. Higher velocity values near the failure location and a larger inundation area than reality is expected, but lower than scenario 1. The velocity field will be reduced by the quantity of sediments within the mixture, thus, the extend of large velocity values will be less than scenario 1. According to the Table 2.1 by O'Brien, a $C_v = 0.45$ is the limit boundary between mud flood and mudflow behaviour, thus different outcomes between both cases are expected. Lower velocity values lead to higher flow depths, since the fluid has more difficulty when flowing and spreading over the area, thus more matter is accumulated along the drainage path. A significant difference is expected regarding the primary and the final inundation area; part of the fluid will not be able to continue flowing due to its amount of sediments and it will deposit.

- Scenario 3 (V_W = V_S): the void ratio is 1.0, therefore there is the same amount of water as sediments. The material is saturated and in a loose state. Compared to the previous cases, larger values for viscosity and yield strength are estimated, which together with the turbulent and dispersive terms, they result in a higher shear stress needed to enable deformation of the fluid. The high velocity field near the failure location is reduced compare to previous cases, since the amount of sediments minimise the ease of flowing of the hyper-concentrated fluid. Thus, the low velocity values and the large amount of sediments will lead to a reduced initial inundated area. Higher flow depths because accumulation of matter are expected due to the low velocity values. The final flooding area will greatly differ from the initial, since the flow will deposit after a long period of failure, making the stream wider along the centerline.
- Scenario 4 (V_W < V_S): for this scenario the amount of water involved is less than the volume of sediments. A large void ratio still indicates a material in a loose state. The large amount of solids will give a larger yield strength, viscosity, turbulent and dispersive terms of the rheological model for the fluid considered. This results in a high shear stress needed to enable deformation of the fluid. Hence, low velocity values are expected near the failure location and those will be decreased even more over distance. The large amount of sediments in the fluid will increase the density of the mixture, leading to a denser and heavier mass. Due to the reduced amount of water, the extension of the initial flooding area is expected to be less than previous scenarios. On the contrary, higher values for the flow depth will be registered near the failure location due to the low velocity values and accumulation of matter. The final flooding area will be less compared to previous situations, due to its difficulty for the fluid to flow, but the depths registered in that case will be higher than for low values of C_v. According to the Table 2.1 by O'Brien, a $C_v = 0.55$ is the limit boundary between mudflow and landslide behaviour.
- Scenario 5 (V_W « V_S): as an extreme situation, when the volume of sediments is larger than water, the material is not considered a fluid anymore. The reduced amount of water is not able to mobilise the material through large distances over the downstream area. According to Table 2.1 from O'Brien, a $C_v = 0.72$ falls into the category of landslide, where flow is not occurring. From the study of the O'Brien quadratic rheological model (see section 3.5), the dispersive term considered for the linear volumetric concentration (λ) sets a maximum value for the maximum volumetric concentration ($C* = 61.5\%$). Once the C_v surpasses the theoretical limit ($C*$), the matter is not considered a fluid with mudflow behaviour anymore. Hence, this scenario is not considered in the subsequent sensitivity analysis.

2. MANNING'S ROUGHNESS VALUE

Based on Table 4.4, the range of values that affect the friction between surface and fluid along the flood plain are divided in 5 categories: small, medium, large, very large and extreme. In FLO-2D the roughness values allowed range between 0.011 - 0.40 (FLO-2D Software, 2019). For this reason, values within the category *small* are not considered for the analyses. Furthermore, values within the category of *extreme* are not contemplated, since *n* values of such category barely allowed the hyper-concentrated fluid to flow. Therefore, the roughness values considered are between the intervals of *medium*, *large* and *very large*. The values are retrieved according to Table 4.4 and described hereafter with a prediction of what to expect:

- Medium, $n = 0.012$: since the friction between fluid and surface is minimum, the extension of the primary impact zone will be larger than reality and also very similar to the final inundated area. High velocity values are expected near the failure location and over a large distance from the breach formation. These large velocities developed will be minimised by the C_v of the mixture and not by the roughness of the surface. An extensive initial inundated area is expected. The ease for the fluid to flow will prevent accumulation of the mixture along the drainage path. Therefore, the flow depths registered will be minimum for this situation. The final inundation area will be similar to the initial, due to high velocities of the fluid and minimum deposition of material.
- Medium, $n = 0.022$: still in the medium range, but the friction between fluid and surface is more significant. Registered velocities are expected to be less than scenario 1 and will cause a reduced

initial flooding area. However, an increase of the flow depths registered is expected. Thus, a more extended final inundated area which will differ from the initial one, more than in scenario 1.

- Very large, $n = 0.055$: in the *very large* range, the roughness of the surface will considerably increase the friction between surface and the hyper-concentrated fluid. The amount of vegetation and obstacles along the drainage path will restrict the flow's mobility along the downstream area. Low velocity values are expected due to this high friction, and the velocity will be further reduced due to the C_v. The primary impact zone will be less compared to previous scenarios because of low velocity values. whereas, high values for flow depths are expected due to the low velocity. The mixture will accumulate along the drainage path when the velocities are not enough to guarantee mobility. Significant differences regarding the initial and final inundated area are estimated, since the material will deposit after a certain time after failure.

- Very large, $n = 0.075$: in the *very large* category, the friction between surface and hyper-concentrated fluid is greater. The sudden release of volume (V_R) will lead to peak velocity values that will be rapidly mitigated by the roughness parameter. Additionally, the volumetric concentration will add limitations to this mobility. Overall, in this scenario the lowest velocity values are expected together with the minimum initial inundated area. The highest values regarding the flow depths are expected in this scenario, due to the small velocities. Therefore, large part of the fluid will deposit after a certain time after failure, which will lead to a larger final inundated area compared to the initial one.

3. FAILURE DURATION

As it was stated by Robertson et al., 2019, the dam B-I was emptied in approximately 6 minutes. To asses the sensitivity of the model against the duration of failure, the breach hydrograph has been modified into the following scenarios:

- Failure duration 3 minutes: the shape of the breach hydrograph is the same as the original hydrograph (Figure 4.5), with a peak discharge of $Q_{peak} = 3.7 * 10^5\ m^3/s$. The sudden release of material will lead to high velocity values near the failure location, but there after will minimise due to the amount of sediments in the mixture and the friction between surface and fluid. The high velocity values will create an extensive flooding are near the failure location, where the mixture will reach further locations. The highest flow depths will be registered for this situation, due to the abrupt release of material. The final inundated area will be grater than the initial one. The high velocities will reach further areas along the drainage path and part of the material will deposit there, leading to a more extended final flooding area (see Figure 5.1).

- Failure duration 12 minutes: the material is released more slowly, since the hydrograph is extended and with a lower $Q_{peak} = 9.2 * 10^4\ m^3/s$. The velocities expected are lower than for the previous case and they will be minimised by C_v. Therefore, the initial flooding area will decrease, since the small velocity values are unable to extend the flood wave to further areas from the drainage path. In this case, the low velocity values will not lead to high flow depths, since the hyper-concentrated fluid is able to flow through the downstream area following the centerline of the narrow stream. Hence, a more reduced final inundated area is expected (see Figure 5.1).

The breach hydrographs considered are plotted together in Figure 5.1.

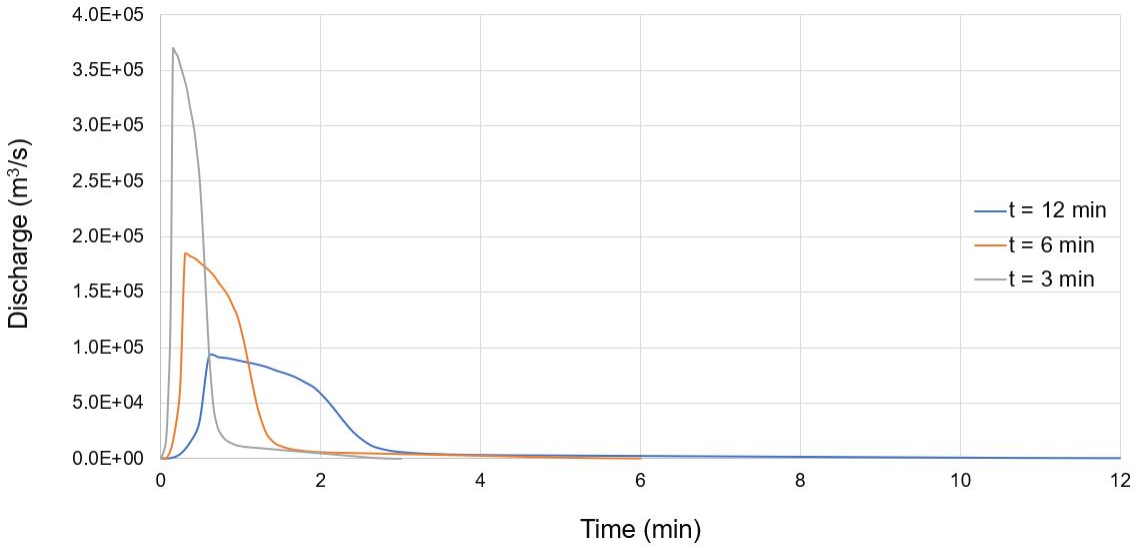

Figure 5.1: Hydrographs for different failure durations.

5.1.2. Simulation results

In this section, the results of the sensitivity analyses are presented. The parameters that are varied are the volumetric concentration (C_v), Manning's roughness (n) and the duration of failure (t), with the values previously explained in section 5.1.1. The results compared and assessed are the initial and final flooding area.

The primary impact zone is delimited with the maximum velocity value registered during the entire simulation time for each element; the final inundation area is calculated with the maximum flow depth value obtained for each cell for the whole simulation time. Two long-sections are used to visualise the differences regarding velocities and depth for a certain time step and for the different scenarios. Figure 5.2 depicts the primary impact zone of the reference case (section 5.1) and the long-sections. Long-section 1 is not completely vertical in order to intersect the front wave of each simulation; long-section 2 is prolonged to cover all the results. The functions plotted in these long-sections are for the same time step, thus the flood wave is expected to be in different positions along the section considering the magnitude of the input parameter.

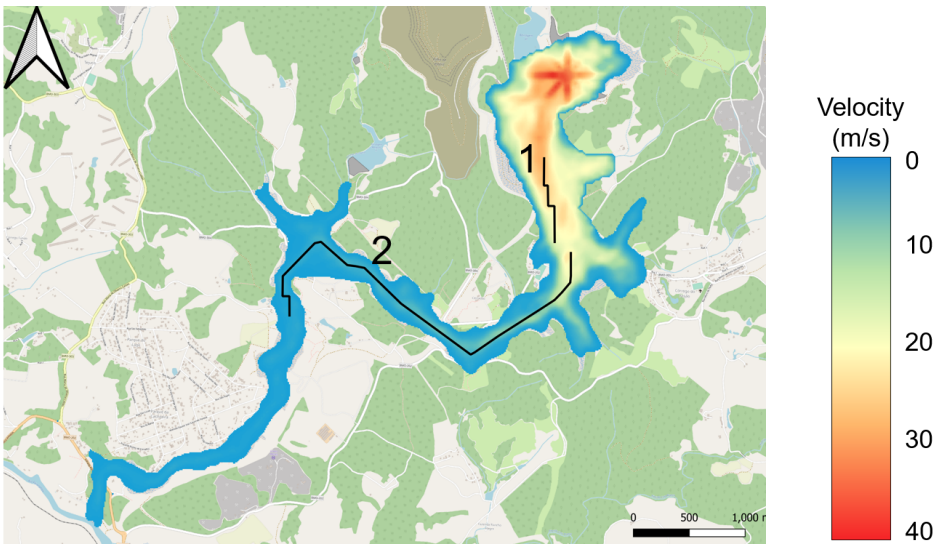

Figure 5.2: Primary impact zone after failure of dam B-I and long-sections.

1. RESULTS: VOLUMETRIC CONCENTRATION

The predictions of what would happen in case of decreasing or increasing the volumes were explained in section 5.1.1. A tentative conclusion drawn was that an increase in the volumetric concentration would lead to low velocity values and a reduced primary impact zone similar to the final inundated area.

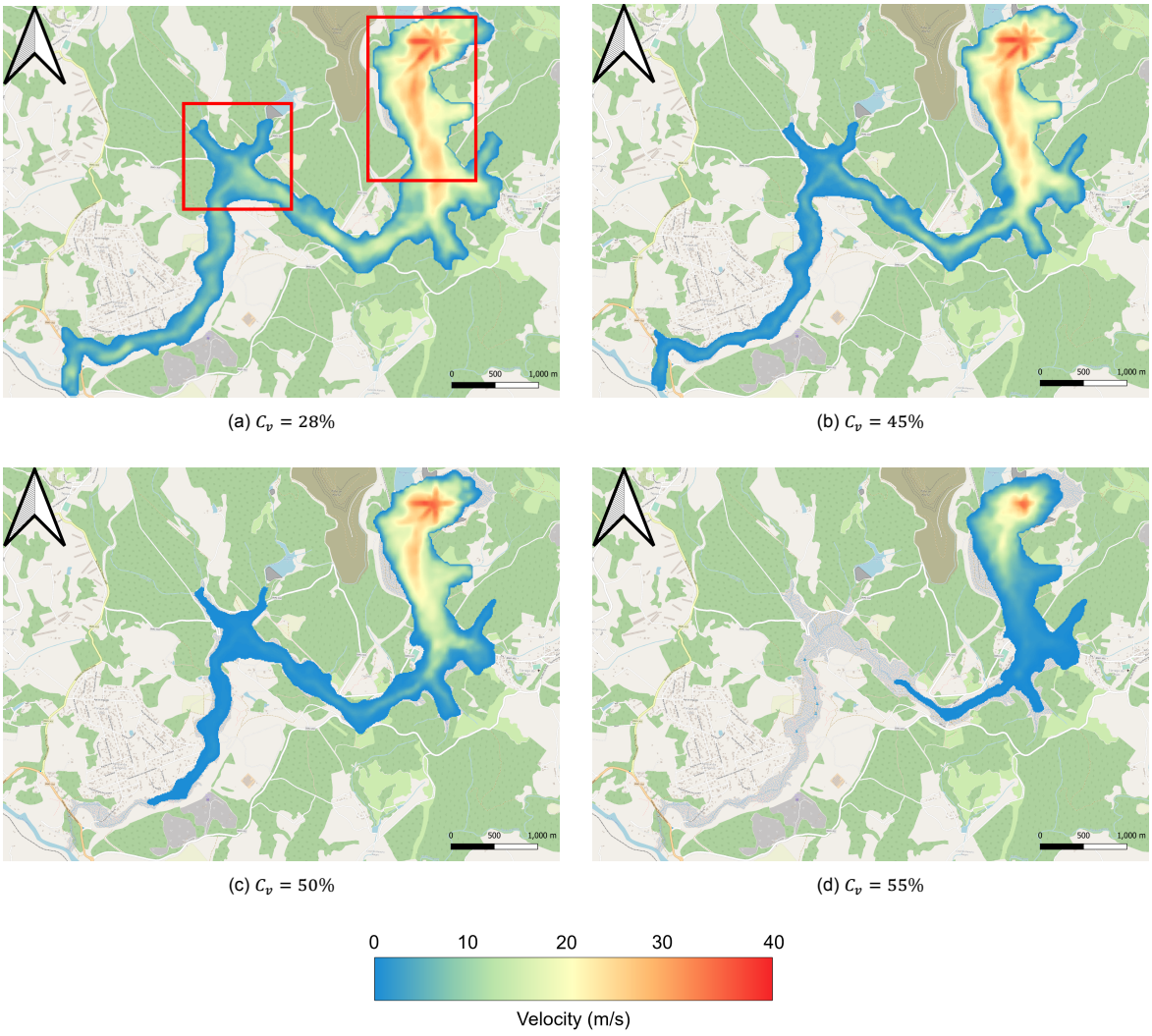

(a) $C_v = 28\%$ (b) $C_v = 45\%$

(c) $C_v = 50\%$ (d) $C_v = 55\%$

Figure 5.3: Primary impact area for different C_v. Rectangles mark examples of area where the flow is accumulated in case of low values of C_v. Note that in those areas, an increase of C_v leads to less fluid accumulation and low velocity values.

Figure 5.3 compares the results between four C_v. The difference regarding the flooding area is significant. For low values of C_v, high velocity values are maintained longer distances, which reduces the arrival time to the river Paraopeda in 28 minutes ($C_V = 28\%$); the high velocity values cause a larger extension of the flood wave through the area in comparison to the rest. The maximum time for the simulations was set to 3 hours, and scenarios $C_v = 50\%$ and $C_v = 55\%$ were not able to reach the downstream boundary condition within that time. The large amount of sediments caused an increment of the viscosity, yield strength the the dispersion forces within the fluid, which caused such decrease in velocity values near the failure location and the overall extension of the flooding area. Variations with respect to inundated area are visible in the areas marked in red rectangles in Figure 5.3 (a); in those locations the flooded region is narrower for high values of C_v.

For long-section 1, the front velocity profiles are plotted for the same time step (108 seconds after failure) for each C_v scenario. Figure 5.4 illustrates the results.

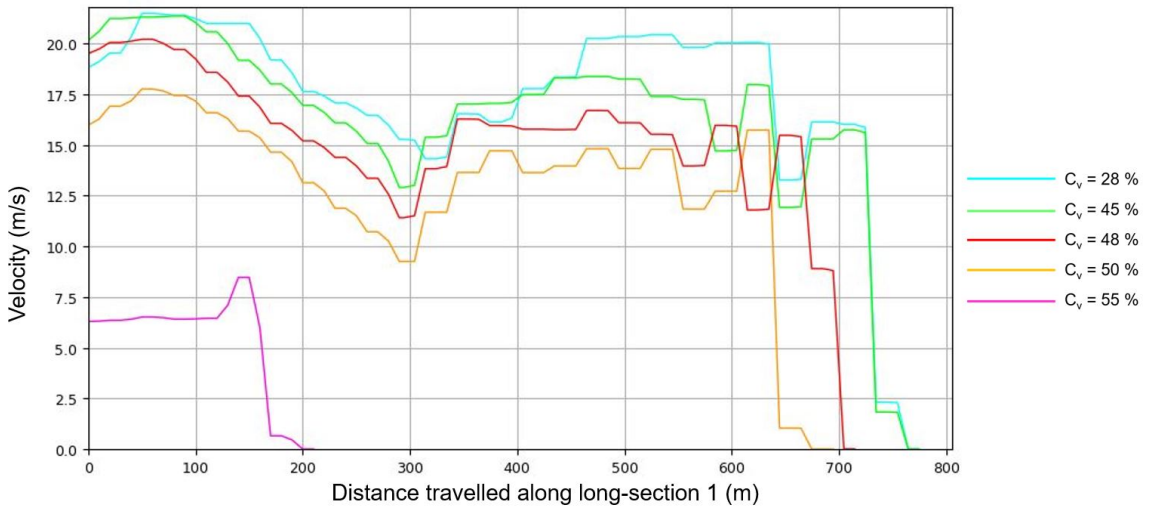

Figure 5.4: Velocity profile along long-section 1 for different C_v.

At 108 seconds after failure, the flood wave of $C_v = 28\%$ is the one with a higher front velocity, followed by $C_v = 45\%$ which has slightly a lower velocity. Thereafter, the average velocity is reduced together with an increase of the volumetric concentration. For the same time step the $C_v = 48\%$ is approximately 60 m behind and a lower front velocity and the same conclusion for $C_v = 50\%$. Note that there are more significant variations with an increase of 5% in the volumetric concentration between $C_v = 50 - 55\%$ than in $C_v = 45 - 50\%$. Even though the material is still in a loose state ($C_v = 55\%$), the reduced amount of water is unable to mobilise the mass at the same velocity as the other scenarios. For long-section 2, the differences in velocity and location are even more visible for the same time step: $C_v = 28\%$ is first on the graph and thereafter the other C_v follows at a slower pace. The velocity values are significantly reduced, to the order of 6 m/s (results in Appendix B).

To examine the final inundated area, the comparison of the four scenarios with the maximum flow depth map is depicted in Figure 5.5.

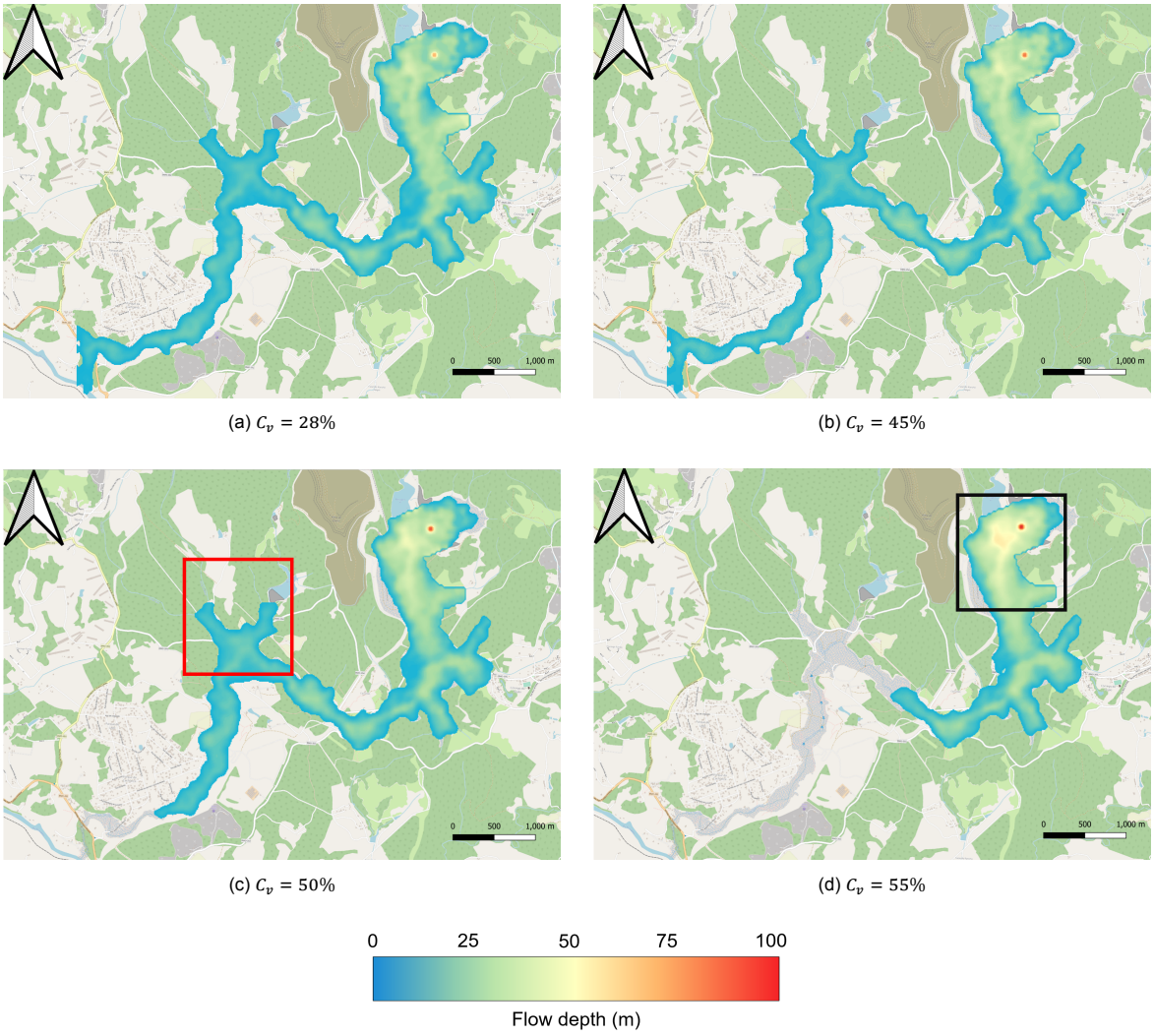

(a) $C_v = 28\%$ (b) $C_v = 45\%$

(c) $C_v = 50\%$ (d) $C_v = 55\%$

Figure 5.5: Final inundated area for different C_v. Red rectangle indicates an example of a region where the mixture is accumulated when increasing C_v. Black rectangle marks the area where the highest flow depths values are found, which are maximum for $C_v = 55\%$ near the failure location.

The extension of the final flooded area is larger for low values of C_v, nevertheless maximum depths are registered for higher values of volumetric concentration. $C_v = 28\%$ and $C_v = 45\%$ present similar results, but $C_v = 50\%$ shows more fluid accumulation at the edges of the flooded area (like in the red rectangle in c) Figure 5.5) and is wider along the drainage path than the previous cases. The highest depths are registered for $C_v = 55\%$, due to slow motion of the mixture and accumulation of it. Maximum depth values are registered for the highest C_v near the failure location (black rectangle in d) in Figure 5.5).

For long-section 1, Figure 5.6 illustrates the depth profiles for 108 seconds after failure and for each C_v scenario.

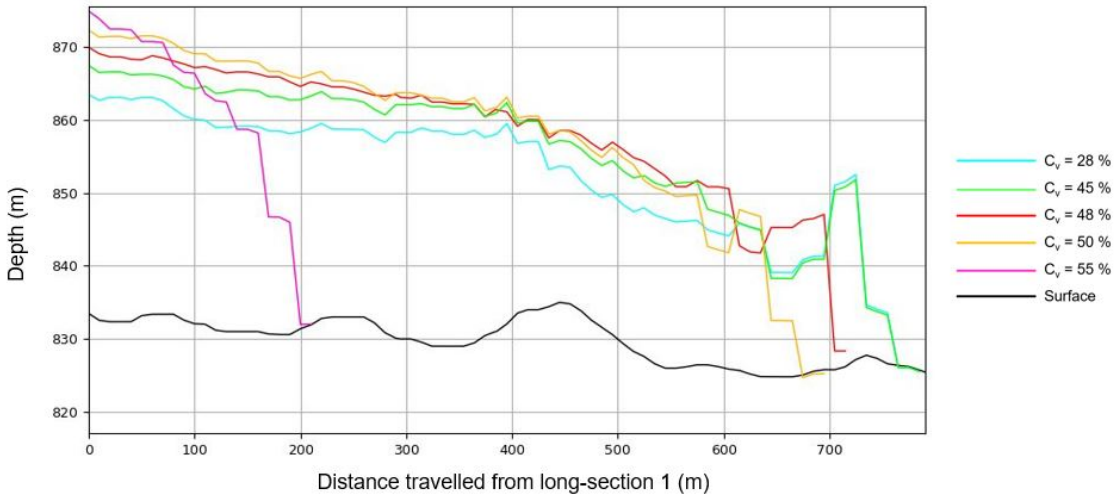

Figure 5.6: Depth profile along long-section 1 for different C_v

The high velocity of $C_v = 28\%$ makes only the front wave taller than the other scenarios, but very similar to $C_v = 45\%$ (as in Figure 5.4). Over distance, the depth is less for low values of C_v due to large velocity values that cause rapid movement of the mixture and prevent accumulation. That is the reason why, along long-section 1 the function $C_v = 50\%$ has the highest depth among the 4 fast flood waves: small velocity values induce to accumulation of material. Case $C_v = 55\%$ deals with lowest velocity values, which cause that for the same time the front wave is approximately 500 m behind the rest and with a higher depth.

Table 5.2 presents the area values for the initial and final inundated surface.

Table 5.2: Area inundated for each C_v

C_v (%)	INITIAL FLOODING AREA (Mm^2)	FINAL FLOODING AREA (Mm^2)
28	4.08	4.04
45	3.31	3.68
48	3.10	3.32
50	2.56	3.14
55	1.41	2.43

Overall, there is a significant variation respect the initial and final inundation area for when decreasing C_V. For $C_v = 55\%$ the change in area results in more than $1\ Mm^2$, due to the deposition of the mixture after a certain time of failure. This difference decreases together with C_v, such as case $C_v = 28\%$ where the initial flooding area is greater than the final, which means that the mixture governed by water has reduced its extension due to its ease to flow. It can be concluded that an augment of the C_v causes an increase of the yield strength, viscosity, dispersive and turbulent forces, thus a larger shear stress is needed to produce deformation.

2. RESULTS: SURFACE ROUGHNESS

The friction intensity between the fluid and the surface regimes the flow velocity over the domain, which it will be higher for low values of *n*.

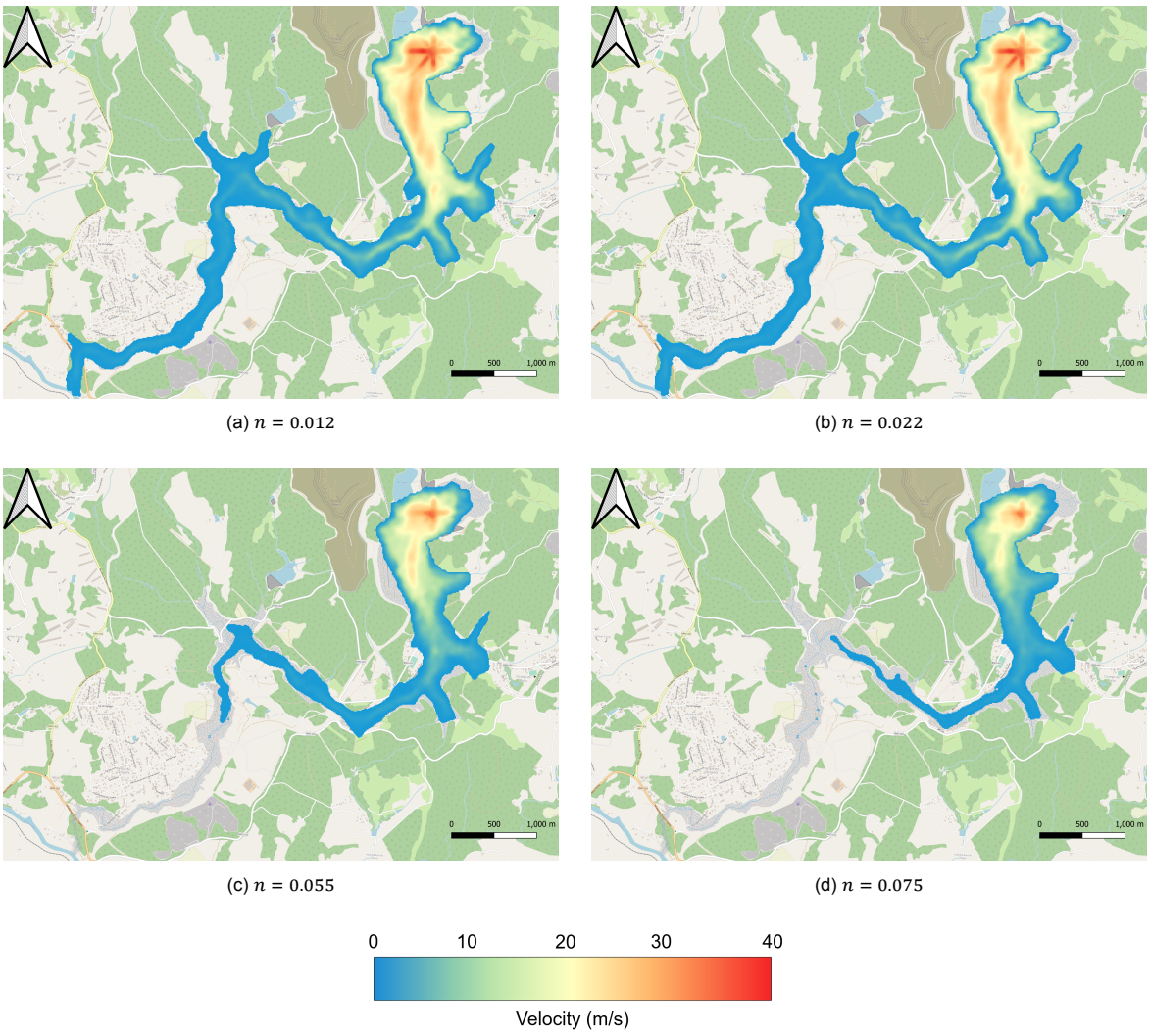

(a) $n = 0.012$ (b) $n = 0.022$

(c) $n = 0.055$ (d) $n = 0.075$

Figure 5.7: Primary impact zone for different Manning's roughness values (n). Note that the high velocity values near the failure location decrease when increasing *n*.

The results obtained with $n = 0.012$ and $n = 0.022$ are similar between them, meaning that for low values of Manning's roughness, the extent of the primary zone and high velocity values is approximately equal. However, for large values of n (cases c) and d) in Figure 5.7), the flood wave does not reach the river in 3 hours and the high velocity field is less extended. In all four scenarios, there are high velocity values near the failure location, but those are mitigated rapidly in case of large n values or smoothed for low n's.

The influence of friction between mixture and surface can be visualised at the first long-section at 108 seconds after failure in Figure 5.8 .

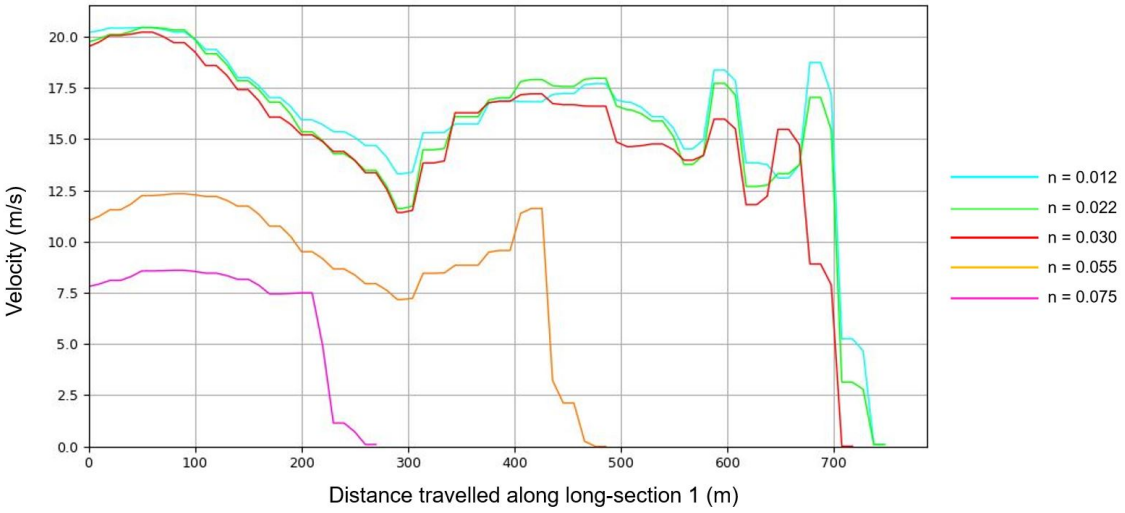

Figure 5.8: Velocity profile along long-section 1 for different n.

For small *n*-values (between 0.012 and 0.022) the differences are insignificant. The front velocity is slightly higher for $n = 0.012$ but very similar to scenario $n = 0.022$, where *n* increases 0.01. Such similarity was expected since both n values are within the range of *medium* amount of vegetation from Table 4.4. There is a bigger contrast between $n = 0.022$ and $n = 0.030$, in which the position of the flood wave is 30 m behind $n = 0.022$ scenario and the average front velocity is minimised. $n = 0.030$ falls in the range of *large* amount of vegetation from Table 4.4, meaning that more obstacles are encountered along the drainage path. Considering a *very large* amount of vegetation ($n = 0.055$ and $n = 0.075$) derives into low velocity values that cause a slower movement of the flood wave. The rate of change in the average front velocity is not constant, for instance: increasing $n = 0.012$ to $n = 0.030$ leads to a reduction in the average front velocity of only 16%. On the contrary, when increasing the $n = 0.030$ to $n = 0.055$ (similar increment as before), the reduction in the average front velocity is 31%. For long-section 2, the velocity values are minimised. The first three scenarios ($n = 0.012$ to $n = 0.030$) are flowing at a similar velocities, which are about $2m/s$ and the flood waves are maintained the same position. Unlike cases $n = 0.055$ to $n = 0.075$, where the friction between mixture and soil caused a reduction in velocity (approximately $1m/s$) and a slower progression of the flood waves (see Appendix B).

Figure 5.9 illustrates the comparison between all n cases for the final inundated area.

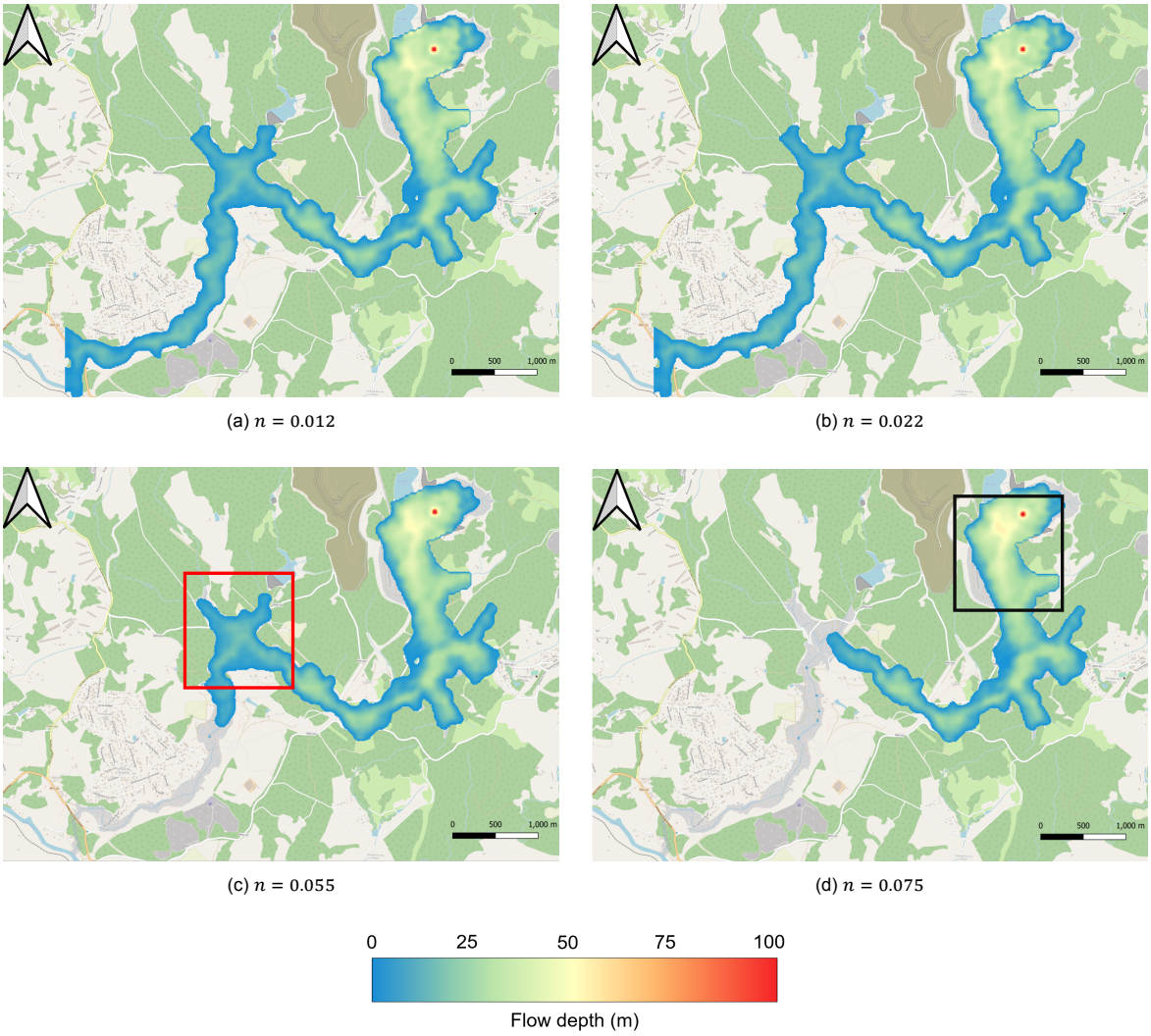

(a) $n = 0.012$ (b) $n = 0.022$

(c) $n = 0.055$ (d) $n = 0.075$

Figure 5.9: Final flooding area for different Manning's roughness values (n). Red rectangle indicates an example of a region where the mixture is accumulated when increasing n. Black rectangle marks the area where the highest flow depths values are registered, which are maximum for $n = 0.075$ near the failure location.

For scenarios a) and b), the inundated area and the depths computed are mainly equal. Such result can be verified with the same velocity values obtained from the previous analyses. In contrast with cases c) and d), where the flood wave is unable to arrive at the downstream area within 3 hours, the fluid is accumulated at the edge of the flooding extension (red rectangle in c) in Figure 5.9). The significant friction between surface and fluid in case d) causes lower velocity values, thus more accumulation of the mixture. Comparing picture a) and b) with c) and d) from 5.9, the yellow areas (black rectangle in d) in Figure 5.9) are more intense near the failure location. Thereafter, those are reduced like with the velocity simulations.

Figure 5.10 shows the flow depths of the front flood wave for each *n* simulation along long-section 1.

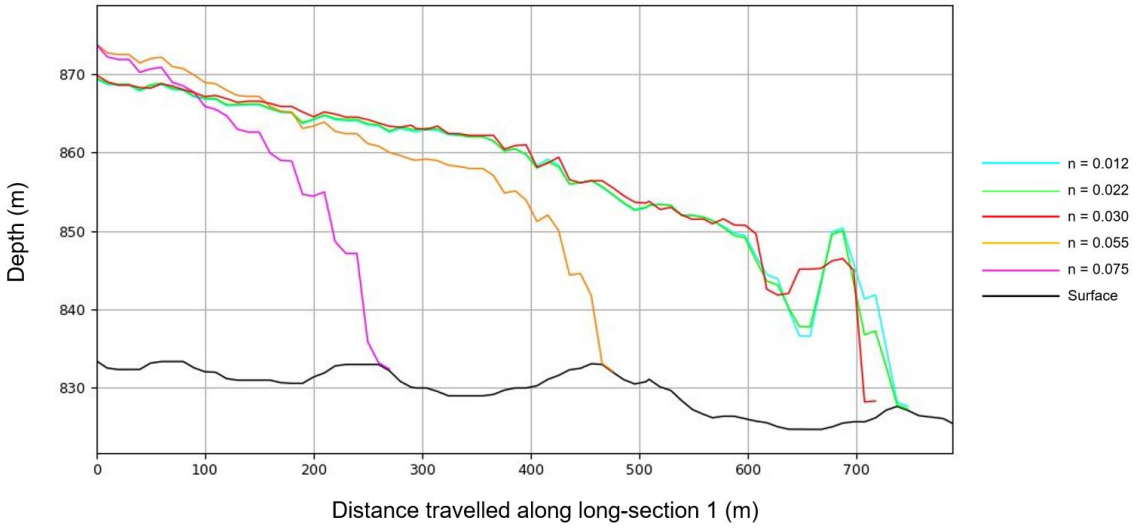

Figure 5.10: Depth profile along long-section 1 for different n.

The high velocity values for the first three cases locate the corresponding flood waves at a similar location, with $n = 0.030$ a bit behind. $n = 0.055$ is placed 300 meters behind with a higher flow depth, respect lower values of n. Lastly, $n = 0.075$ presents the highest flow depth at the left-hand side of the graph, since it is 500 meters behind and the high friction between soil and surface make difficult its spread over the surface.

Table 5.3 shows the area values for the initial and final flooding ares for different *n*-values.

Table 5.3: Area inundated for each n

SURFACE ROUGHNESS	INITIAL FLOODING AREA (Mm^2)	FINAL FLOODING AREA (Mm^2)
$n = 0.012$	3.52	3.62
$n = 0.022$	3.37	3.54
$n = 0.030$	3.10	3.32
$n = 0.055$	2.19	2.82
$n = 0.075$	1.77	2.71

In general, there is a reduction of both areas when increasing the roughness value. Additionally, such increase of *n* also causes a greater difference between initial and final flooding area. For instance, for $n = 0.012$ the initial and final area are very similar, with only a $0.1Mm^2$ difference caused by the accumulation of fluid after a certain time. The same conclusion is derived for $n = 0.022$ (but with more difference between areas), since both *n* fall into the same category of amount of vegetation. Therefore, values within the range of *small*, *medium* and the lower boundary of *large* give results that are comparable, they differ within a variation of 12% respect the initial flooding area and 8 % the final one (comparison between $n = 0.012$ and $n = 0.030$). For values $n > 0.030$ both areas are significantly reduced. The initial inundated area is 43% less for $n = 0.075$ compared to $n = 0.030$; the final flooding area is 23% less between them.

3. FAILURE DURATION

The time of failure is basically reflected on the velocity values near the breach location. The failure duration is linked with the volume within the reservoir and the velocity needed for the mixture in order to leave the reservoir in that period of time. The original duration of failure was 6 minutes; to assess the effects of such time for the flooding areas, it has been reduced in half and also doubled: 3 and 12 minutes (Figure 5.1).

The primary impact zone is illustrated in Figure 5.11, for times: 3, 6 and 12 minutes. The reference case for Brumadinho (6 minutes) has been added to make an easier comparison.

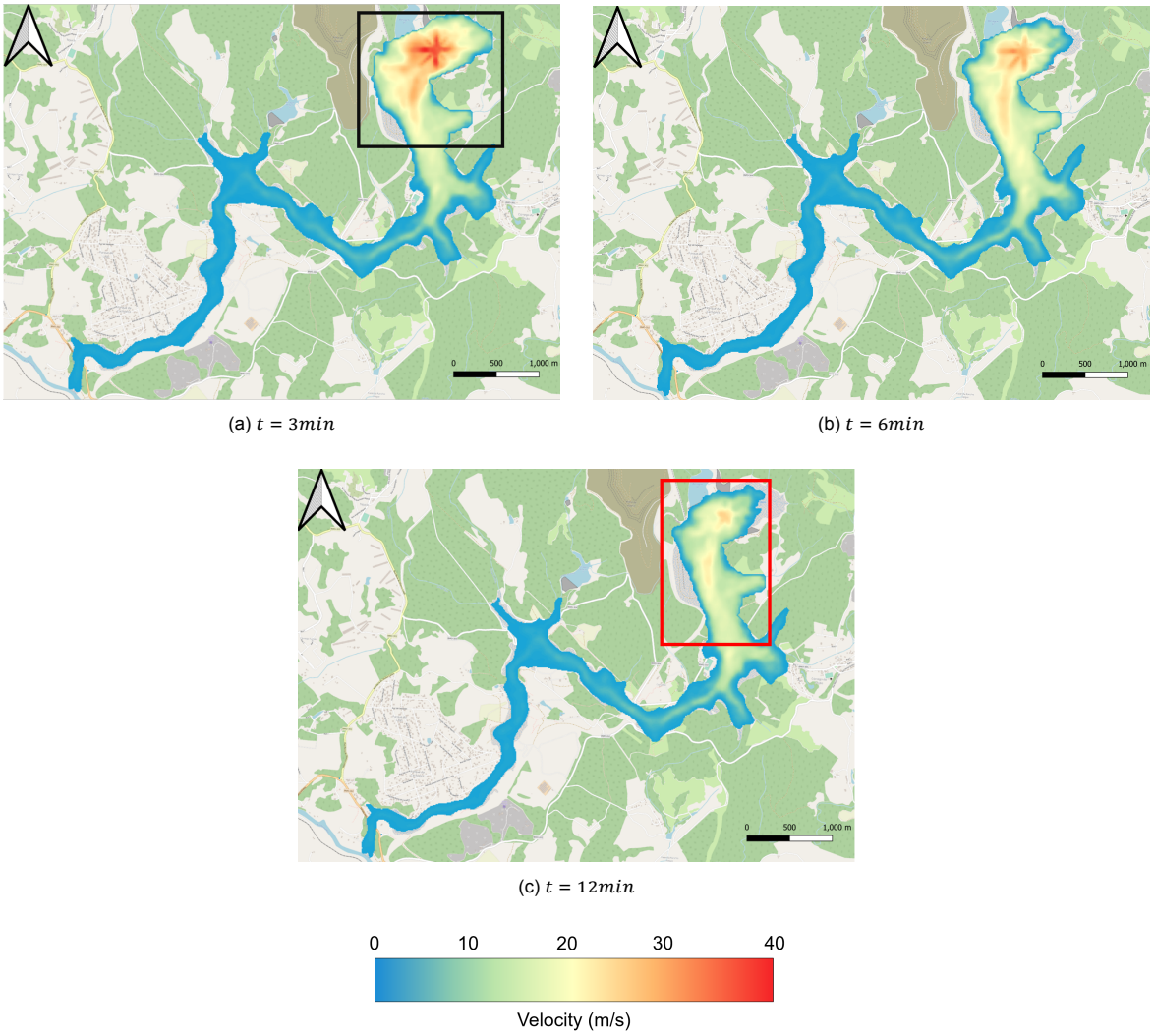

(a) $t = 3min$

(b) $t = 6min$

(c) $t = 12min$

Figure 5.11: Initial flooding area for different failure duration. Black rectangle indicates the area where the maximum velocity values are registered for low values of t, which decrease when increasing the failure duration. The red rectangle marks the reduction of the inundated area near the failure location when increasing the hydrograph time.

For all three cases, the flood wave arrives at the river Paraopeda within 3 hours but at different velocities. The main differences are near the failure location, which is where all the volume is released at different rhythm. For $t = 3\ min$, the extent of the high velocity field and the area inundated is larger compared to two other situations (black rectangle in (a) in Figure 5.11). At that same region, for $t = 12\ min$, the velocities are lower and also the area inundated is less (red rectangle in (c) in Figure 5.11).

For 108 seconds after failure, the velocity profiles are plotted for long-section 1 in Figure 5.12 .

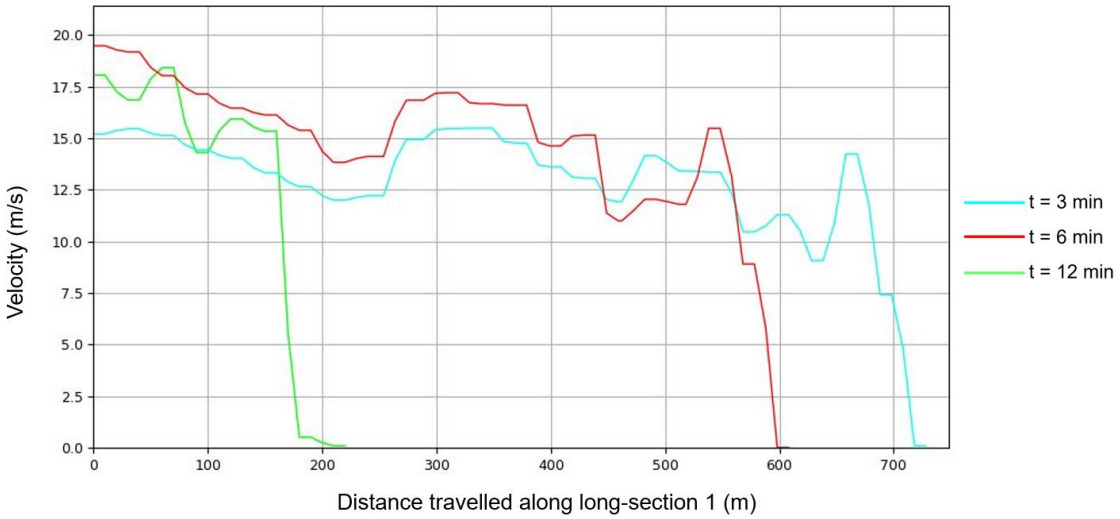

Figure 5.12: Velocity profile along long-section 1 for different failure times.

From the previously analyses, it was concluded that for shorter failure times the velocity values near the breach were higher. Therefore, in long-section 1 (Figure 5.12) the fastest function is $t = 3\ min$. Notice that between the functions of $t = 6\ min$ and $t = 12\ min$, the fast curve is 400 m in front of the slow one, but both have the same average front velocity ($\sim 8m/s$). This displacement in space (400 m) but for the same time step indicate that when the red curve was at 200 m from long-section 1, it had a higher velocity than the green curve. Thus, $t = 12\ min$ curve flows in a slower pace. The same conclusions are drawn for long-section 2, where the distance between each curve is even larger and the velocity values are reduced to $\sim 2m/s$.

Figure 5.13 depicts the final inundation areas for each duration of failure.

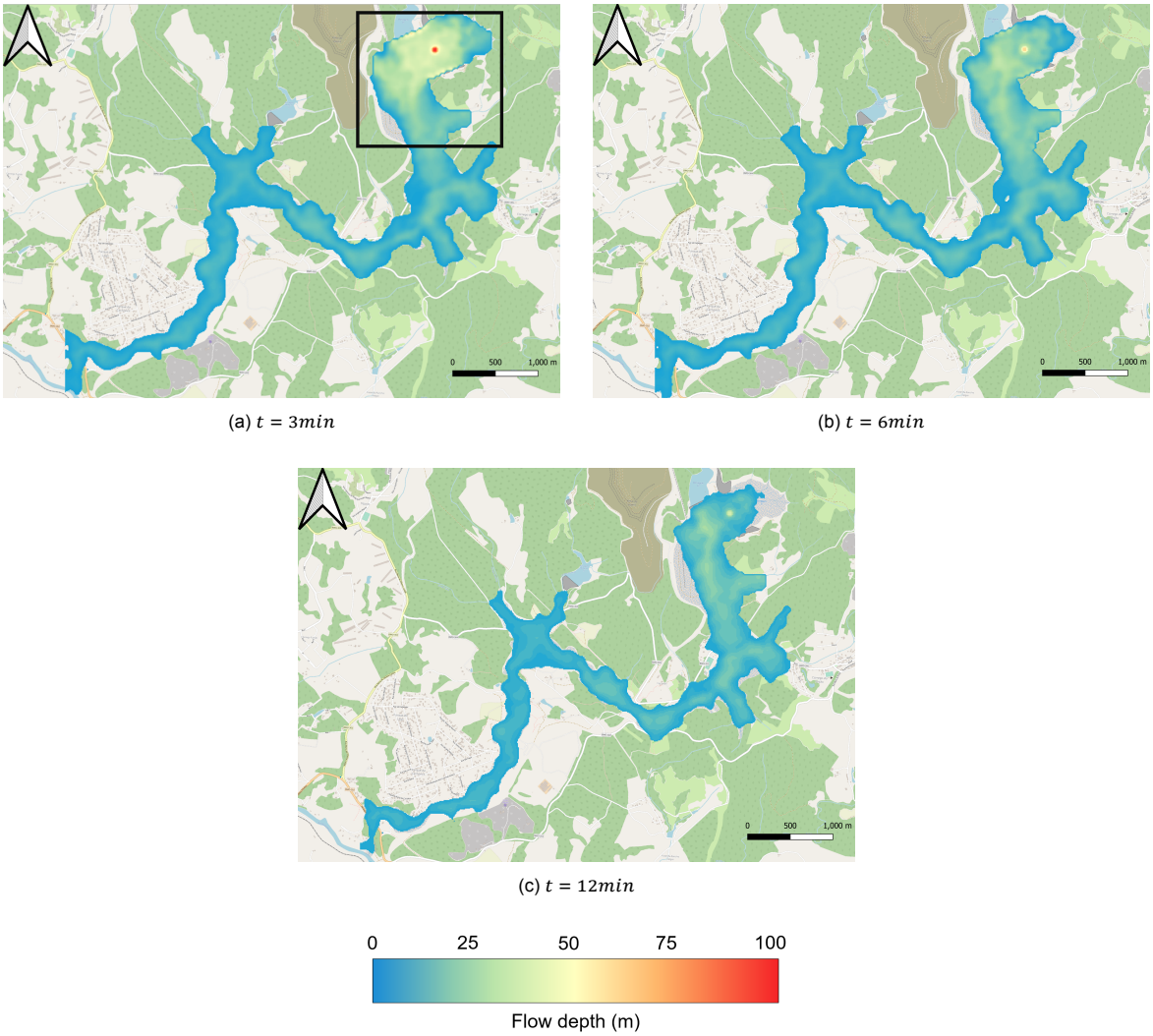

(a) $t = 3min$ (b) $t = 6min$

(c) $t = 12min$

Figure 5.13: Final flooding area for different failure duration. The black rectangle marks the area where highest flow depths are registered and the extension of the flooding area in that location, which is maximum for low values of t.

In Figure 5.13 for $t = 3\ min$, the high velocities make the final inundation area larger compared to the other times, due to fast accumulation and deposition of fluid at the edges of the flooded area. In these analyses the highest flow depths are registered for $t = 3\ min$, due to the sudden release of volume that causes an increase in the height of the front part of the flood wave (black rectangle in a) in Figure 5.13). In that same area for $t = 12\ min$, the depths estimated are lower and also the extent of the inundated surface. Note as well that the width of the flooding area is reduced for $t = 12\ min$, the low values in velocity mitigate the spread of the flood wave along the drainage path.

Figure 5.14 shows the flow depth variations at long-section 1 for 108 seconds after failure.

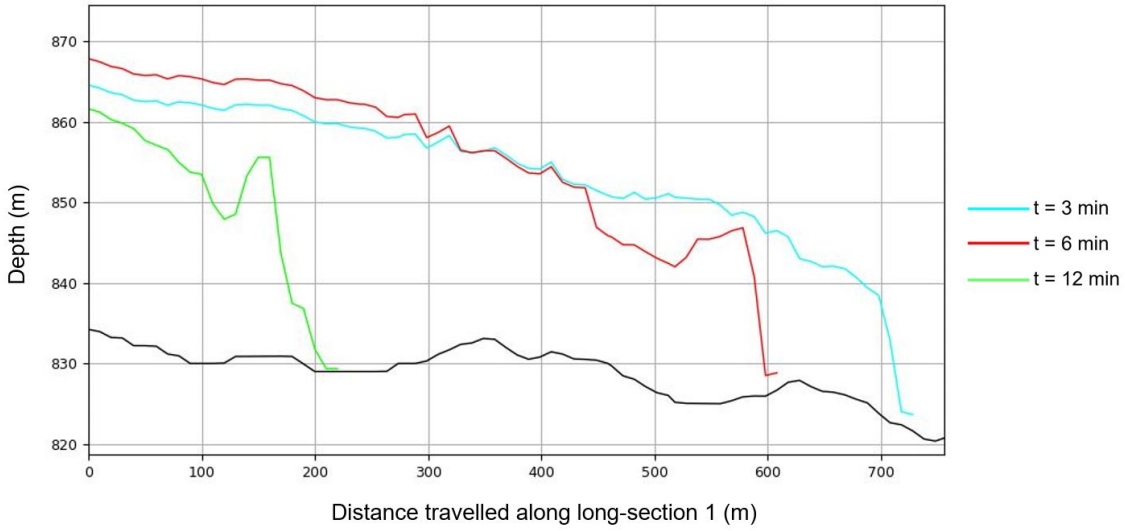

Figure 5.14: Depth profile along long-section 1 for different failure times.

The position of long-section 1 does not capture the highest flow depth values near the breach location. However, it can be seen in Figure 5.14 that the $t = 3\ min$ curve is in a more advanced location respect the others and with a $H = 14\ m$ approximately. For the same time step, the $t = 6\ min$ flood wave is 100 m behind and it is 21 m high; for $t = 12\ min$ the front wave is 24 m high and it is located 400 m behind the previous case. Thus, by the time the $t = 12\ min$ reaches the same location as $t = 3$ and $t = 6\ min$, the flow depth will be less compared to the other two functions at that same place.For long-section 2, the distances between each flood wave are within the range of 500 meters. The average flow depths are around 3 meters (see results in Appendix B).

The measured inundated areas before and after failure are summarised in Table 5.4.

Table 5.4: Area inundated for each duration of failure

DURATION OF FAILURE	INITIAL FLOODING AREA (Mm^2)	FINAL FLOODING AREA (Mm^2)
$t = 3\ min$	3.56	4.21
$t = 6\ min$	3.10	3.32
$t = 12\ min$	2.72	3.04

Both areas increase for a short failure duration. As it was stated before, the same amount of volume needs to be released from the reservoir, therefore a shorter time leads to higher velocities. The largest difference between the initial and final failure is for $t = 3\ min$, $0.65 Mm^2$. The high velocity of the flow causes a further spread of the material along the drainage path and, thereafter, part of the fluid is depositioned there. On the contrary, $t = 12\ min$ involves lower velocities, which make the fluid to follow the centerline of the drainage path more accurately and with less deviations towards the edges.

5.1.3. Results: Initial flooding area

Figure 5.15 illustrates which input parameter is most sensitive to the model regarding the primary impact zone.

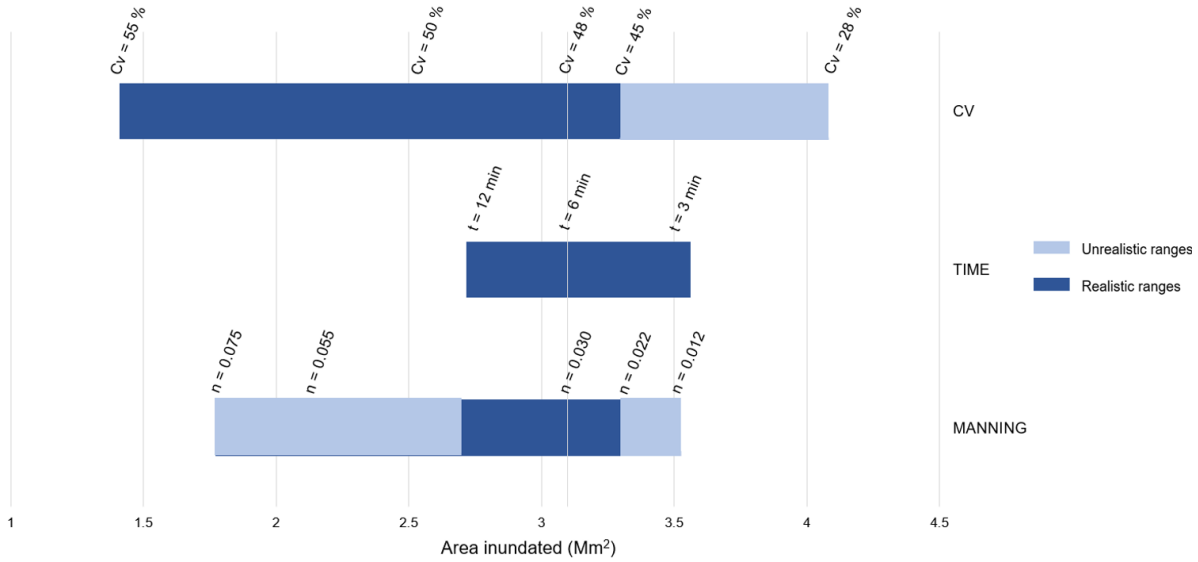

Figure 5.15: Chart to indicate the impact on the calculated initial inundation area based on a range of input input parameters.

From the diagram in Figure 5.15, a tentative conclusion can be drawn that the most sensitive parameter is the volumetric concentration, followed by the Manning's roughness value and the duration of failure. A further segmentation of the ranges between realistic and unrealistic can be done in order to understand the realism of the parameter ranges. Therefore, the range for each parameter has been divided according to the following reasons:

- $28 < C_v < 45$ %: it is considered unrealistic to have a volumetric concentration that accounts twice the volume of water than sediments (as in $C_v = 28\%$). Water within the reservoir and mine tailings dams significantly influences the stability of such structures, leading to lower values of safety of factor and higher risks of liquefaction (Ruiz et al., 2021). Drainage systems are installed within the impoundment to reduce the phreatic level as much as possible. Thus, in case of dam break and for low water levels, a mud flood behaviour should not be expected. That is the reason why, the range $45 < C_v < 55$ % which corresponds to mudflow behaviour is more suitable for the situation. A $C_v = 55\%$ means that the volume of water is less than the sediments, therefore the correct use of drainage systems and a low phreatic level are ensured.

- $0.040 < n < 0.075$: According to Google Earth, before failure the amount of vegetation through the drainage path was not very large and there were also some buildings and agricultural fields. Therefore, the category of *very large* from Table 4.4 considers the simulations made with $n = 0.055$ and $n = 0.075$, which are accounted for unsuitable values. Furthermore, the unrealistic range for Manning's roughness is extended until high values within the range of *large* (0.040) for the same reasons just mentioned.

- $0.012 < n < 0.022$: from the satellite images before failure and according to the description given by Arcement and Schneider, 1989, roughness values within the category of *medium* are not realistic for this case.

From Figure 5.15 and the reasons just explained, it can be concluded that the most sensitive parameter is the volumetric concentration. A large amount of sediments ($C_v = 55\%$) gives an increase in each component of the rheological quadratic model (equation 3.18). Thus a higher total shear stress is needed to mobilise the mixture, and as a consequence, the primary impact zone is reduced. The second most sensitive parameter is the duration of failure. For the same C_v, the breach hydrograph

determines the velocity of the flood wave, which is large near the failure location but gets smaller with distance due to the rheological properties of the fluid. The primary impact zone is more influenced by a reduction in the failure duration of only 3 minutes than an increment of failure duration of 6 minutes. Lastly, Manning's roughness value has a lower impact but still considerable.

Comparing $C_v = 45\%$ and $t = 3\ min$ in the upper boundary of the tornado chart, the reduced failure duration with $C_v = 48\%$ has more impact on the primary inundated area than $t = 6\ min$ with $C_v = 45\%$. The reduced times of the breach hydrograph cause high velocity values that are difficult to reduce by the $C_v = 48\%$. On the other hand, for larger failure times and $C_v = 28\%$, the amount of sediments will have little effect on the spread of the mudflow through the area. Furthermore, the initial flooding area is smaller for larger values of C_v than large failure duration. The relatively large volume of solids will increase the shear stresses within the fluid, thus the deformation of is minimised.

5.1.4. Results: Final flooding area

Figure 5.16 illustrates the results obtained from the maximum depth values per element from each simulation done for the simulation of the failure of dam B-I.

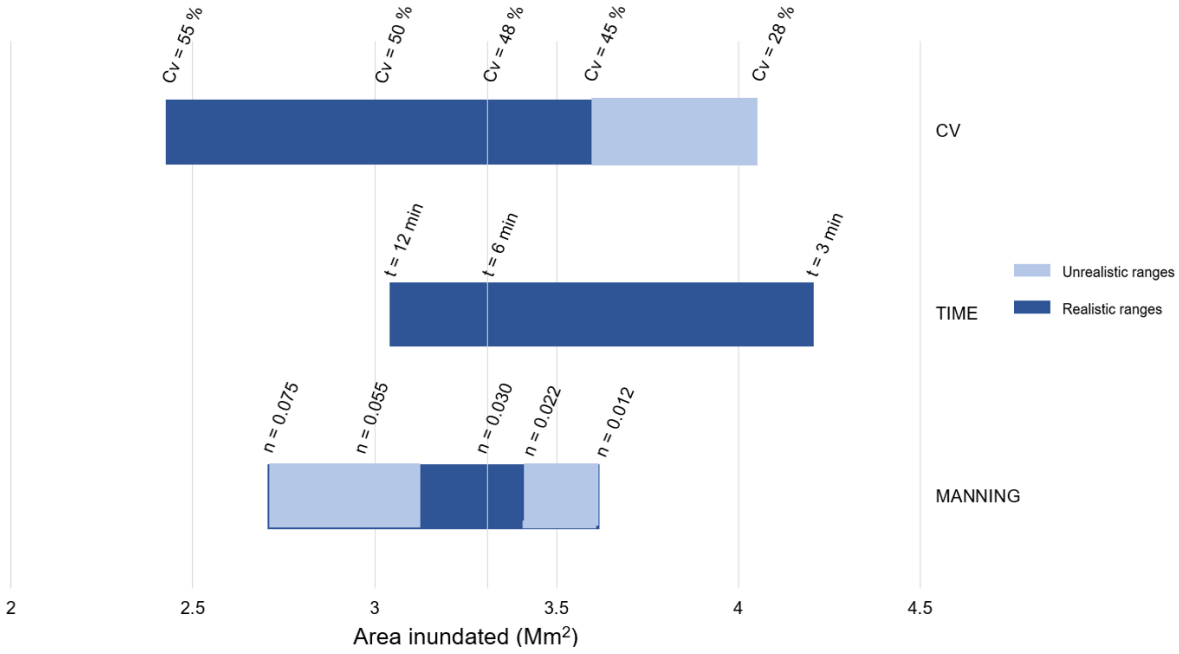

Figure 5.16: Chart to indicate the impact on the calculated final inundation area based on a range of input input parameters.

From Figure 5.16, it is concluded that the most sensitive parameter is the duration of failure together with the volumetric concentration and finally the Manning's roughness value. However, from the assumptions stated before in section 5.1.3 about the realism of each value, the ranges of influence are reduced but the conclusions are maintained.

Comparing the results of C_v and t, on the right hand side of the graph in Figure 5.16, the value for the final flooding area for $t = 3\ min$ and $C_v = 48\%$ is larger than $t = 6\ min$ and $C_v = 28\%$. The high velocities caused by the sudden release of V_R for $t = 3\ min$ drive the hyper-concentrated fluid to further locations than $C_{=}28\%$. Since $t = 3\ min$ considers a $C_v = 48\%$, part of the fluid will deposit over the inundated area. On the other hand, $C_{=}28\%$ involve high velocity values that are unable to spread as far as $t = 3\ min$ scenario and the large amount of water will reduce accumulation of matter.

Furthermore, on the left hand side of the chart, the final inundation area result is comparable when increasing the C_v with a 2% and keeping the duration of failure constant with 6 minutes; or increasing

the duration of failure with 6 minutes and keeping constant the C_v.

5.2. HEC-RAS: Dam B-I failure

The failure of dam B-I has also been simulated with HEC-RAS in order to compare the results with FLO-2D. HEC-RAS has the option that the user can choose which rheological model is used: Bingham plastic model, Herschel-Bulkley model or the O'Brien quadratic model (see in section 2.3.2). FLO-2D has the O'Brien quadratic model implemented. Section 4.2 explained the governing equations used for HEC-RAS. A one characteristic with respect to FLO-2D was the use of the Shallow Water Equations for debris flows and the turbulent eddy viscosity in them. Therefore, to compare the how each model performance, the same simulation is done with different values for the volumetric concentration provided in section 5.1.3.

For this Msc thesis, the latest version 6.0 of HEC-RAS is used. One of the new features of this version is the possibility to introduce rheological properties, such as viscosity and yield strength, an use non-Newtonian fluids in the simulations. It is stated in the HEC-RAS User's Manual (Brunner, 2016) and in their website that it is a trial version and there are no complex simulations performed yet with that new feature. At the first attempt to use HEC-RAS to model the resulting flood wave of failure of dam B-I, some problems were encountered with the arrival times of the flood wave to the river Paraopeba, which was 55 minutes. A large difference between the actual arrival time and FLO-2D simulation (2.5 hours). Stanford Gibson (member of the HEC-RAS development team) explained (personal comment in email 04/12/2021) that the non-Newtonian feature is still a *beta* version and that the O'Brien method was still not tested, which could explain the unexpected results. Additionally, it was suggested to use the Bingham plastic model, since it was tested against a flume experiment with mud (Gibson et al., 2021). Therefore, the simulations performed are as follows.

1. Using water and a different cell size to asses the accuracy (cell size of 20, 30 and 40 m).
2. O'Brien quadratic model for $C_v = 45\%$, $C_v = 48\%$ and $C_v = 55\%$.
3. Bingham plastic model for $C_v = 45\%$, $C_v = 48\%$ and $C_v = 55\%$.

5.2.1. Water

HEC-RAS was calibrated in section 4.5 with the formulas of fluid motion. In this section, the front wave velocity is determined with water along long-section 1 (same as in Figure 4.7) to assess the influence of the cell size in the results. Three cell sizes are chosen: 20, 30 and 40 m. The results show that the average front velocity is maintained and there are slight changes on the location of the flood wave along the drainage path (Figure 5.17). It can be compared with the front velocity obtained with FLO-2D at a similar location (Figure 4.7), where the front velocities are comparable ($\sim 20m/s$). Furthermore, the arrival times of water at the river Paraopeba for cell size 30 m is 25 minutes and only 30 seconds more and less between the two other simulations. Therefore, the average value of 30 as the cell size is chosen for the next simulations.

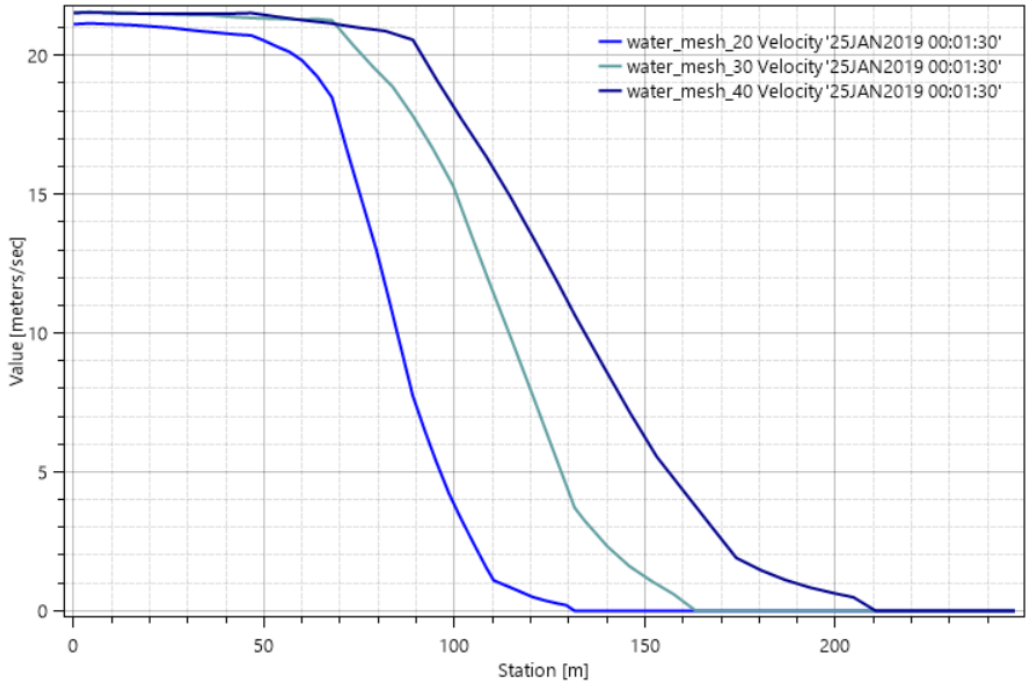

Figure 5.17: Front velocity at time 1.30 minutes after failure for different cell sizes.

5.2.2. O'Brien Quadratic model

The constant input parameters for the model are the Manning's roughness value ($n = 0.030$) and the breach hydrograph with a duration of 6 minutes (Figure 4.5). Regarding the rheological model, the input parameters are printed in Table 5.5.

Table 5.5: Input data for the non-Newtonian properties

C_v (%)	τ_y (N/m^2)	μ $(N \cdot s/m^2)$	ρ_m (kg/m^3)	d_s (m)	ρ_s (kg/m^3)
45	100	177	1970	0.000055	3155
48	243	478	2034	0.000055	3155
55	1914	4852	2185	0.000055	3155

Figure 5.18 illustrates the front part of the flood wave at $t = 90s$ and the first and second long-sections in HEC-RAS. It also shows the location of long-sections 1 and 2.

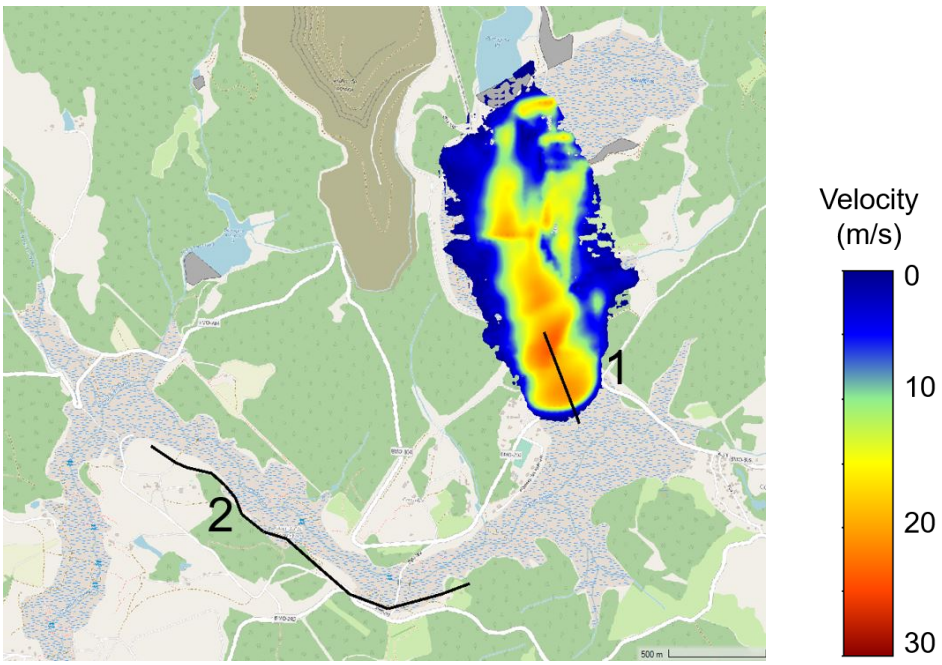

Figure 5.18: Flood wave at time 90 seconds after failure and along long-section 1. $C_v = 48\%$.

Figures 5.19 and 5.20 compare the front velocity for different C_v along long-section 1. For FLO-2D, the time is 108 seconds after failure and for HEC-RAS 90 seconds after failure.

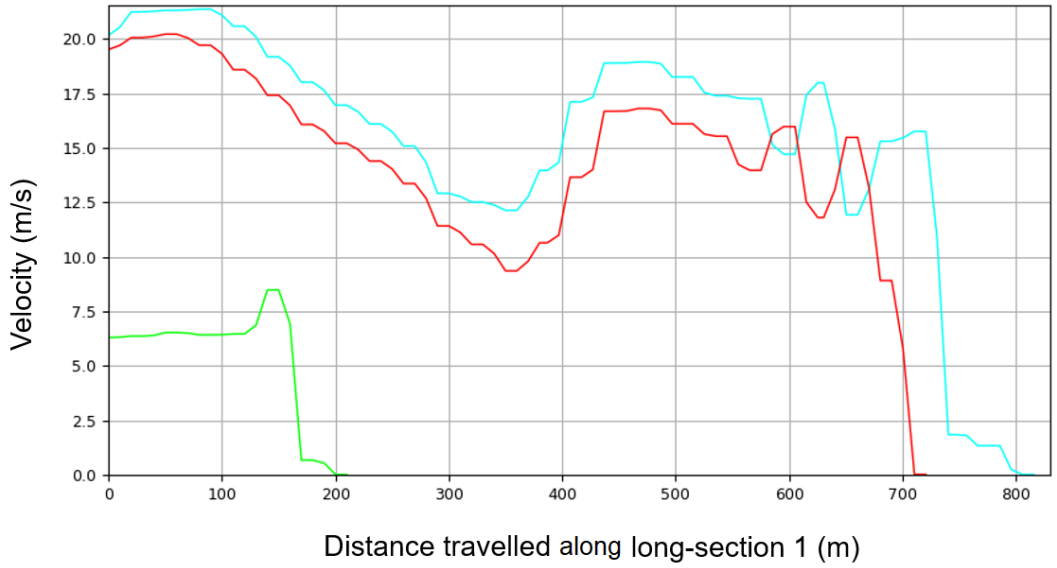

Figure 5.19: Front velocities along long-section 1 for different C_v. FLO-2D results. O'Brien quadratic model.

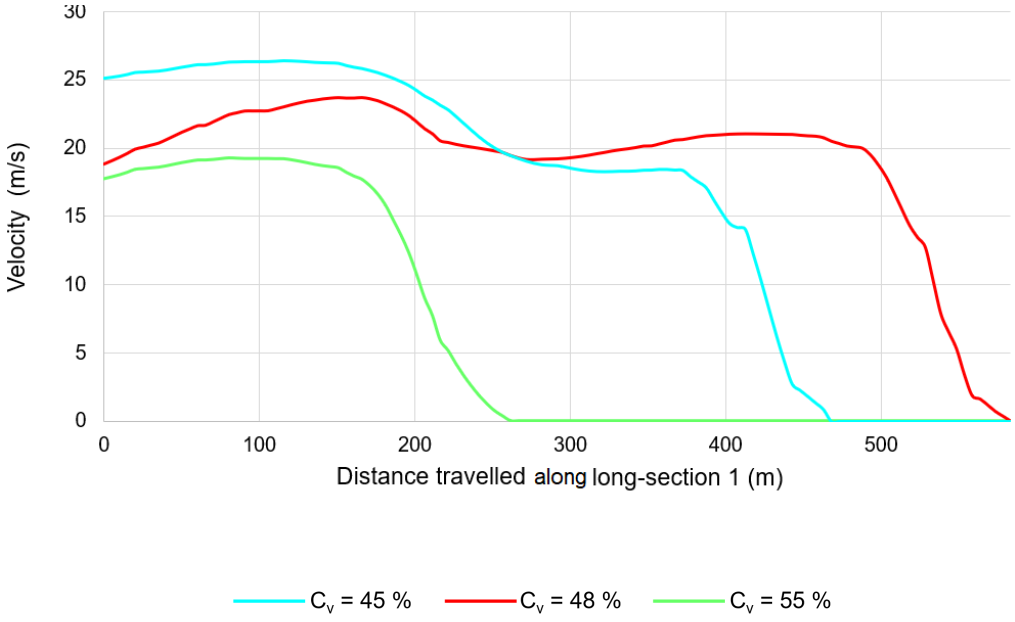

Figure 5.20: Front velocities along long-section 1 for different C_v. O'Brien quadratic model. HEC-RAS results.

The fluid modelled with HEC-RAS arrives approximately 20 seconds before at the same location compared to FLO-2D. This is explained by the lower velocity values obtained with FLO-2D (Figure 5.4). However, what it is unclear is the location of $C_v = 48\%$, respectively $C_v = 45\%$ for HEC-RAS. The three flow curves should be positioned in a descending order, i.e., first the $C_v = 45\%$, then the $C_v = 48\%$; and finally the $C_v = 55\%$. The front velocities are also different, approximately 5 m/s higher estimated to HEC-RAS.

For long-section 2 (marked in Figure 5.18), the situation is different. See Figure 5.21.

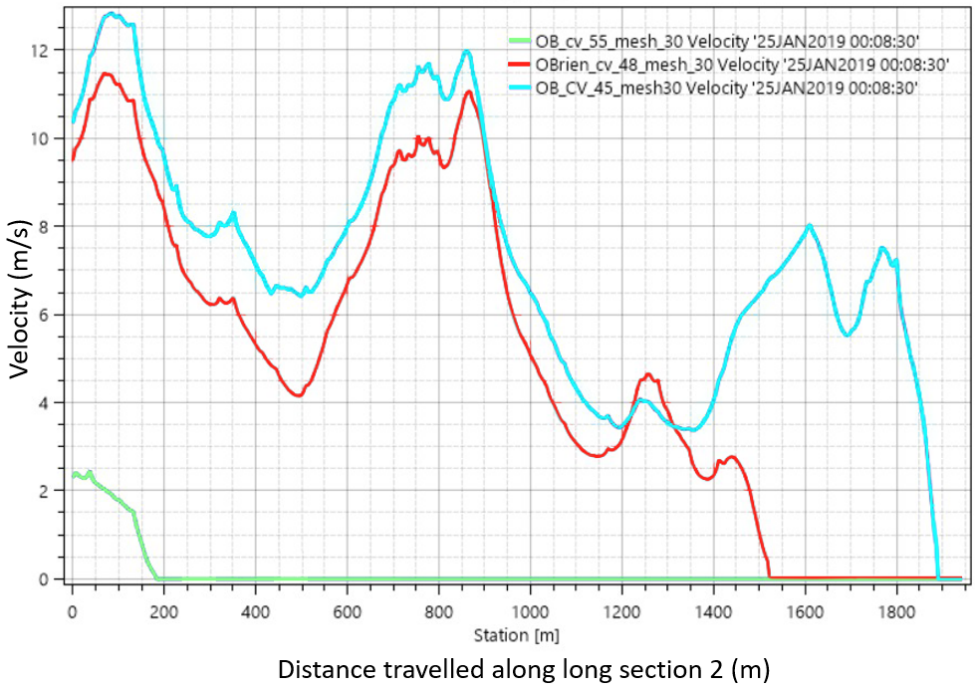

Figure 5.21: Front velocity at time 8:30 minutes after failure for different C_v. O'Brien quadratic model.

For long-section 2, the position of each flow curve follows the logic behind the theory explained: faster flood wave for low C_v. The low amount of sediments allows the hyper-concentrated fluid to flow at high velocities. Thus, it is unclear how it is possible that for long-section 1 the front velocity for $C_v = 48\%$ is higher than $C_v = 45\%$ and for long-section 2 the situation is the opposite. Also, the arrival times for the C_v flood waves along long-section 2 are on average 20 minutes, whereas HEC-RAS calculates the fluid at a similar location within 9 minutes after failure.

5.2.3. Bingham Plastic model

In section 2.3.2 the Bingham plastic model was introduced including the input parameters needed, which are the yield strength and the viscosity. For different C_v, these are obtained following the equations presented for O'Brien in section 3.4 and the values shown are in Table 5.5. The results are also obtained for long-sections 1 and 2 used in FLO-2D (Figure 5.2).

Figure 5.22 illustrates the front velocity profiles for each C_v flood wave.

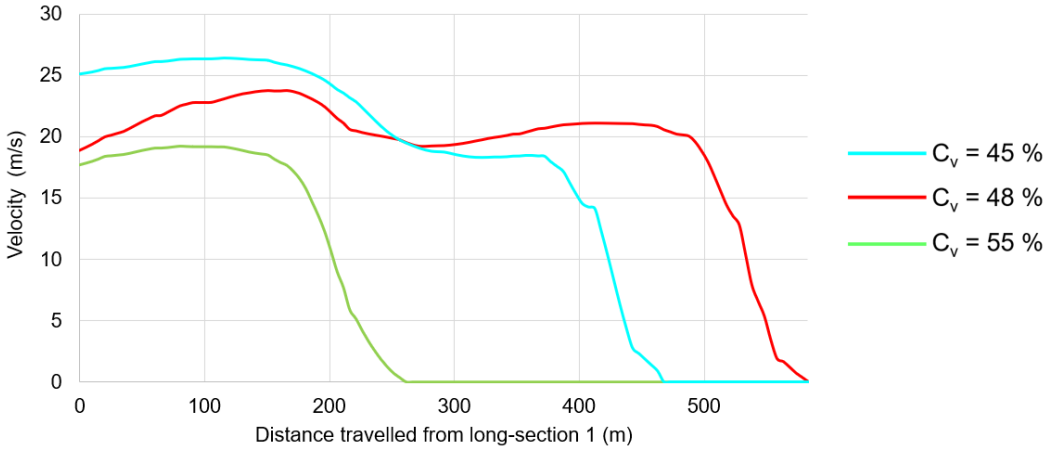

Figure 5.22: Front velocity at time 1.30 minutes after failure for different C_v. Bingham Plastic model

It was expected that the results with the Bingham plastic model would follow a logic order of the flood waves along long-section 1, however the problem remains as in the previous analysis. The front part of the $C_v = 45\%$ is behind the $C_v = 48\%$. Additionally, the shape of the resulting velocity curves is exactly the same when using the O'Brien model, which means that the specific modelling parameters parameters that make the models different are disregarded (such as turbulent and dispersive shear stresses in the O'Brien model). For long-section 2, the exact same change happens for the Bingham simulation: the $C_v = 45\%$ flood wave is more advance in space than $C_v = 48\%$, which is logic. The shape and values of the velocity curves is the same as in the O'Brien simulation and the arrival time along long-section 2 is still too short compared to FLO-2D and the actual (Figure **??** in the Appendix A).

5.2.4. Discussion

Stanford Gibson mentioned in a personal comment that the Bingham plastic model was tested successfully for a flume experiment. However, a dam break simulation is different and a large-scale situation. As a preliminary conclusion, more attention should be given to the implementation of the rheological models in HEC-RAS; it is still a *beta* version, thus some inconsistency could have been expected. Bingham and O'Brien rheological models are different: O'Brien accounts for turbulent and dispersive shear stresses within the mixture (where turbulent is the normative one with large values), whereas, Bingham only considers the yield strength and viscosity terms. From the sum of all the shear stresses on each rheological model, a predicted result was that the Bingham model would lead to faster flood waves with lower total shear stresses from the yield strength and viscosity; and the O'Brien a slower flood wave with a higher values for the total shear stresses (due to the turbulent shear stress).

6

Applications

Tailings dam breach studies are expected and required when operating and planning tailings storage facilities. Dam break studies include the description of a hypothetical dam breach, flood wave routing, inundation mapping and evaluation of environmental and socio-economical impacts in the society. From the analyses performed with FLO-2D and HEC-RAS, a preliminary conclusion was that when non-Newtonian fluids are considered, HEC-RAS is unable to obtain consistent results; whereas FLO-2D is more convenient and efficient. Therefore, is this section only FLO-2D is used.

Before this master thesis began, an internship project was done between November 2020 until January 2021 at Cohere Consultants. The objective of the internship was to perform a non-regret analysis, based on gathering information related with the dimensions of tailing storage facilities in the state of Minas Gerais (Brazil), their purpose, structure and current state. Available data was used to determine which tailings dams are most likely to fail, thus those need immediate assistance. A simple method to delimit the flooded area was developed for the 10 most unstable upstream dams, as a first approximation instead of using complex models. In the internship report, the 10 most unstable tailings storage facilities were analysed, according to the volume within the reservoir, the height of the dam and the risk level associated to each structure. For this project, two of the most unstable dams (Forquila I and B. Rejeitos) are considered and modelled with FLO-2D.

6.1. Methods used

Two different methods are used to delimit the initial flooding area for two unstable upstream dams. The first approach is called Energy-line method, which is based on two empirical equations that correlate the volume of the reservoir with the distance travelled by the mixture (Corominas, 1996). The second method is the application of FLO-2D and the corresponding O'Brien rheological model. A third comparison with HEC-RAS is not carried out due to the inconsistent results obtained in section 5.2.

6.1.1. Energy-line method

This method is based on an empirical equation that relates the impoundment volume (V_T) in reservoir with the angle of reach (α). The angle of reach is described as the ratio of the elevation difference between the highest point of the material before flowing and the more advanced point after deposition (*H'*) and the total travelled distance of the waste material (*L'*) (Corominas, 1996).

$$\frac{H'}{L'} = 0.973 \cdot V_T^{-0.105} \tag{6.1}$$

$$\tan(\alpha) = \frac{H'}{L'} \tag{6.2}$$

The angle of reach was used to create an energy plane that had the same elevation value as the crest of the mine tailing dam and then it was extended through the downstream area according to α. Thus, the limit of the inundated area was defined by the intersection of the energy plane with the topography. Figure 6.1 is a sketch of the energy-line method.

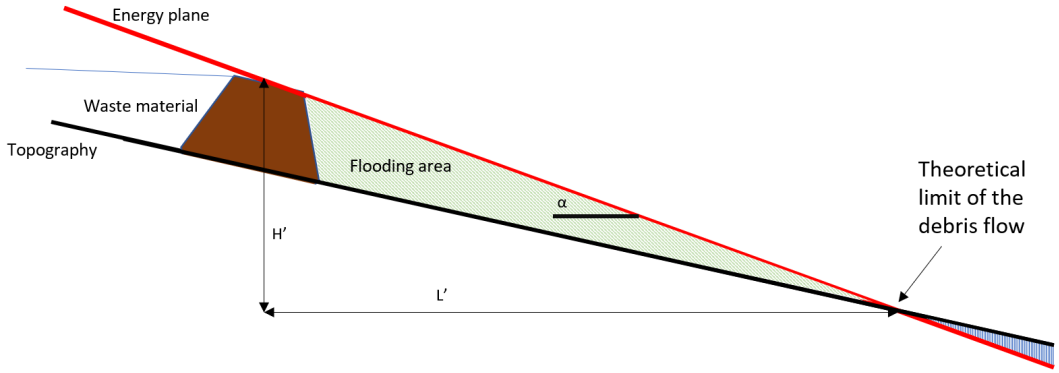

Figure 6.1: Sketch of the energy plane.

6.1.2. FLO-2D

The results provided in this section comprise a range of solutions for the flooding area and the time needed for the flood wave to stop flowing. The range of values is given according to the most sensitive parameters for FLO-2D for the primary impact zone: the volumetric concentration and the time of failure. Thereafter, the initial inundated area obtained with the maximum velocity value per cell for the entire simulation time is compared with the result that was obtained with the energy-line method.

The input parameters considered are:

- Volumetric concentration: 45%, 50% and 55%.
- Duration of failure: 3, 6 and 12 minutes.

6.2. Forquilha I

Forquilha I is an upstream mine tailings dam in the state of Minas Gerais, Brazil. It is an iron mine, property of VALE S.A. According to FEAM *(Fundação Estadual do Meio Ambiente)* and ANM *(Agência Nacional de Mineração)*, dam Forquilha I has an emergency level of 3, which indicates imminent failure, and a high potential damage associated.

The main characteristics of Forquilha I are:

1. Volume of the reservoir: 12.8 Mm^3
2. Height of the dam: 98.3 m

1. VOLUMETRIC CONCENTRATION

The three realistic values obtained from the sensitivity analysis are used for this flooding prediction. A lower boundary value of $C_v = 45\%$ in the case where $V_W > V_S$, a medium value of $C_V = 50\%$ when $V_W = V_S$ and an upper boundary value $C_v = 50\%$ for $V_W < V_S$. Note that for the study performed in section 5.1, the released volume considered was less than the impounded volume (since it was known). Whereas, for the following predictions, the total volume of the reservoir is considered, leading to more conservative results. The duration of failure for the simulations is 6 minutes, with a peak discharge of $Q_{peak} = 2.4 * 10^5\ m^3/s$.

The primary impact zone and the time needed for the flood wave to stop flowing are summarised in Table 6.1.

Table 6.1: Results obtained for each C_v

C_v (%)	INITIAL FLOODING AREA (Mm^2)	DURATION ($hours$)
45	3.58	> 10
50	2.79	9
55	1.97	5

The results obtained agree with the conclusions drawn in section 5.1. Low values of C_v lead to a less extended flooded area. From Table 6.1, there are more differences when increasing a 5% the volumetric concentration between $C_v = 50\%$ and 55% than for lower values of it (results in Appendix D). Comparing the results of FLO-2D with the energy-line method, the approach used with equations 6.1 and 6.2 results in an overestimation of the flooding area (Figure 6.2).

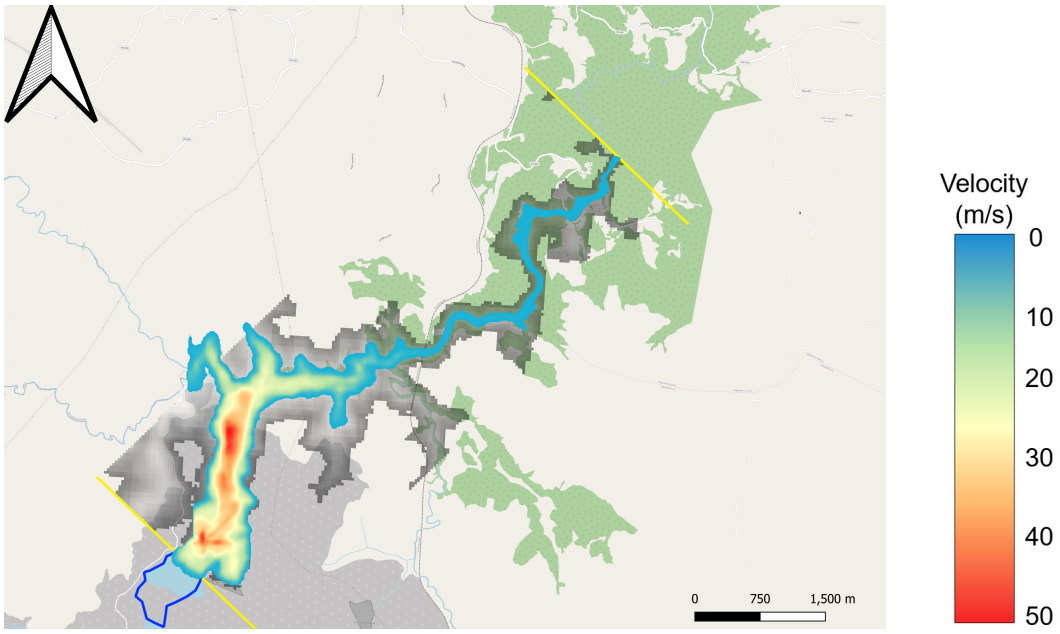

Figure 6.2: Comparison between the inundated area obtained with FLO-2D for $C_v = 50\%$ (coloured area) and the energy-line method (grey area). Yellow lines mark the beginning and end of the flooding area. Blue line delimits the reservoir.

2. FAILURE DURATION

Three different hydrographs are implemented for each situation. The times used are the sames as in the failure of dam B-I:

- $t = 3\ min$ with a $Q_{peak} = 4.8 * 10^5\ m^3/s$
- $t = 6\ min$ with a $Q_{peak} = 2.4 * 10^5\ m^3/s$
- $t = 12\ min$ with a $Q_{peak} = 1.2 * 10^5\ m^3/s$

The primary inundated area and the duration of flow are summarised in Table 6.2.

Table 6.2: Results obtained for each failure duration

t (min)	INITIAL FLOODING AREA (Mm^2)	DURATION $(hours)$
3	3.58	7
6	2.79	9
12	2.10	6

For the same volumetric concentration, a larger time to release all the volume leads to lower velocity values near the failure location and a reduced inundated area. For a sudden release of mine tailings material ($t = 3\ min$), the high velocity values will give more force for the material to flow. However, the rheological properties within the fluid will minimise the driving forces that move the fluid along the downstream area. The result obtained with the energy-line method exceeds the area delimited by FLO-2D for all situations (results in Appendix D). Figure 6.3 illustrates the inundation area for a duration failure of $t = 12\ min$ (coloured area) in comparison with the flooded area obtained with the energy-line method (grey area.

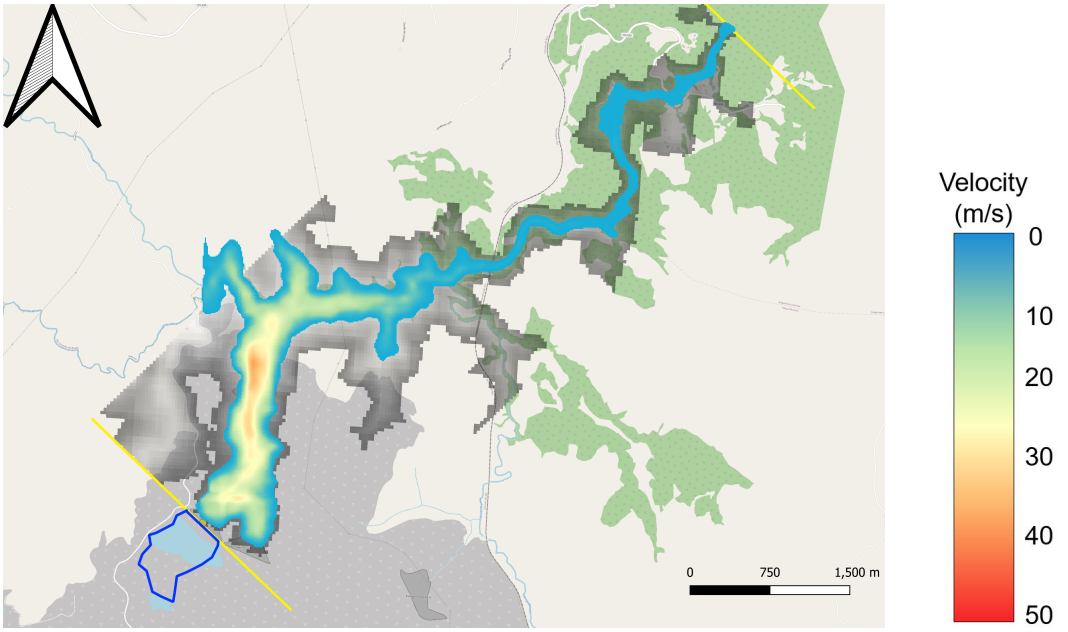

Figure 6.3: Comparison between the inundated area obtained with FLO-2D (coloured area) for $t = 12\ min$ and the energy-line method (grey area). Yellow lines mark the beginning and end of the flooding area. Blue line delimits the reservoir.

6.3. B. Rejeitos

Rejeitos is an upstream mine tailing dam in the state of Minas Gerais, Brazil. It is owned by Arcelormittal Mineração Serra Azul S.A. and it is an iron mine. FEAM and ANM assigned an emergency level of 2 and a high potential damage associated.

The main characteristics of Forquilha I are:

1. Volume of the reservoir: 5.25 Mm^3
2. Height of the dam: 89 m

1. VOLUMETRIC CONCENTRATION

The range of C_v considered is the same as the previous case. The results obtained are presented in Table 6.3.

Table 6.3: Results obtained for each C_v

C_v (%)	**INITIAL FLOODING AREA** (Mm^2)	**DURATION** ($hours$)
45	2.99	> 10
50	2.26	8.50
55	1.21	6

The higher the C_v is, the less extensive is the inundated area (see Appendix D). The flooding duration also decreases since the fluid will stop flowing before due to the low velocities. In this situation, the energy-line approach results in an excess of the measured flooding area. However, the extension of the inundated area along the drainage path matches with both methods for a $C_v = 50\%$ (Figure 6.4).

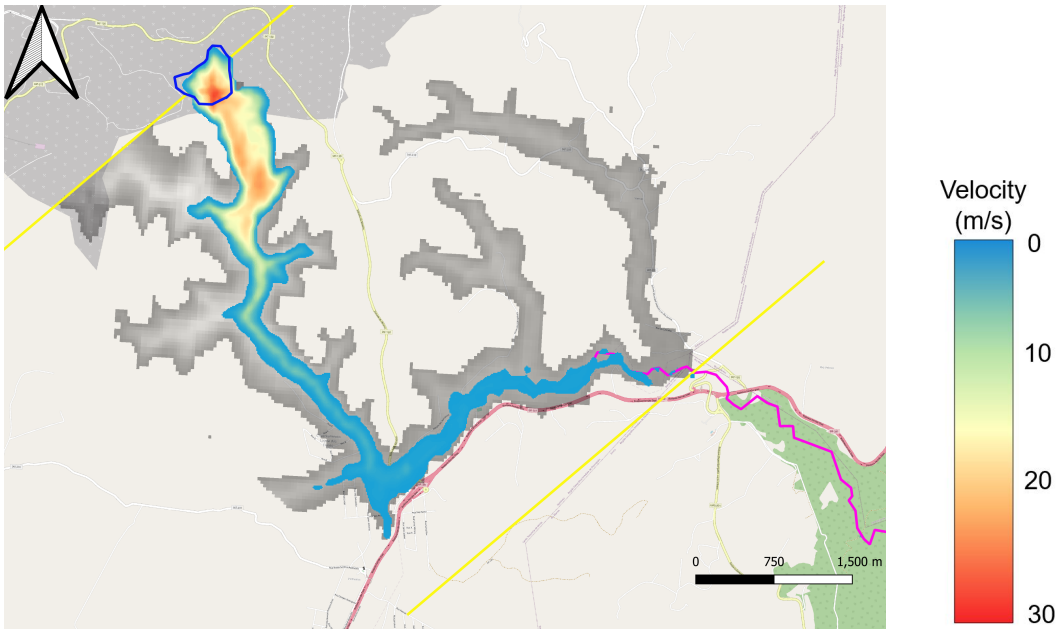

Figure 6.4: Comparison between the inundated area obtained with FLO-2D (coloured area) for $C_v = 50\%$ and the energy-line method (grey area). Yellow lines mark the beginning and end of the flooding area. Blue line delimits the reservoir. Pink line the drainage path.

2. FAILURE DURATION

The breach hydrograph obtained with FLO-2D depends on the volume in the reservoir and the duration of failure. The shape of the hydrograph is the same as in Figure 4.5 and the peak discharges for each time are:

- $t = 3\ min$ with a $Q_{peak} = 2.0 * 10^5\ m^3/s$
- $t = 6\ min$ with a $Q_{peak} = 1.0 * 10^5\ m^3/s$
- $t = 12\ min$ with a $Q_{peak} = 5.0 * 10^4\ m^3/s$

The results obtained from different failure times are summarised in Table 6.4.

Table 6.4: Results obtained for each failure duration

t **(*min*)**	**INITIAL FLOODING AREA (Mm^2)**	**DURATION (*hours*)**
3	2.29	9.50
6	2.26	8.50
12	2.20	7

According to Table 6.4 and for different failure times, the inundated areas are less different between them than previous analyses. For $t = 12\ min$, the energy-line method results in an overestimation of the flooded area (see Figure 6.5). The grey areas that do not match with the flooded area delimited with FLO-2D represent areas where the energy plane is above the topography, but it should be neglected when delimiting the possible flooding area, since the drainage path does not cover that region (see Appendix D for the other analyses).

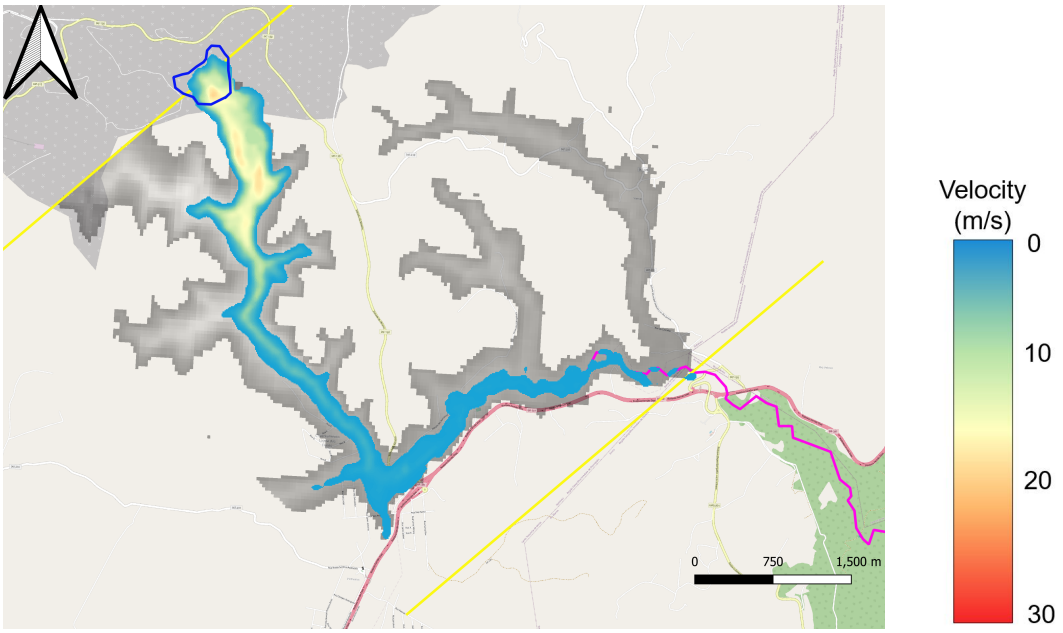

Figure 6.5: Comparison between the inundated area obtained with FLO-2D (coloured area) for $t = 12\ min$ and the energy-line method (grey area). Yellow lines mark the beginning and end of the flooding area. Blue line delimits the reservoir. Pink line the drainage path.

7

Discussion

The main objective of this study is to investigate which parameters dominate the behaviour of mudflow in case of failure of a tailing storage facility. This study was done through a sensitivity analysis on all the parameters of the rheological model used. In this way, a better understanding of the possibilities and the limitations of the models was gained.

7.1. Rheological model

The O'Brien quadratic rheological model was selected as the basis for the sensitivity analysis. Other rheological models exist, but the O'Brien model is more complex and it was expected more accurate outcomes. When assessing the terms at the sensitivity analysis of the 4 shear stresses that compose the model, it has been proven that the dispersive shear term has no bearing on the overall shear stress. If the dispersive term could be ignored, the average sediment size parameter could be ignored as well, requiring fewer inputs to run the model.

Furthermore, from the sensitivity analysis the turbulent shear stress is the normative term in the rheological model, due to the squared Prandtl mixing length. For large flow depths, such as the flood wave resulting from a dam break, terms such as molecular viscosity and yield strength are not comparable with the turbulent component. They depend on two empirical coefficients derived from O'Brien's research, but further study regarding the physics of those coefficients should be carried out.

7.2. Volumetric concentration

From the sensitivity analyses carried out with FLO-2D, it was observed that the volumetric concentration influences the initial and final flooding area the most. Five different scenarios were compared according to different volumes, and the conclusion drawn was that the higher the C_v, the less extended is the inundated area. The explanation is that large amount of sediments within the fluid will lead to high density values of the mixture and together with large flow depths, the turbulent shear stress will greatly increase. Thus, if the mixture becomes denser, the internal and external forces acting to mobilise the fluid are insufficient to produce large velocity values.

Furthermore, from the sensitivity analysis in the rheological model, there were visible differences between the functions $C_v = 20\%$ and $C_v = 45\%$. However, the velocity and depth profiles along longsection 1 show the same location for both C_v for the same time step. A slight variation between flood waves front position was expected, since the front velocities present small differences. The differences between initial and final flooding area are more apparent for higher C_v due to accumulation of solids after a certain time of failure.

7.3. Manning's roughness

Regarding the front velocity profile and for a similar increase in roughness, there are less differences between $n = 0.012$ and $n = 0.022$ than $n = 0.055$ and $n = 0.075$. Each of both cases fall in the same category according to Table 4.4, but the results converge for values within the category of *medium*. The same statement is not applicable for *n*-values within the range of *very large*.

7.4. Failure duration

The output hydrograph created by the Tailings dam tool in FLO-2D is extended and reduced, with different peak discharge values. The failure time determines the velocity field near the breach location. For small failure time, for instance $t = 3\ min$, a large volume is released at a high velocity, which causes an increase in the flow depth. This increase, in turn, increases the Prandtl mixing length, resulting in a large turbulent shear stress. The large velocities in the model are reduced according to the rheological properties of the mixture. For the same volumetric concentration, properties like viscosity act more intensively to minimise the high velocity values for a low failure duration. On the contrary, for $t = 12\ min$, the velocity values are in the same order of magnitude near the breach location.

7.5. Flooding areas

The volumetric concentration is the most sensitive parameter for the initial flooding area. Whereas, for the final flooding area, the volumetric concentration and the duration of failure are both sensitive. A large failure duration gives similar values regarding initial and final flooded areas, since the velocities are small and the fluid will flow and deposit simultaneously. For high C_v, the difference between initial and final inundated area is more significant. The fluid will rapidly spread near the failure location; but once it reduces its pace, it will accumulate and deposit along the drainage path. Thus, it is concluded that for initial and final flooding areas, higher C_v values lead to a lower flooded surface.

7.6. HEC-RAS

FLO-2D and HEC-RAS do not compare well. The basis of the governing equations is the same, but HEC-RAS uses a different approach. HEC-RAS is suitable for using water as the main fluid. Whereas for non-Newtonian fluids, the model is still underdeveloped. The results obtained with the Bingham plastic model and O'Brien quadratic rheological model are exactly the same, which means that these models are not yet properly implemented in HEC-RAS. The fact that the non-Newtonian feature in HEC-RAS is still a trial version, it means that more validation tests and adjustments need to be applied in the model.

7.7. Limitations

The non-Newtonian fluid considered for this study is assumed to have a constant volumetric concentration during all the simulation. Mine tailings are composed of particles and water and when failure occurs, these mix and flow along the downstream area. Once the flow velocity can no longer sustain coarse particles anymore due to its high unit weight, they will deposit near the failure location, while the finer particles will continue flowing as suspended load. Deposition of particles imply that the volumetric concentration will reduce, therefore the mixture should show a reduction in volumetric concentration over distance. Thus, a 2-phase flow approach should be considered, which implies a more complex perspective, i.e: the fluid on top will have higher velocity values, less sediments and scour the layer below; while the layer below flows slowly, with more sediments that part of them will deposit or being scoured by the fluid.

From this study, the duration of failure was chosen as one of the most influential parameters according to the sensitivity analysis. Nonetheless, the resulting hydrograph does not account for all of the elements that affect a breach formation. The breach formation depend on several factors such as the type

of failure (e.g:overtopping; piping; foundation failure), embankment geometry, material, construction method and reservoir dimensions. The breach hydrograph is obtained with FLO-2D according only to the failure duration and volume released, which means that there is a lack of information regarding the dam characteristics that may influence the resulting hydrograph.

8

Conclusions and Recommendations

8.1. Conclusions

This chapter present the answers to the main research question:

How does the flow behaviour affect the area impacted by a hyper-concentrated sediment fluid resulting from a dam break?

The main question has been divided into 6 sub-questions.

1. What properties affect flow behaviour of a hyper-concentrated sediment fluid?

Based on the results of the sensitivity analysis carried out and the parameters in the rheological model, it can be concluded that the property that affects the flow behaviour the most is the volumetric concentration. Other components of the rheological model are also C_v-dependant. The yield strength and viscosity have the C_v in an exponential form; density of the mixture will increase when C_v increases, resulting in a larger turbulent shear stress and the linear volumetric concentration ratio in the dispersive term. When increasing C_v, all the shear terms in the rheological model increase, thus high shear stress values are needed to mobilise the hyper-concentrated sediment fluid. Other properties such as the density of sediments have a lower impact in the shear stress; since the density of sediments only accounts for the density of mixture in the turbulent term, but the normative value in that component is the Prandtl mixing length. The magnitude of the dispersive shear stress term is low compared to the other shear stresses, thus parameters such as the sediment size will not alter the shear stress significantly.

2. Which parameters are the most critical for modelling the dam break flow model?

When evaluating the O'Brien rheological model, the volumetric concentration is the property that governs the flow behavior. When using complex models to simulate dam failure, such as FLO-2D or HEC-RAS, the volumetric concentration and the period of failure are important characteristics to consider. The breach hydrograph is calculated based on the volume released and the time it takes for the failure to occur. Therefore, larger volumes with less time will result in higher peak discharges. The high velocity field is specially extended near the failure location, but thereafter decreases according to the shear stress for the chosen C_v.

3. In what way does a non-Newtonian fluid model perform better than water based model for breach modelling?

The large volume of sediments in mine tailings material plays an important part in the development of the mudflow wave in the event of a dam breach. The fluid's viscosity will increase as the volumetric concentration increases, increasing the fluid's resistance to flow. Hyper-concentrated sediment fluids show a shear-thinning behaviour, which means that the viscosity decreases when increasing the shear rate. If the viscosity increases due to C_v, the shear rate will decrease. The C_v also affects the yield strength, which will be higher for larger values of C_v. A higher shear stress will be necessary to initiate movement and allow the fluid to deform. Non-Newtonian properties are ignored when utilizing water-based models, resulting in larger flow velocities and larger inundated areas than in practice would occur.

4. From the properties of mine tailing materials, is it possible to accurately determine beforehand the flow behaviour?

If a range of values is considered, it is possible to estimate which case will have the largest impact on the affected area. For instance, classifying the scenarios by order of rheological properties such as viscosity or yield strength, or fluid properties like volumetric concentration. Another option would be to classify the input parameters of the model, i.e. discharge values of the breach hydrograph, duration of failure or Manning's roughness value. However, for both classifications, only a comparison of the predictions can be obtained, not an exact result. Since the volumetric concentration was the parameter that influence the flow behaviour the most, a possible first approximation could be done by using different values of it. To obtain a realistic range of solutions, the values should be logical according to the situation, i.e. if mudflow is considered, use C_v values that range from 45-55%.

5. What are the limitations of the existing modelling softwares used?

When it comes to setting up a simulation, both softwares are comparable. The main distinction is in the capability that each application offers. FLO-2D was created to simulate flooding events on urban topographies, and as a result, it offers a wide range of urban modeling options. The component that is used to predict mud and debris flow hazards is still under development, with several parts still missing. HEC-RAS is developed to perform hydraulic calculations for natural or man-made environments with water as the primary component. The non-Newtonian capability was added in the most recent beta version, thus it is still under development and there are not simulations that can be used as examples.

HEC-RAS is more user-friendly than FLO-2D. HEC-RAS includes its own graphical user interface, which allows the user to see all of the input parameters and outcomes at a glance. FLO-2D, on the other hand, is an executable program that requires at least 8 text files containing all of the input parameters. It can utilise QGIS as an interface to define the text files, but it must run separately afterwards; MapperPro is a viewer application to visualise the results, and from there the results can be exported to QGIS again.

6. Are the simpler methods an accurate approach to delimit the inundated area?

The energy-line concept results in an overestimation of the flooding area, therefore it's a conservative approach. When complex models are not an option, it is an alternative way to get a first approximation of the inundated region. However, only the surface inundated along the drainage path is obtained, without information on flow velocities or flow depths.

8.2. Recommendations

The following recommendations are proposed according to the results, discussions and conclusions of this study. The recommendations and future research proposals are addressed to: a better operation of tailings storage facilities, how to reduce the uncertainty regarding the material involved and its behaviour in case of failure, possible improvements for FLO-2D and HEC-RAS models.

The following recommendations are suggested for a proper operation and maintenance process of tailings storage facilities:

- Record of planning and operating procedures.
- Registration of the impounded volume.
- Good monitoring system.
- Site investigation to determine the geotechnical properties of mine tailings materials.
- Drainage system to lower the volume of water within the reservoir.
- To prevent damage in the downstream area in case of failure, create obstacles along the drainage path to reduce velocity of the flood wave in case of dam failure.

Recommendations given for improvement of FLO-2D are:

- Variable cell size along the grid. Add the possibility to refine or coarsen the mesh in certain locations over the computational domain.
- Unify all the software in one program. With its own GUI and viewer for results.
- According to the bathymetry, estimate the volume of the reservoir.
- Further reduction of the interval time steps.
- Possibility to use other rheological models.
- Make the software usable for small-scale simulations in order to reproduce laboratory experiments.

Recommendations given for improvement of HEC-RAS are:

- Correct implementation of rheological models.
- Estimate the volume of the reservoir with the bathymetry.
- Creation of its own breach hydrograph.

The following suggestions are proposed for future research based on the findings of this project.

- 2-phase flow approach for mine tailings dam failure. Distinction of the fluid phase with low volumetric concentration from the mudflow phase.
- Consider precipitation. Make a distinction between dry or rainy day by adding extra water in the reservoir.
- Non-constant volumetric concentration if only mudflow is considered. Deposition of solids along the drainage path.
- Consideration of the breach formation and the type of failure. Assess how it would affect the outflow rate and the duration of failure.
- 3D modelling to obtain more detailed solutions.

Bibliography

Akan, A. O., & Iyer, S. S. (2021). *Open channel hydraulics*. Butterworth-Heinemann.

Alderman, N. (1997). Non-newtonian fluids: Guide to classification and characteristics. *London: ESDU*.

Anderson, J. D., & Wendt, J. (1995). *Computational fluid dynamics* (Vol. 206). Springer.

Arcement, G. J., & Schneider, V. R. (1989). Guide for selecting manning's roughness coefficients for natural channels and flood plains.

Bagnold, R. A. (1954). Experiments on a gravity-free dispersion of large solid spheres in a newtonian fluid under shear. *Proceedings of the Royal Society of London. Series A. Mathematical and Physical Sciences*, *225*(1160), 49–63.

Bagnold, R. A. (1956). The flow of cohesionless grains in fluids. *Philosophical Transactions of the Royal Society of London. Series A, Mathematical and Physical Sciences*, *249*(964), 235–297.

Berghe, J.-F. V., Ballard, J., Wintgens, J., & List, B. (2011). Geotechnical risks related to tailings dam operations. *Proceedings Tailings and Mine Waste*.

Bhanbhro, R., Auchar Zardari, M., Ahmed Memon, B., Ali Soomro, M., Edeskär, T., & Knutsson, S. (2021). Mechanical properties and particle breakage of uniform-sized tailings material. *Journal of Materials in Civil Engineering*, *33*(3), 04020481.

Boger, D. V. (2013). Rheology of slurries and environmental impacts in the mining industry. *Annual review of chemical and biomolecular engineering*, *4*, 239–257.

Boger, D., Scales, P., & Sofra, F. (2006). Rheological concepts. *Paste and Thickened Tailings-A Guide*, 25–37.

Brunner, G. W. (2016). *Hec-ras river analysis system. hydraulic reference manual. version 5.0.* (tech. rep.). Hydrologic Engineering Center Davis CA.

Bureau, T.-S. (2017). Periodic review dam mine safety stream bean - dam b-i. technical report. *IBC - RISK MANAGEMENT GEOTECHNICAL*.

Chien, N., & Wan, Z. (1999). Mechanics of sediment transport.

Corominas, J. (1996). The angle of reach as a mobility index for small and large landslides. *Canadian Geotechnical Journal*, *33*(2), 260–271.

Coussot, P. (2005). Rheometry of pastes, suspensions, and granular materials: Applications in industry and environment.

Davies, M. P. (2002). Tailings impoundment failures are geotechnical engineers listening? *GEOTECHNICAL NEWS-VANCOUVER-*, *20*(3), 31–36.

Du, J., Hu, L., Lin, D., & Zhang, L. (2018). Experimental study on physical and mechanical properties of iron tailing materials. *GeoShanghai International Conference*, 187–194.

Dutch Risk Reduction Team. (2019). DRR Team Mission Report Minas Gerais state, Brazil.

Elger, D. F., LeBret, B. A., Crowe, C. T., & Roberson, J. A. (2020). *Engineering fluid mechanics*. John Wiley & Sons.

F Gama, F., Mura, J. C., R Paradella, W., & G de Oliveira, C. (2020). Deformations prior to the brumadinho dam collapse revealed by sentinel-1 insar data using sbas and psi techniques. *Remote Sensing*, *12*(21), 3664.

FLO-2D Software, I. (2019). Flo-2d. reference manual. *User's manual*.

Franco, J. M., & Partal, P. (2010). The newtonian fluid. *Rheology*, *1*, 74–95.

Ghahramani, N., Mitchell, A., Rana, N. M., McDougall, S., Evans, S. G., & Take, W. A. (2020). Tailings-flow runout analysis: Examining the applicability of a semi-physical area–volume relationship using a novel database. *Natural Hazards and Earth System Sciences*, *20*(12), 3425–3438.

Gibson, S., Floyd, I., Sánchez, A., & Heath, R. (2021). Comparing single-phase, non-newtonian approaches with experimental results: Validating flume-scale mud and debris flow in hec-ras. *Earth Surface Processes and Landforms*, *46*(3), 540–553.

Guardian, T. (2019). Terrifying moment of brazil dam collapse caught on camera. Retrieved December 21, 2021, from https://www.youtube.com/watch?v=sKZUZQytads&ab_channel=GuardianNews

Haan, C. T., Barfield, B. J., & Hayes, J. C. (1994). *Design hydrology and sedimentology for small catchments*. Elsevier.

Hanes, D. M., & Bowen, A. J. (1985). A granular-fluid model for steady intense bed-load transport. *Journal of Geophysical Research: Oceans*, *90*(C5), 9149–9158.

Hergarten, S., & Robl, J. (2015). Modelling rapid mass movements using the shallow water equations in cartesian coordinates. *Natural Hazards and Earth System Sciences*, *15*(3), 671–685.

Highland, L., Bobrowsky, P. T. et al. (2008). *The landslide handbook: A guide to understanding landslides*. US Geological Survey Reston.

Hu, L., Wu, H., Zhang, L., Zhang, P., & Wen, Q. (2017). Geotechnical properties of mine tailings. *Journal of Materials in Civil Engineering*, *29*(2), 04016220.

Hydronia, L. (2017). Riverflow2d, two-dimensional flood and river dynamics model, reference manual.

Iverson, R. M. (1997). The physics of debris flows. *Reviews of geophysics*, *35*(3), 245–296.

Julien, P. Y., & Lan, Y. (1991). Rheology of hyperconcentrations. *Journal of Hydraulic Engineering*, *117*(3), 346–353.

Kossoff, D., Dubbin, W., Alfredsson, M., Edwards, S., Macklin, M., & Hudson-Edwards, K. A. (2014). Mine tailings dams: Characteristics, failure, environmental impacts, and remediation. *Applied Geochemistry*, *51*, 229–245.

Krishnan, J. M., Deshpande, A. P., & Kumar, P. S. (2010). *Rheology of complex fluids*. Springer.

Lumbroso, D., Davison, M., Body, R., & Petkovšek, G. (2021). Modelling the brumadinho tailings dam failure, the subsequent loss of life and how it could have been reduced. *Natural Hazards and Earth System Sciences*, *21*(1), 21–37.

Mathieu, J., & Scott, J. (2000). *An introduction to turbulent flow*. Cambridge University Press.

Mikoš, M., & Bezak, N. (2021). Debris flow modelling using ramms model in the alpine environment with focus on the model parameters and main characteristics. *Frontiers in earth science*, (8), 1–11.

Minussi, R. B., & Maciel, G. d. F. (2012). Numerical experimental comparison of dam break flows with non-newtonian fluids. *Journal of the Brazilian Society of Mechanical Sciences and Engineering*, *34*(2), 167–178.

Miranda, L. S., & Marques, A. C. (2016). Hidden impacts of the samarco mining waste dam collapse to brazilian marine fauna-an example from the staurozoans (cnidaria). *Biota Neotropica*, *16*(2).

Morgenstern, N. R., Vick, S. G., Viotti, C. B., & Watts, B. D. (2016). Report on the immediate causes of the failure of the fundão dam. *Prepared for Vale Ltd*, *12*.

Morris, M., West, M., & Hassan, M. (2018). A guide to breach prediction. *Dams and Reservoirs*, *28*(4), 150–152.

O'Brien, J. S., Julien, P. Y., & Fullerton, W. (1993). Two-dimensional water flood and mudflow simulation. *Journal of hydraulic engineering*, *119*(2), 244–261.

O'Brien, J. S., & Julien, P. Y. (1988). Laboratory analysis of mudflow properties. *Journal of hydraulic engineering*, *114*(8), 877–887.

O'Brien, J., & Julien, P. (1985). Physical properties and mechanics of hyperconcentrated sediment flows. *Proc. ASCE HD Delineation of landslides, flash flood and debris flow Hazards*.

Palu, M., & Julien, P. (2019). Review of tailings dam failures in brazil. *Proc Conf: XXIII Simpósio Brasileiro De Recursos Hídricosat*.

Petkovšek, G., Hassan, M. A. A. M., Lumbroso, D., & Collell, M. R. (2021). A two-fluid simulation of tailings dam breaching. *Mine Water and the Environment*, *40*(1), 151–165.

Raman, A., & Liu, F. (2019a). An investigation of the brumadinho dam break with hec ras simulation. *arXiv preprint arXiv:1911.05219*.

Raman, A., & Liu, F. (2019b). An investigation of the brumadinho dam break with hec ras simulation. *arXiv preprint arXiv:1911.05219*.

Robertson, P., de Melo, L., Williams, D., & Ward Wilson, G. (2019). Report of the expert panel on the technical causes of the failure of feijão dam i. *Prepared for Vale Ltd*, *12*.

Ruiz, E., Huamaní, L., Paucar, J., Larota, J., Jiménez, C., & Gallo, Y. (2021). Planning the dewatering of a tailings storage facility. *Mine Water and the Environment*, *40*(1), 270–284.

Saasen, A., & Ytrehus, J. D. (2019). Viscosity models for drilling fluids: Viscosity parameters and their use. *ASME 2019 38th International Conference on Ocean, Offshore and Arctic Engineering*.

Shook, C. A., & Roco, M. C. (2015). *Slurry flow: Principles and practice*. Elsevier.

Southard, J. (2000). An introduction to fluid motions and sediment transport. *Eastern Section SEPM Short Course*.

Spee, E. (2010). Waqua/triwaq–two-and three-dimensional shallow water flow model. technical documentation. version 3.15, march 2010. ministry of transport. *Public Works and Water Management*.

Stanford, G., & Sánchez, A. (2020). Hec-ras mud and debris flow.

Vreugdenhil, C. B. (1994). *Numerical methods for shallow-water flow* (Vol. 13). Springer Science & Business Media.

Wallingford, H. (2019). A review of the risks posed by the failure of tailings dams.

White, F. (2003). Fluid mechanics.

A

Benchmark test

A.1. HEC-RAS

Results for a coarser mesh (444 cells):

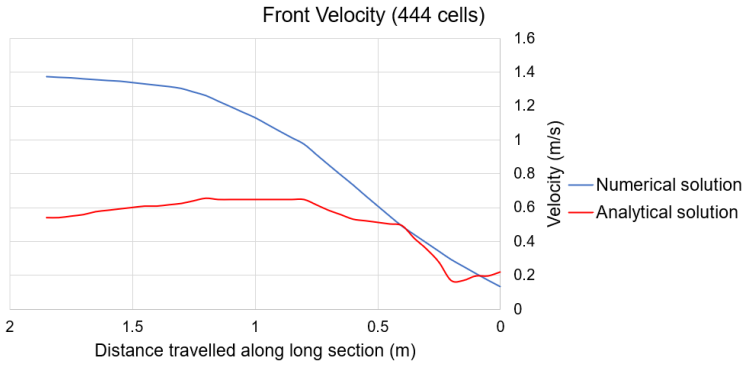

Figure A.1: Front velocity for a coarser grid.

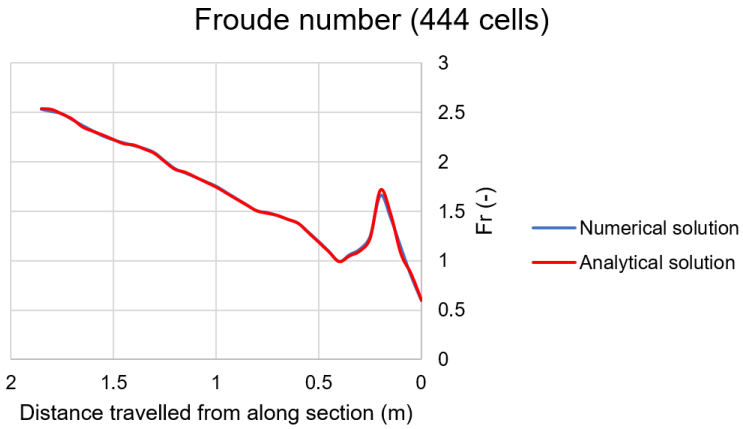

Figure A.2: Froude number for a coarser grid.

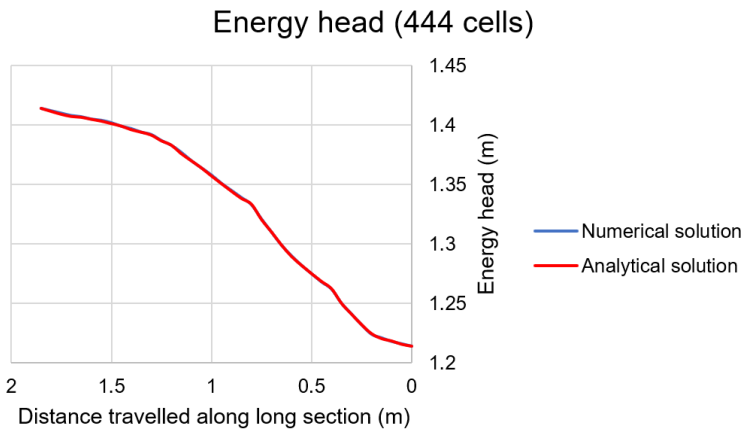

Figure A.3: Energy head for a coarser grid.

Results for a finer mesh (35964 cells):

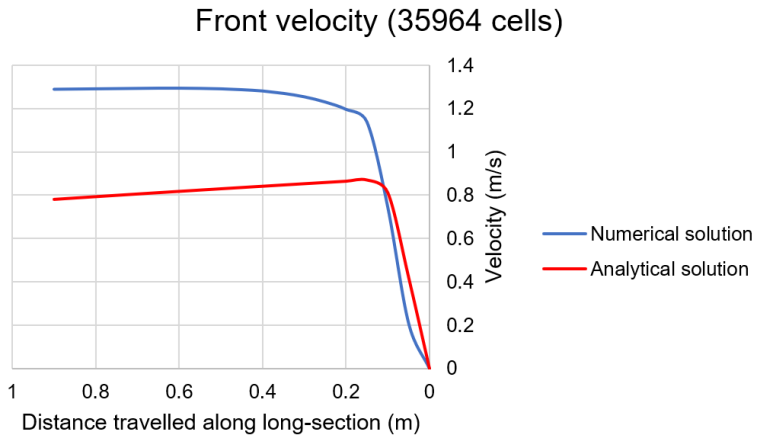

Figure A.4: Front velocity for a finer grid.

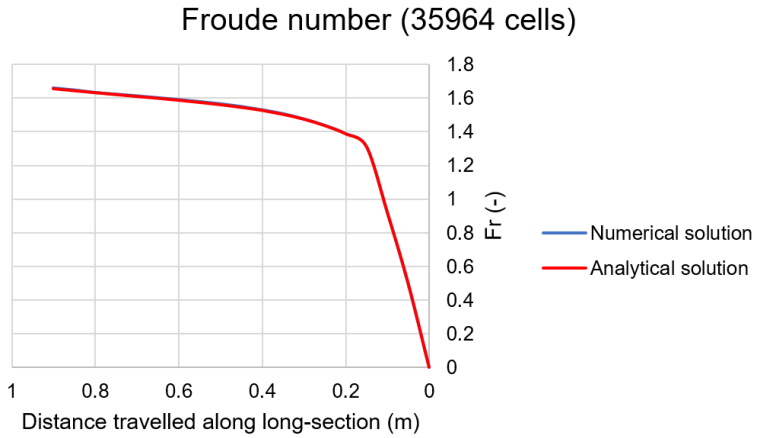

Figure A.5: Froude number for a finer grid.

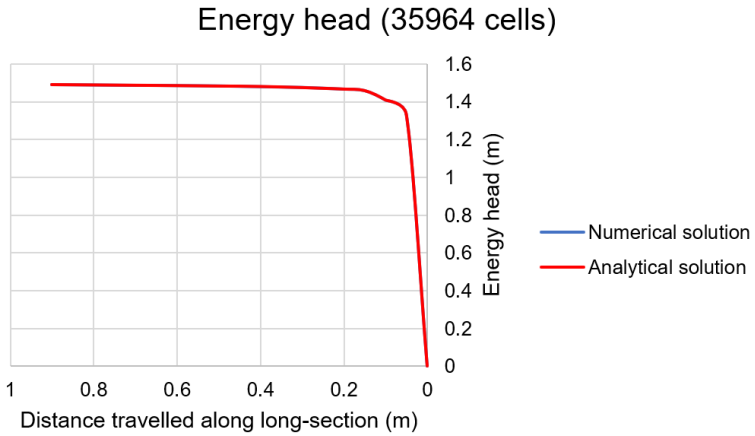

Figure A.6: Energy head for a finer grid.

A.2. FLO-2D

Water as the main fluid. Results of the analytical and numerical solution for the front velocity.

LONG -SECTION 1. Time 0.72 seconds after failure.

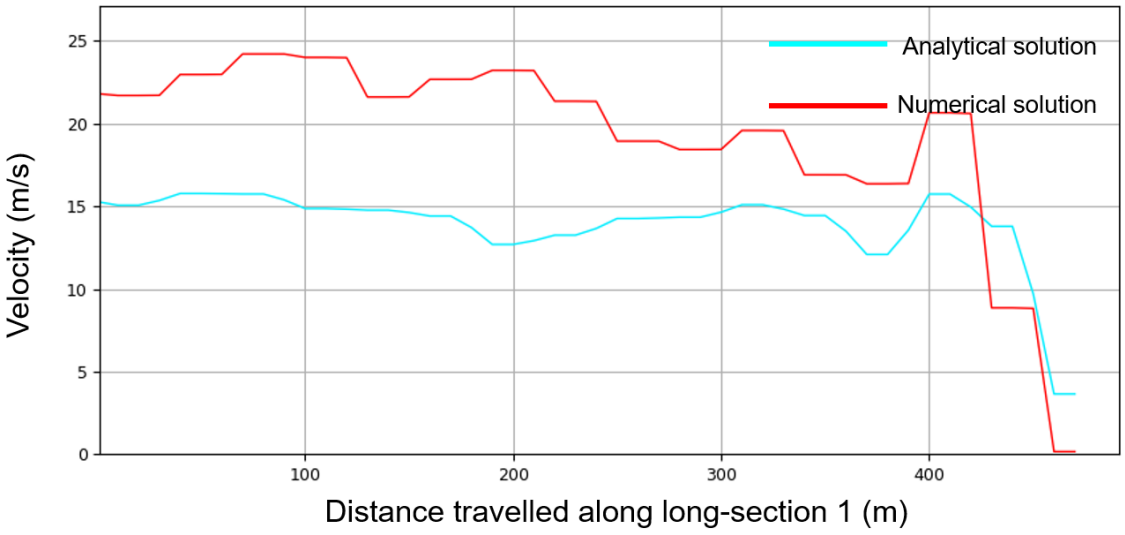

Figure A.7: Front velocity along long-section 1.

LONG -SECTION 2. Time 108 seconds after failure.

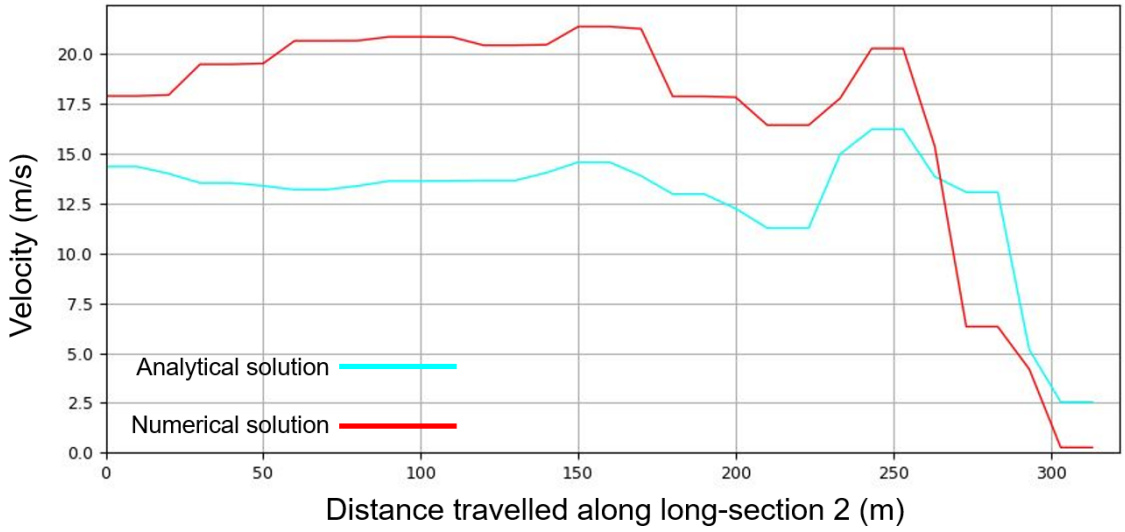

Figure A.8: Front velocity along long-section 2.

LONG -SECTION 4. Time 252 seconds after failure.

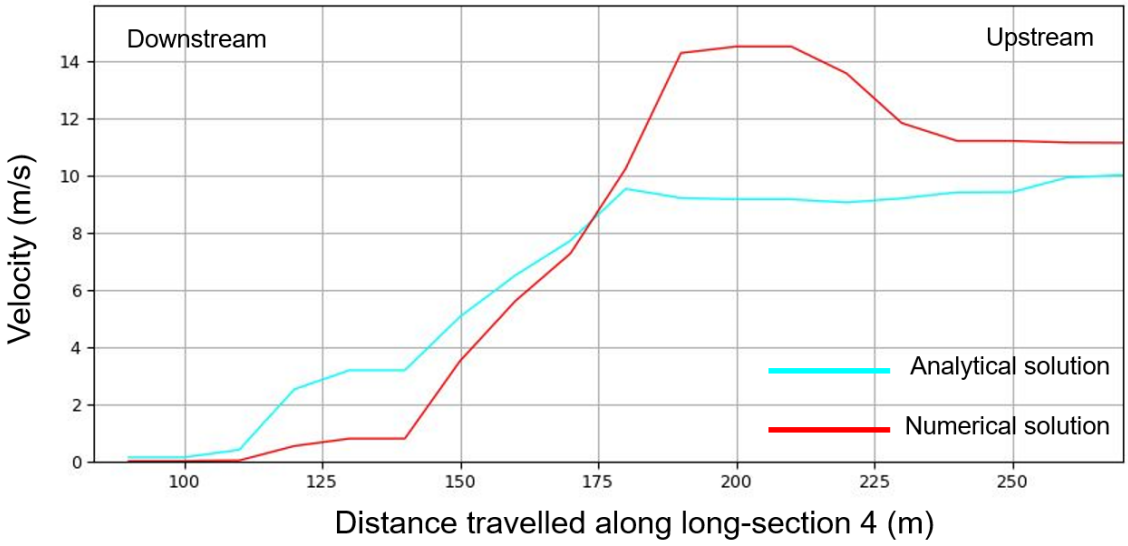

Figure A.9: Front velocity along long-section 4.

B

Sensitivity analysis. FLO-2D results

VOLUMETRIC CONCENTRATION

Long section 2. Velocity profiles

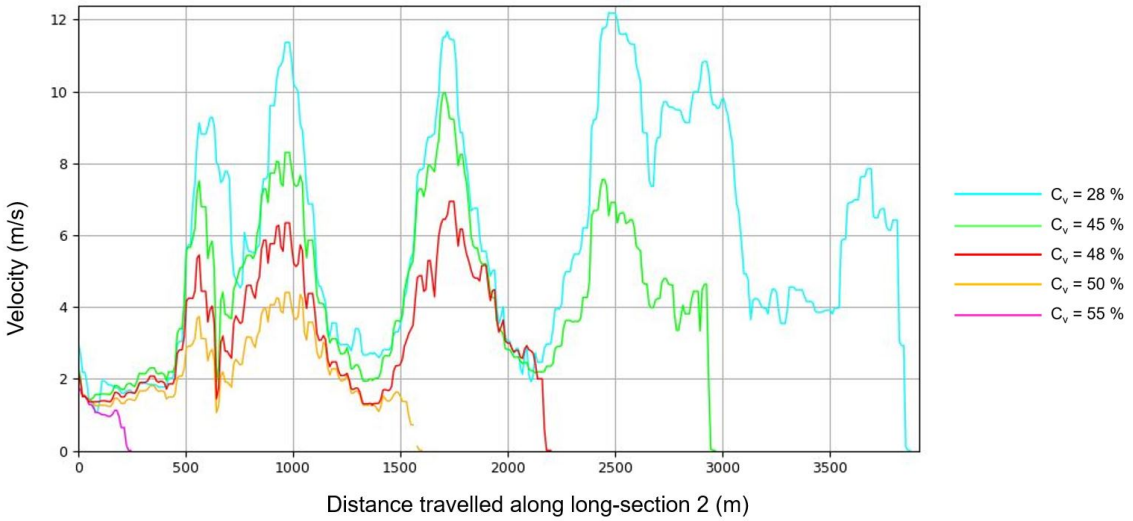

Figure B.1: Front velocity along long-section 2 for different C_v.

Long section 2. Flow depth profiles

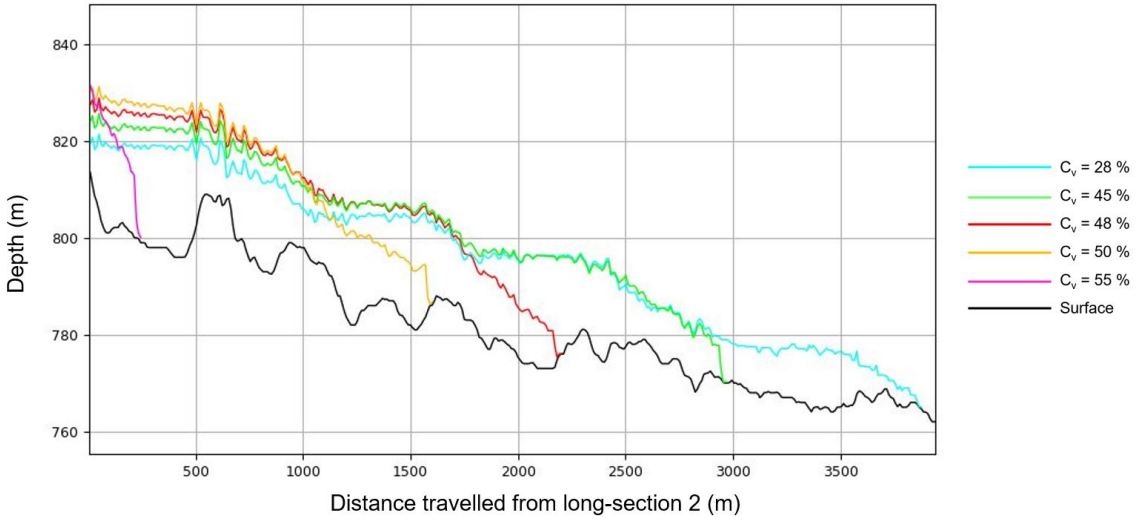

Figure B.2: Flow depth along long-section 2 for different C_v.

MANNING'S ROUGHNESS

Long section 2. Velocity profiles

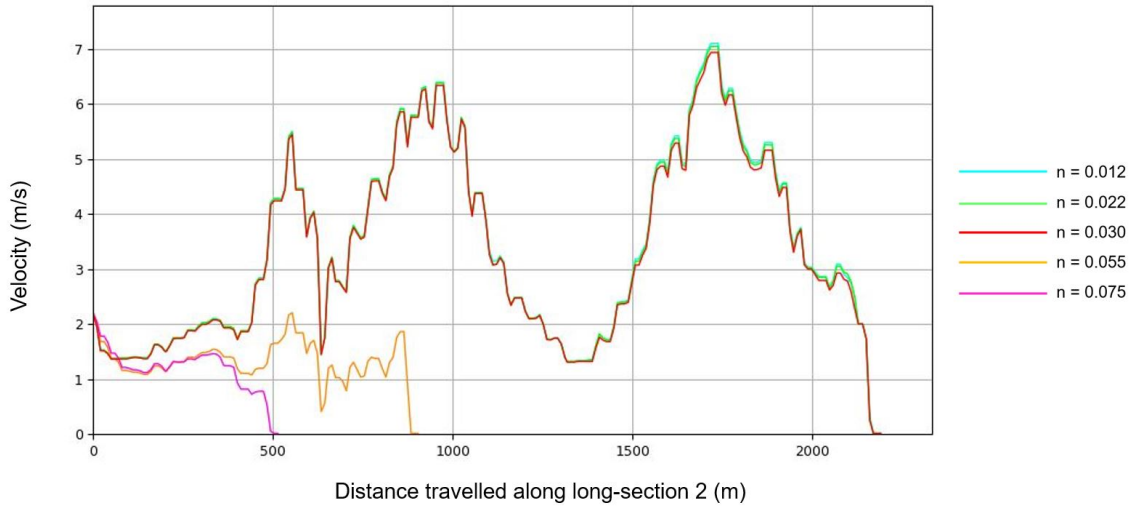

Figure B.3: Front velocity along long-section 2 for different n.

Long section 2. Flow depth profiles

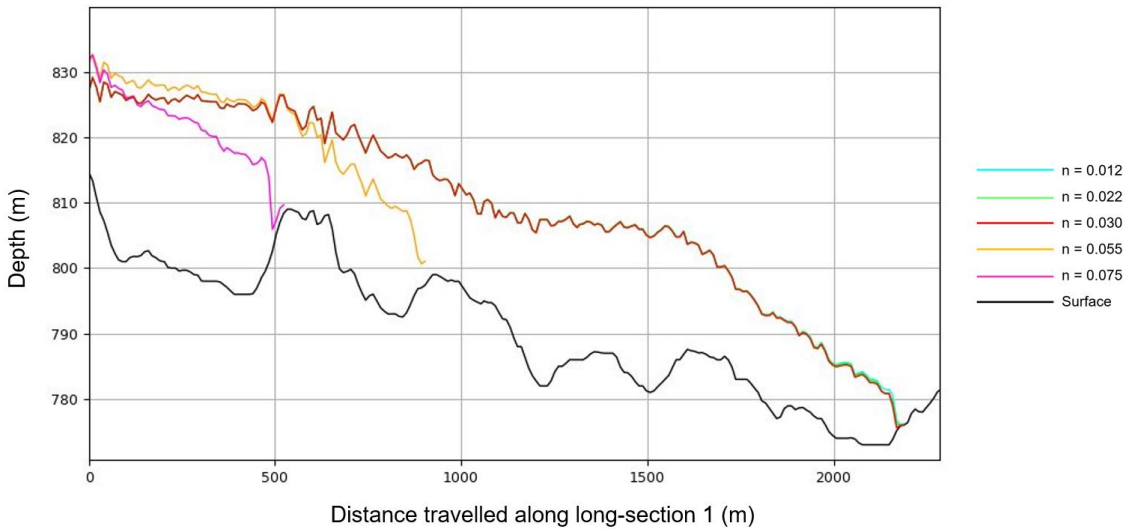

Figure B.4: Flow depth along long-section 2 for different n.

FAILURE DURATION

Long section 2. Velocity profiles

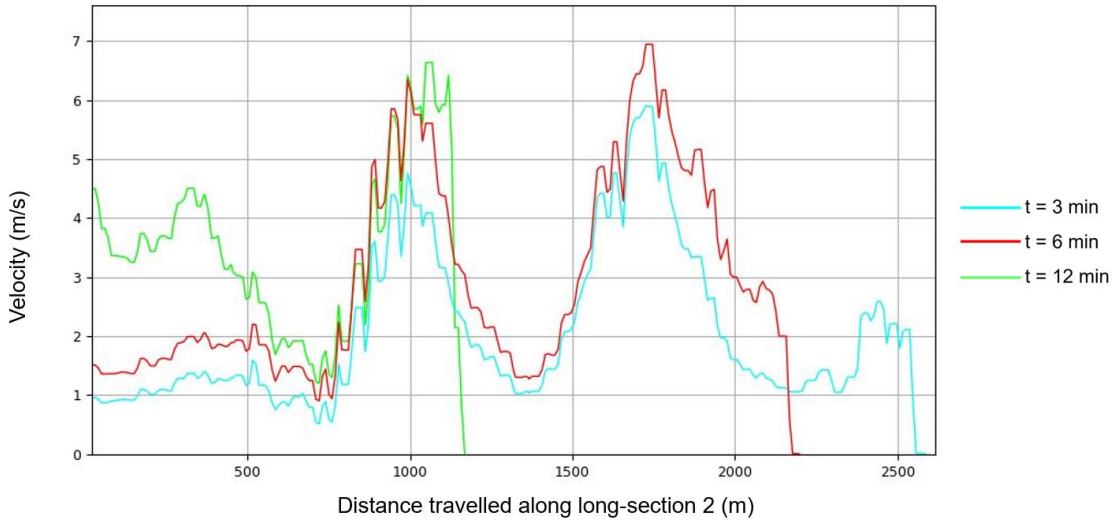

Figure B.5: Front velocity along long-section 2 for different t.

Long section 2. Flow depth profiles

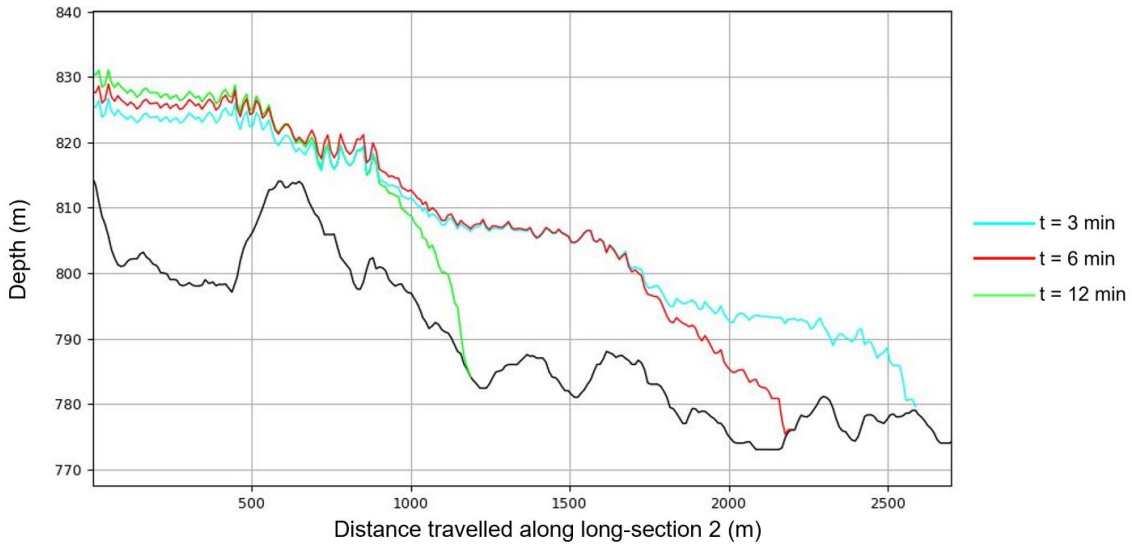

Figure B.6: Flow depth along long-section 2 for different t.

C

Sensitivity analysis. HEC-RAS results

Front velocity at time 8:30 minutes after failure for different C_v. Bingham Plastic model.

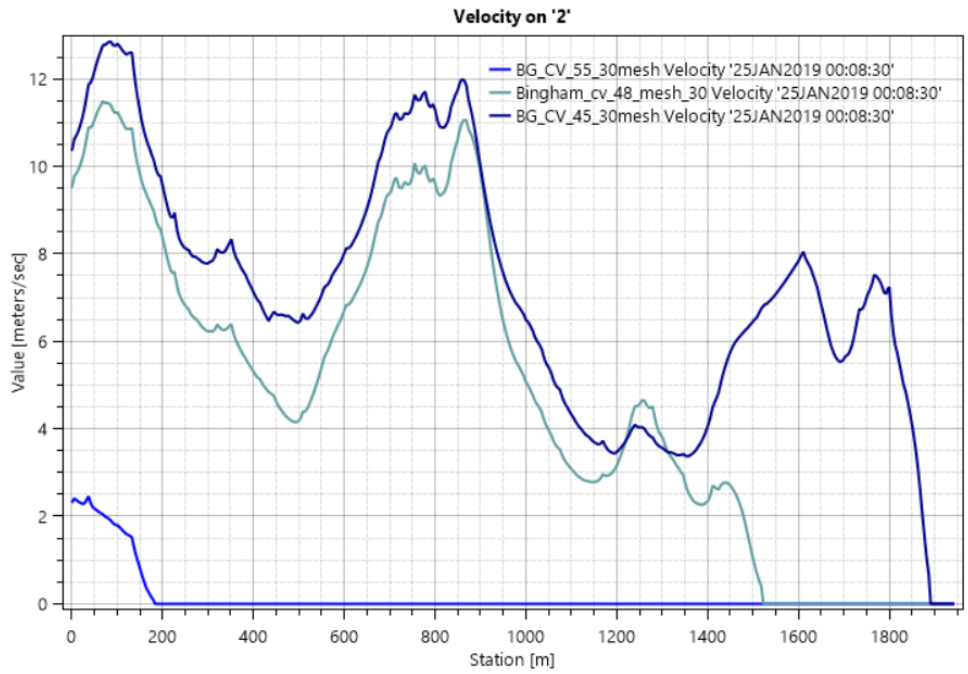

D

Applications

FORQUILHA I

Primary impact zone for different C_v.

$C_v = 45\%$

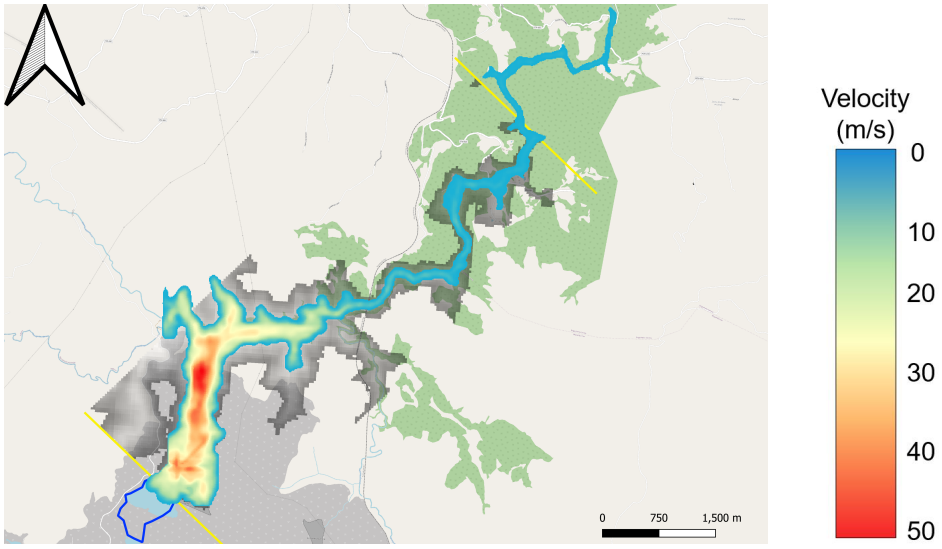

Figure D.1: Comparison between the inundated area obtained with FLO-2D for $C_v = 45\%$ (coloured area) and the energy-line method (grey area). Yellow lines mark the beginning and end of the flooding area. Blue line delimits the reservoir.

$C_v = 55\%$

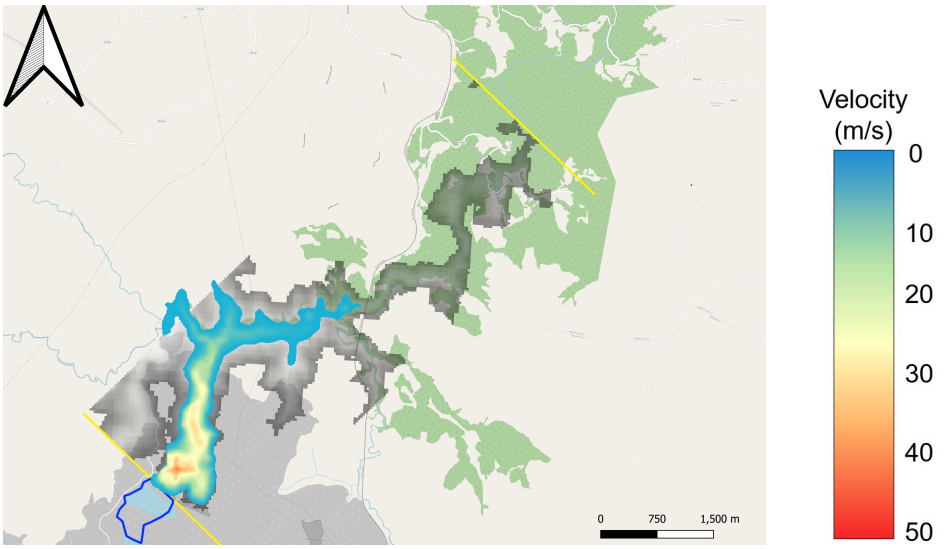

Figure D.2: Comparison between the inundated area obtained with FLO-2D for $C_v = 55\%$ (coloured area) and the energy-line method (grey area). Yellow lines mark the beginning and end of the flooding area. Blue line delimits the reservoir.

Primary impact zone for different t.

$t = 3\ min.$

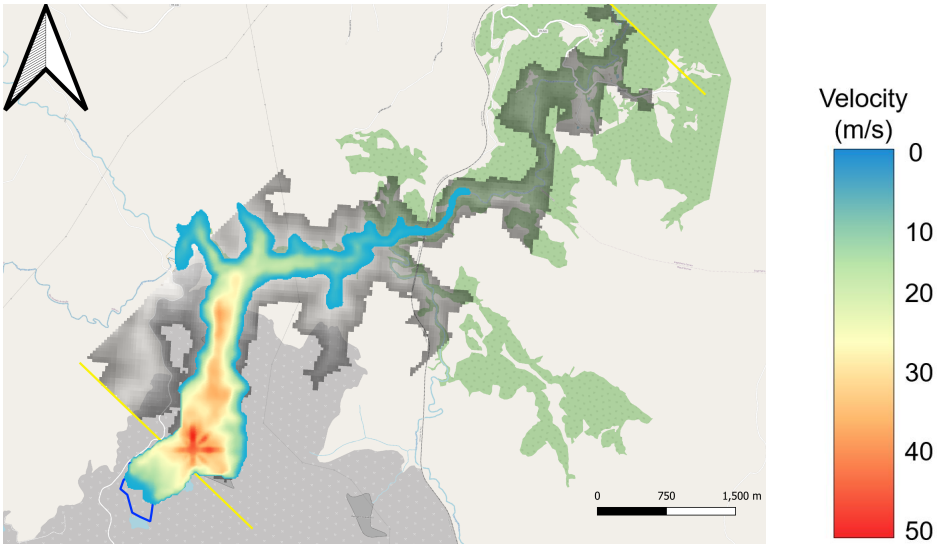

Figure D.3: Comparison between the inundated area obtained with FLO-2D (coloured area) for $t = 3\ min$ and the energy-line method (grey area). Yellow lines mark the beginning and end of the flooding area. Blue line delimits the reservoir.

B. REJEITOS

Primary impact zone for different C_v.

$C_v = 45\%$

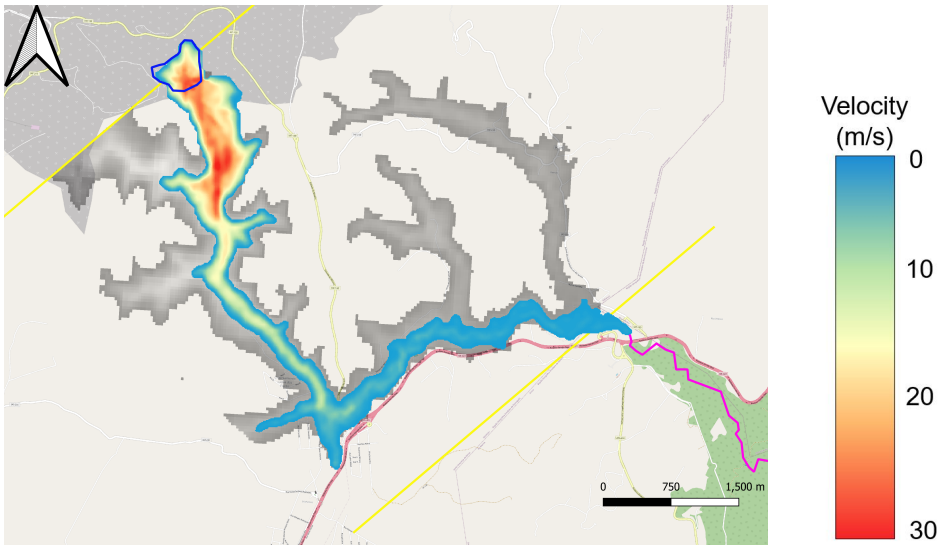

Figure D.4: Comparison between the inundated area obtained with FLO-2D (coloured area) for $C_v = 45\%$ and the energy-line method (grey area). Yellow lines mark the beginning and end of the flooding area. Blue line delimits the reservoir. Pink line the drainage path.

$C_v = 55\%$

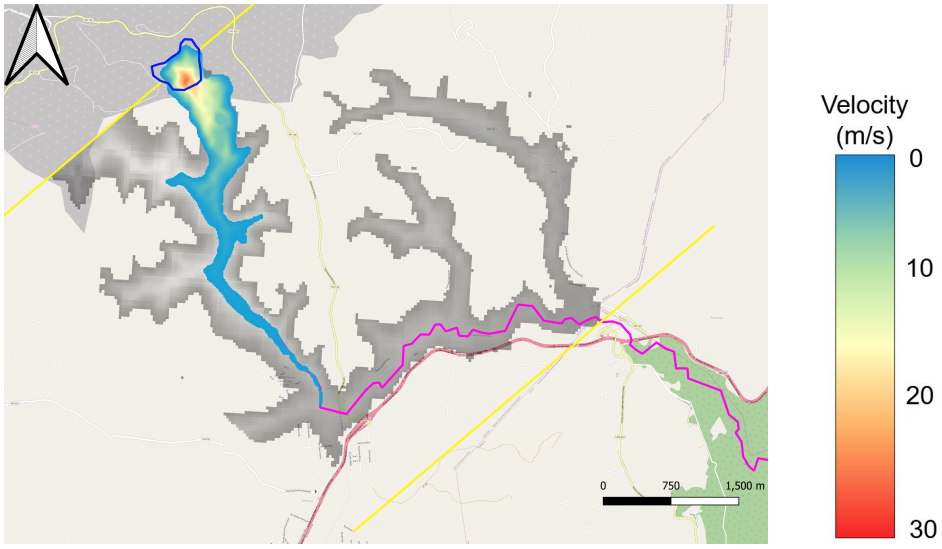

Figure D.5: Comparison between the inundated area obtained with FLO-2D (coloured area) for $C_v = 55\%$ and the energy-line method (grey area). Yellow lines mark the beginning and end of the flooding area. Blue line delimits the reservoir. Pink line the drainage path.

Primary impact zone for different t.

$t = 3\ min$.

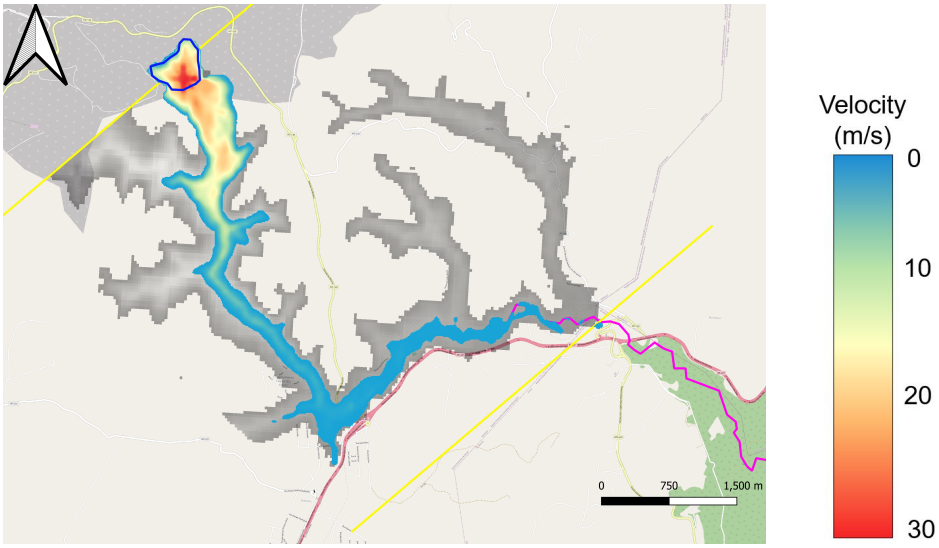

Figure D.6: Comparison between the inundated area obtained with FLO-2D (coloured area) for $t = 3\ min$ and the energy-line method (grey area). Yellow lines mark the beginning and end of the flooding area. Blue line delimits the reservoir. Pink line the drainage path.